NASA CONTRACTOR REPORT

NASA CR-26

NASA CR-2683

EXPERIMENTAL STUDIES ON THE AERODYNAMIC PERFORMANCE AND DYNAMIC RESPONSE OF FLOW DIRECTION SENSING VANES

P. S. Barna and Gary R. Crossman

Prepared by
OLD DOMINION UNIVERSITY
Norfolk, Va. 23508
for Langley Research Center

NATIONAL AERONAUTICS AND SPACE ADMINISTRATION • WASHINGTON, D. C. • MAY 1976

1. Report No.	2. Government Accession No.	3. Recipient's Catalog No.
NASA CR-2683		

4. Title and Subtitle	5. Report Date
Experimental Studies on the Aerodynamic Performance and Dynamic Response of Flow Direction Sensing Vanes	May 1976
	6. Performing Organization Code

7. Author(s)	8. Performing Organization Report No.
P. S. Barna Gary R. Crossman	75-T7
	10. Work Unit No.

9. Performing Organization Name and Address	11. Contract or Grant No.
School of Engineering Old Dominion University Norfold, VA 23508	NSG 1143
	13. Type of Report and Period Covered
12. Sponsoring Agency Name and Address	Contractor Report
National Aeronautics and Space Administration Washington, D.C. 20546	14. Sponsoring Agency Code

15. Supplementary Notes

Technical Monitor, David D. Kershner, Flight Instrumentation Division, NASA Langley Research Center, Hampton, VA

Topical Report

16. Abstract

Systematic investigations were performed on a variety of aerodynamic surfaces to obtain their potential for possible application to wind vanes. Among the surfaces tested were:

(a) single vanes consisting of flat plates of various planforms having aspect ratios between 0.5 and 5;

(b) bi-vanes with aspect ratio 2.5;

(c) various cone and box vanes; and

(d) various cruciform configurations.

These models were subjected to windtunnel tests in the Engineering laboratories at Old Dominion University. In addition to lift and drag force measurements, damping and frequency test were performed under a variety of flow conditions.

These tests were performed in the range of Reynolds numbers 3×10^4 to 1.3×10^5.

17. Key Words (Suggested by Author(s))	18. Distribution Statement
flow-direction indicators angle of attack dynamic response wind vanes	Unclassified-unlimited Subject Category 06

19. Security Classif. (of this report)	20. Security Classif. (of this page)	21. No. of Pages	22. Price*
Unclassified	Unclassified	123	$5.25

*For sale by the National Technical Information Service, Springfield, Virginia 22161

EXPERIMENTAL STUDIES ON THE AERODYNAMIC PERFORMANCE AND DYNAMIC RESPONSE OF FLOW DIRECTION SENSING VANES*

By

P.S. Barna**

and

Gary R. Crossman***

SUMMARY

Systematic investigations were performed on a variety of aerodynamic surfaces to obtain their performance characteristics and determine their potential for possible application to wind vanes. Among the surfaces tested were:

(a) single vanes consisting of flat plates of various planforms having aspect ratios between 0.5 and 5;

(b) bi-vanes with aspect ratio 2.5;

(c) various cone and box vanes; and

(d) various cruciform configurations.

These models were subjected to windtunnel tests in the Engineering laboratories at Old Dominion University. In addition to lift and drag force measurements, damping and frequency tests were performed under a variety of flow conditions.

These tests were performed in the range of Reynolds numbers 3×10^4 to 1.3×10^5.

---

* This report includes results of research performed under tasks NAS1-9434-49, NAS1-11707-10, and NAS1-11707-40.

** Professor of Mechanical Engineering, School of Engineering, Old Dominion University, Norfolk, Virginia 23508

*** Assistant Professor of Engineering Technology, School of Engineering, Old Dominion University, Norfolk, Virginia 23508.

INTRODUCTION

The simplest wind vane is the "weathercock" which has been known for some considerable time and has been used to visually determine the "climatic" wind direction in the open air. In comparison to modern standards, these devices were relatively crude instruments with generally slow response and thus have had limited scientific application. Recently, however, more sophisticated wind vanes have been developed to accurately and promptly determine the direction of airflow under a variety of flow conditions. In some instances, when determination of wind speed is also desired, a propeller finds application and together with the wind vane this type of sensor has gained popularity in various fields of application. In aircraft testing, vanes are employed to accurately determine such variables as airspeed, gust velocity*, angle of attack, angle of slide-slip, etc. In meteorology, increased emphasis on atmospheric turbulence studies has resulted in a renewed interest in meteorological sensors which would rapidly respond to high frequency disturbances. As a result of this demand numerous investigators have set out to review the existing theory of oscillating wind vanes and to design and test various models in order to determine--preferably also to improve--their overall performance.

These efforts produced a variety of designs which are described in numerous papers listed in the reference section. However, after reviewing these papers it was felt that additional studies were needed to answer some questions still outstanding concerning the pertinent parameters and design procedures which ultimately would lead to instruments with optimum response. In order to attain this a test program was instituted which centered around systematic investigations relating to the aerodynamic performance and dynamic response of vanes or fins under steady flow conditions. Accordingly, in this program the performance and response characteristics of numerous model vanes of various sizes and shapes were obtained. The results of these studies are summarized in this paper.

SYMBOLS

a	lift curve slope $dC_L/d\alpha$, radians
A.C.	aerodynamic center (center of pressure) assumed 1/4 chord distance from leading edge

* Usually coupled with a windmill.

AR	aspect ratio, b^2/S
b	span of a wing, m
C	chord, m
$\overline{C}$	mean chord, S/b
C_r	chord at root, m
C_n	normal force coefficient of single vane
$\overline{C}_v$	average torque coefficient for bi-vanes
C_L	lift coefficient of vane
C_D	drag coefficient of vane
C_M	moment coefficient of vane
C.G.	center of gravity of vane
d	distance between bi-vanes, m
D	damping of vane
D_C	critical damping
E	Young's modulus of elasticity
F_n	normal force acting on vane, N
f_n	natural frequency, Hz
f_d	damped frequency, Hz
h	overshoot ratio
I	mass moment of inertia, kg/m^2
I_A	area second moment, m^4
l_R	response length, m
m_v	mass of vane
N	unit of torque, Nm/degree
$r_{C.G.}$	radial distance from pivot to center of gravity of vane, m

r_n	armlength, radial distance of normal force to pivot, m
R_v	armlength of bi-vanes, m
q	dynamic pressure, $\frac{1}{2}\rho U^2$
S	vane area, m^2
t	time, sec
t_R	time response for amplitude to decrease from β_o to β_R, sec
t_v	vane thickness, m
T	torque generated by bi-vanes, Nm
Δt	time required for β_o to decrease to $\frac{1}{2}\beta_o$, sec
U	approach air velocity, m/s
w	load per unit span of wing, N/m
$x_{A.C.}$	distance from leading edge to A.C., m
α	angle of incidence enclosed between a chord and airstream, degrees
β	displacement or oscillations, radians
β_o	initial displacement or offset angle, radians
β_R	amplitude after time lapse of t_R, radians
γ	arm angle of bi-vanes, degrees
ν	kinematic visocity of air, m^2/s
ω	angular frequency of oscillations, rad/s
ϕ	vane setting or trim angle, degrees
ρ	density of air, kg/m^3
ρ_v	density of vane material, kg/m^3
ξ	damping ratio
σ	relative deflection
τ_R	specific time response when $2\pi \ln \beta_o/\beta_R = 1$
Λ	peak ratios of successive amplitudes of oscillations

CONSIDERATIONS CONCERNING VANE DESIGN

The term wind vane or weather vane refers to a simple system generally consisting of three components: (a) an aerodynamic surface which is the vane itself, (b) an arm, to which the vane is attached at one end, and (c) a counterweight at the other end of the arm that statically balances the vane. Between the vane and counterweight a pivotal axis is located generally at the center of gravity of the system about which motion takes place. It is a necessary condition that the vane under consideration is free to rotate about the axis so it can align itself parallel with the airstream without restraint. It is understood that, when a well designed vane is displaced from equilibrium and is subsequently released, it always promptly returns to its former equilibrium position parallel to the direction of the wind through a few oscillations with rapidly diminishing amplitude.

Generally a vane design should satisfy various criteria of different origin. These criteria may be divided into three major categories, namely, (a) aerodynamic, (b) structural, and (c) manufacturing criteria, each of which embraces a different field of study.

The pertinent parameters related to vane design and performance are influenced by the interaction between these three criteria. More specifically, aerodynamic criteria concern dynamic responses such as frequency and damping of the system resulting from aerodynamic forces acting on the particular vane configuration. The structural criteria relate to stiffness or rigidity of the vane configuration and it can readily be seen that the physical properties of vane material such as density and elasticity, as well as dimensions, affect mechanical strength. Since, however, the mass and shape of the vane combined with its component's configuration determines inertia, a scope for optimization emerges because both damping and frequency depend on inertia as well as on aerodynamic forces. Furthermore, since aerodynamic forces depend on vane planform, ultimately strong interdependence between aerodynamic and structural aspects become evident. Finally, the design should preferably be simple and so lend itself to easy, low-cost manufacture which generally adds to the commercial attractiveness of the product.

The design of a vane also depends a great deal on the particular mode of

application, such as steady or unsteady flow, subsonic or supersonic speed and so on. For example, vanes designed for sensing incidence angles of the air from an aircraft may differ considerably from vanes employed at a meteorology station. A vane designed to withstand handling under field conditions will have to be more rugged and thus would have more inertia than a vane used in a laboratory under controlled conditions. But even a light vane must be adequately stiff to ward off aero-elastic effects.

Thus each particular application will probably result in a different design which must satisfy specific requirements. However, in order to design vanes for a particular purpose, their aerodynamic performance characteristics must first be established. Under aerodynamic performance is listed the lift, drag, and aerodynamic moment of a particular vane configuration.

Performance Parameters

The dynamic behavior of wind vanes may be characterized as a damped periodic oscillatory motion analytically represented by a second order differential equation which is linear as long as the torque produced by aerodynamic forces is linear with angle of incidence. In practice, torque is indeed found to be linear under steady flow conditions for small angles of incidence provided the vane is isolated (single). The relevant theory is summarized in Appendix A. The accuracy of theoretical predictions, however, falls short for some bi-vane configurations and for small aspect ratio vanes with short armlength.* The relevant theory for bi-vanes is presented in detail in Appendix B.

It is noted that periodic oscillatory vane motion is desirable because the aperiodic, critically** damped motion theoretically requires infinite time for the displaced vane to return to its equilibrium, zero-displacement position. Periodic motion provided with adequate damping, however, will enable the vane to swiftly return to its equilibrium position through a few oscillations with rapidly decreasing amplitude.

Results of linear theory furnish the following expressions for damping ratio,

---

* The study of vanes with short armlength is considered to be beyond the scope of this paper.

** Or more than critical.

natural and damped frequency, and time response, respectively, for isolated (single) vanes:

Damping Ratio:

$$\xi = \frac{1}{2}\left(\frac{\rho}{2}\right)^{1/2}\left(\frac{aSr_n^3}{I}\right)^{1/2} \tag{1}$$

Natural Frequency:

$$\omega_n = 2\pi f_n = \left(\frac{\rho}{2}\right)^{1/2}\left(\frac{aSr_n}{I}\right)^{1/2} U \tag{2}$$

Damped Frequency:

$$\omega_d = 2\pi f_d = 2\pi f_n \sqrt{1 - \xi^2} \tag{3}$$

Time Response:

$$t_R = 2\pi \frac{\ln \beta_o/\beta_R}{f_n \xi} \tag{4}$$

From the above expressions the following appear:

(1) since $I \propto r_n^2$ (see Appendix C), the linear theory, by eq. (1), predicts that damping, for a specified vane size, shape and mass, becomes directly proportional to the square root of the armlength $(r_n^{1/2})$ whereas the natural frequency of the oscillation, by eq. (2) becomes inversely proportional to the square root of the armlength $(r_n^{-1/2})$. From this, it appears that if armlength is considered the main variable, damping can only be increased at the expense of frequency response. One may also observe that damping is independent of--while frequency is proportional to--AIRSPEED.

(2) on the other hand, assuming a constant armlength and vane size, *both* damping and natural frequency become inversely proportional to the square root of inertia of the system. Thus both damping and frequency *can be* simultaneously improved by reducing inertia to a possible minimum. This may be attained through

reducing mass by either employing lighter materials or by decreasing the thickness of the material or both.

(3) damped frequency depends on both natural frequency and damping ratio (see eq. (3)). Thus the experimenter generally recognizes that the observed damped frequency decreases with increasing damping and vice versa.

(4) effects of damping and natural frequency combine in the time response parameter (eq. (4)) which predicts the actual time required for the amplitude of a damped oscillation to decrease to a certain preselected value. For example, assuming $\beta_R = 0.01\beta_o$, the quantity $2\pi \ln(\beta_o/\beta_R) = 29$ approximately, thus $t_R = 29/f_n\xi$.

In order to express time response in terms of design "constants" eqs. (1), (2), and (4) are combined, resulting in

$$t_R = \text{const} \frac{I}{a^{1/2}\, U\, Sr_n^{\,2}} \tag{5}$$

where

$$\text{const} = \frac{64\pi^2}{\rho} \ln(\beta_o/\beta_R)$$

In a first approximation the secondary masses may be neglected. Thus for the vane alone

$$I = I_v \propto \rho_v\, t_v\, Sr_n^{\,2}$$

hence

$$t_R \propto \frac{\rho_v t_v}{a^{1/2} U} \tag{5a}$$

It may be noticed that eq. (5a) appears to be independent of armlength. Thus for a specified airspeed U, eq. (5a) predicts that light vanes with high lift-curve slope will yield the most satisfactory time response. However, where the term I includes the inertia of both counterbalance and support shaft, the expression is no longer free of armlength. Still, for optimum response the arm

needs to be the shortest possible in order to minimize inertia, and this may be attained in practice by attaching the vane directly to the pivotal shaft of oscillations (ref. [11]).

By multiplying time response with velocity one obtains the response length

$$l_R = Ut_R \propto \frac{\rho_v t_v}{a l/2} , \tag{5b}$$

which is a characteristic constant for a specific design configuration and therefore is a convenient parameter, being independent of air speed.

As far as the stiffness of the vanes is concerned a design parameter can be established from the simple theory of beams, assuming that the vane deflects only under aerodynamic forces and its deflection follows the laws of cantilevered beams.

It is proposed to relate the deflection of the tip of a vane under consideration to its semi-span and compare this with the stiffness of a rectangular vane of the same semi-span and surface area. The relative deflection or the stiffness parameter of a rectangular wing with assumed uniform loading

$$\sigma = \frac{\delta}{(b/2)} = \frac{wb^3}{64EI_A} \tag{6}$$

where $I_A = C_r t_v^3/12$. For non-uniform loading, such as the elliptical lift distribution, the expression requires correction.

Clearly, the vane planform (shape) affects the second moment of the vane at the root where the maximum bending occurs, thereby influencing the deflection of the tip. For example, a vane with a trapezoidal planform of the same thickness and surface area equal to that of a rectangular wing will be stiffer because its section modulus will be larger at the root. The stiffness of the trapezoidal vane, however, can be made equal to that of the rectangular vane by reducing its thickness, thus making the vane lighter.

Furthermore, the vane planform also affects damping because the lift curve slope $a = C_n/\beta$ is strongly aspect ratio-dependent as shown by experiments. In particular, since the lift curve slope for rectangular and trapezoidal planforms is about the same, for equal relative deflection the latter vane shape is preferable to the former due to its lesser thickness.

TEST EQUIPMENT

All experiments relating to aerodynamic characteristics of vanes were performed in the windtunnels at Old Dominion University.* More particularly, these experiments were first concerned with force and moment measurements of all the models under consideration. These were subsequently followed by separate tests concerning damping and frequency. Finally, most model configurations were also subject to determination of inertia.

(a) The force measurements included both the lift and the drag components. The models were mounted to a calibrated strain-gage sting-balance system** which was furnished by NASA Langley Research Center complete with readout equipment. The sting was supported by a support mechanism that allowed the angle of attack to be varied between plus and minus 15 degrees, or between zero and 30 degrees. The apparatus also registered moment about the point of support. The general arrangement of the balance and readout equipment set up at the exit of the open windtunnel is shown in Figure 1, while the sting and support mechanism set up in the closed windtunnel is shown in Figure 2.

(b) The damping characteristics were obtained with the aid of a mechanism that allowed the models to swing freely about a vertical axis. The models were mounted in a vertical position to the downstream end of a light horizontal rod, while the upstream end of the rod was provided with an adjustable counterbalance for static balancing. With the aid of a potentiometer and amplifier, the oscillations of the models were transmitted to a suitable recorder which printed the motions graphically. A trigger mechanism was provided to enable the models to be set initially at a desired offset angle in the airstream and then released manually to oscillate freely about the axis. The general arrangement of this apparatus is shown in Figure 3.

(c) For the moment of inertia measurements of the models, a small portable horizontal turntable supported by a vertical shaft was employed. In order to produce oscillatory motion a spiral spring with linear characteristics was wound around the shaft and thus provided the returning torque. To minimize friction, the shaft was guided by air bearings, to which the air was supplied from the

* In the first set of experiments the open-end windtunnel was employed, but in subsequent tests the 3 ft x 4 ft (.914 m x 1.219 m) return circuit tunnel was utilized.

** The balance support was specially designed for this project by the investigators.

compressed air system of the Engineering School, and the pressure was regulated by a reducer as shown in Figure 4.

(d) Models tested may be classified into the following categories:

1. Isolated (single) vanes
2. Bi-vanes (2 separate vanes)
3. Box-and-cone-vanes
4. Cruciform-vane configurations.

1. Isolated (single) vanes consisted of flat plates featuring various planform configurations. They were made of .0625 in. (1.6 mm)-thick hard aluminum with approximately 20 in.^{2} (.0128 m^2) projected surface area.* All models were provided with rounded leading and trailing edges. Altogether 14 different configurations were tested with various aspect ratios ranging from 0.5 to 5. Details of model configurations are shown in Figures 5(a) and 5(b).

2. Bi-vane models consisted of flat plates arranged in pairs, each having 10 in.^{2} (.0064 m^2) projected surface area and the same aspect ratio of 2.5. In one of the models the vanes were separated by a fixed distance of 5.1 in. (.129 m) while in the other model the distance between the vanes was variable. In the model with the fixed distance the vanes were provided with hinges with the pivot situated at half chord distance under the surface, and the angle of incidence of each vane could be changed by turning the vane about its pivot. In the other model each vane was fastened to an arm which could be rotated about a single pivot located on the axis of symmetry. In both models the vanes could be aligned parallel with the airstream, or could be offset to either form a diverging vane pair known as a "diffuser" or a converging vane pair known as a "contraction". As will be seen later, positive offset angles denote diffusing configuration while the negative offset angles refer to contracting stream. Details of bi-vane models are given in Figures 6(a) and 6(b).

---

* Surface area of one side only.

3. Box-and-cone-vane models consisted of vanes joined at their tips and thus forming a continuous surface like the sides of an open box or a cone. Since the trailing vortices were eliminated (due to joined tips), the aspect ratio designated as being 2.5 in reality loses its close association with the theory of finite wings. Four cone-vanes, each having approximately 5 in. (.127 m) mean diameter and 2 in. (.0508 m) width were fabricated with enclosed angles of 0, 10, 20, and 30 degrees.* These models were provided with cruciform supports as shown in Figure 7, while the box vane, also shown on the photograph in Figure 6, was provided with only a single vertical support. The cone and box vanes were made of 0.04 in. (1 mm)-thick aluminum.

4. The cruciform-vane models were rectangular, delta, trapezoidal, and sweptback planform each having 20 in.^{2} (.128 m^2) projected area and were made of 0.04 in. (1 mm)-thick aluminum, as shown in Figure 8. These models were vanes tested first as flat vanes.

All of the models described above were fitted, in turn, to a small streamline-shaped adaptor about 2 in. (0.051 m) long, that was provided at one end with suitable slits into which the models fitted, while a 0.25 in. (6.3 mm) hole was bored into the other end of the adaptor. This end fitted over the sting balance for the force measurements or over the downstream end of the shaft employed for damping experiments.

The shaft employed for damping was a light 0.25 in (6.3 mm) diameter aluminum tube which was plugged at the upstream end, facing the stream, with a streamlined fairing. A small moveable jockey weight was employed for counterbalancing. During the experiments, shafts with trailing lengths ranging from 1 in. (.025 m) to 21 in. (.534 m) in length were employed.

EXPERIMENTAL METHOD

All experiments were performed under steady flow conditions.

(a) Force Measurements

The model under consideration was carefully installed on the sting and the leveling screws were adjusted until zero lift was recorded on the readout

---

* Half of the enclosed angle is referred to later as divergence (when positive).

equipment. After noting this position as the zero incidence angle, the airflow was stopped. Subsequently normal and axial force, and pitching moment, were recorded at one-degree steps of incidence angle, from zero to 15 degrees, with no air flow present. These readings were necessary to correct steady flow values. The air flow was then restarted and the same recordings were made of normal and axial force, and pitching moment. Both in the open-end and closed tunnel, experiments were performed with an airspeed of 66 ft/sec (20.1 m/sec). This procedure was repeated for each model tested.

Extreme care was exercised during the tests to shield the sensitive strain-gage balance from any excessive force. It was always protected by a covering shield except while in use.

(b) Damping and frequency experiments.

The assembled model, with shaft and counterweight, was first statically balanced about the vertical axis,* with the vertical axis set at a predetermined distance from the vane aerodynamic center. The airstream was then established, the recorder started, and the model allowed to trail freely.

In early tests of the single vanes the model was set to a desired initial offset angle, then released and the oscillations recorded. Initial offset angles consistently employed during the tests were 5, 10, or 15 degrees. In addition to these angles, the model was also "plucked" at random angles and these oscillations recorded. For all later tests involving the bi-vanes, box-and-cone vanes, and cruciform vanes, approximately 10 degree offset angle was used.

Damping experiments were first performed primarily with constant-moment arm; that is, the aerodynamic center of all models was at the same distance (r_n) from the vertical axis. A 5-in. (0.127 m) moment arm was used for each model when practical. This resulted in a different moment of inertia for each model. Subsequent tests were performed with various moment arms.

(c) Inertia Tests

Moments of inertia of the models were obtained by measuring the time of

* The vertical axis was turned into horizontal position for this procedure.

oscillations of the turntable. The moment of inertia included the mass of the model, counterweight, and supporting shaft.

The models were first assembled with the supporting shaft and counterweight, and the assembly was subsequently placed on the turntable. Their centers of gravity, which had been marked prior to the model being tested, were located at the (vertical) axis of rotation. The spring constant of the table had been obtained earlier, by measuring the oscillations of several cylindrical steel rods for which the moments of inertia were calculated prior to each test.

RESULTS OF EXPERIMENTS

Lift, drag and pitching moment coefficients were evaluated from the measured normal and axial forces and moments for each model vane tested.

For establishing lift, drag, moment and aerodynamic center the following procedures were used: the strain gage balance employed for the experiments was designed to measure normal F_n and axial F_a forces as well as pitching moment. With the measured normal and axial force the lift L and drag D force respectively become

$$L = F_n \cos \alpha - F_a \sin \alpha \ , \quad D = F_n \sin \alpha + F_a \cos \alpha$$

and by definition the lift and drag coefficients become

$$C_L = \frac{L}{qS} \ , \quad C_D = \frac{D}{qS} \ .$$

Since the moment was measured about the balance center, a procedure was adopted to transfer this to a moment about the leading edge. Accordingly, by dividing the moment with the measured normal force the aerodynamic center distance as measured from the balance center was located. Subsequently this length was subtracted from the distance between the leading edge and the balance center, hence the aerodynamic center A.C. measured from the leading edge was established. This length is expressed as fraction of the mean the chord $x_{A.C.}/c$, and by definition, the moment coefficient about the

leading edge

$$C_M = \frac{F_n \, x_{A.C.}/c}{qS} .$$

The results of these tests are shown in Figures 9 to 23, in which variation of C_L, C_D, and C_M with incidence is presented. Because of some speed fluctuations present in the airstream, the data recorded show some scatter, especially at lower angles of incidence. However, when the mean values are plotted, the curves appear as fairly continuous lines, indicating satisfactory consistency.

The damping coefficients were obtained from both calculations and direct experiments. Strictly speaking both results are semi-empirical in nature and employ experimentally obtained data for calculations. The calculated damping coefficient for single vanes was obtained from eq. (1) where experimentally obtained values were employed for both the lift curve slope a, and inertia I. The experimental damping coefficient was evaluated with eq. A(9)* from the oscillations recorded. The peaks were first read from charts that had been made by the recording apparatus, and subsequently, a weighted peak-ratio technique was applied to obtain a mean from the first three peaks recorded after the vane was released from its initial offset angle position. The mean was calculated from the "weighted" formula

$$\Lambda_m = \frac{3\Lambda_1 + 2\Lambda_2 + \Lambda_3}{6} \qquad (7)$$

where Λ_1, Λ_2, Λ_3 are the first three peak ratios obtained from the oscillagrams as shown on the accompanying sketch.

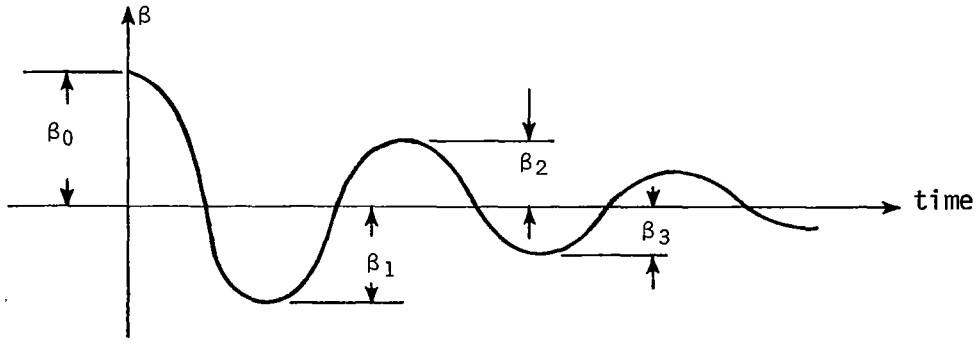

$$\Lambda_1 = \frac{\beta_1}{\beta_0} , \quad \Lambda_2 = \frac{\beta_2}{\beta_0} ; \quad \Lambda_3 = \frac{\beta_3}{\beta_0}$$

Results on damping are presented in Figures 24 to 88.

Results of frequency are shown in Figure 29 where a sample of the experimental observations is presented. Since all other results show a similar pattern, they are presented more completely in Table II, where all damping, frequency and response length data is listed.

The time response characteristic of some vanes is presented in Figures 30 to 33 where specific time response $\tau_R = 1/f_n \xi$ is plotted against airspeed.

The location of the aerodynamic center A.C. from the leading edge, or in the case of swept wings, from the leading apex, is shown in Figure 34.

Discussion of the Results

From the experimental observations, the aerodynamic performance of various model wings may be assessed. Since all models were of equal surface area (20 sq. in. or .0129 m^2) and of equal moment arm (5 in. or .127 m) in many instances, direct comparison between the models can be made.

Lift, drag and moment

As may be anticipated from three-dimensional airfoil theory, lift characteristics and lift-curve slope (a) of single flat vanes appear to be strongly affected by aspect ratio. All the curves show in Figure 9 a non-linear relation between lift-coefficient C_L and incidence, α, accompanied by the variation of the lift-curve slope $dC_L/d\alpha$. While there appears some similarity between the three sets of curves at low incidences, (in the range $0 \leq \alpha \leq 8$ degrees) a marked difference occurs at higher incidences. Naturally, at low incidence angles, the lift curve steadily increases with increasing incidence for all curves.

For the higher aspect ratio (AR ≒ 5) planforms the lift curve slope decreases after about 8 degrees and stall occurs at about 11 degrees for models 1, 9 and 14. No stall is experienced within the test range with model 7, this being characteristic to swept wings, although some change in the lift curve slope may be observed.

For the medium aspect ratio (AR ≒ 2.5) planforms the largest variation of the lift-curve slope appears at low incidences (in the range $0 \leq \alpha \leq 4$ degrees) and remains almost constant at higher incidences.

For the low aspect ratio (AR ≒ 1) planforms the general trend for the lift curve slope is to increase with increasing incidence all the way through the test range.

Since the theory is based on small oscillations, the results obtained over about half the test range (0-8 degrees) may be considered important, while the other half (8-16 degrees) is of academic interest. While the lift-curves are shown in Figure 9, some pertinent results also appear tabulated in Table I where a comparison is made between theoretical and experimental lift-curve slopes. It appears that the highest lift-curve slope is attained with the AR ≒ 5 models and both the rectangular (#1) and elliptic (#9) planforms yield about the same average $dC_L/d\alpha$ value (about 4.97 and 4.89, respectively) over the first eight degrees of incidence.* The lowest lift-curve slope was found to be about 1.6 for the delta-wing model (#12) with AR ≒ 1, while even the half-aspect ratio model (#8) showed a higher value, 2.12.

It is of interest to note that these experimental results are in fair agreement with theory as predicted by the "lifting-line" theory for lift-curve slope given by the result:

$$\frac{dC_L}{d\alpha} = 2\pi \frac{AR}{2 + AR}$$

However, they are generally in a surprisingly poor agreement with the corrected formula

$$\frac{dC_L}{d\alpha} = 2\pi \frac{AR}{2 + (E)AR}$$

---

* The slope near origin is called the "initial" lift-curve slope, a_o .

where E is the semi-perimeter of the wing plan.

It is of some interest to note that variation of the Reynolds number influenced the "initial" lift curve slope to some extent, but produced only a negligible effect on the values averaged over the first eight degrees.

Results on drag (Fig. 10) indicate that the wing (#1) which produced the highest lift also produced the highest drag; consequently, the lowest drag of flat plates plays no significant role in the theory of oscillating single vanes. However, drag forces are significant for bi-vanes.

The moment coefficient, of the vanes shown in Figure 11, follows the pattern of the lift coefficient and has application in locating the aerodynamic center, hence establishing the moment arm.

Results of experiments on lift of bi-vanes is of considerable interest as damping can attain high values with this type of design.* Since the model employed had the same aspect ratio in all experiments, the only parameter was the trim angle, that is the setting angle of each vane to the flow direction. In one set of experiments the distance between the vanes was varied while in another set it remained constant.

It appears that the lift-curve slope becomes dependent on trim angle as well as of incidence and it decreases with increasing trim. In fact, the initial lift-curve slope can become negative at origin or near zero incidences as shown in Figures 12(a), (b) and 15. In addition, the lift coefficient can also vanish at some incidence different from zero, thus creating an additional "equilibrium" position where no moment is developed. Depending on the oscillatory motion the bi-vane may "hang up" at this position or return to its zero equilibrium position. It was observed that this only occurred at trim angles greater than 15 degrees.

The "hang-up" is, of course, due to the drag component significantly adding to the torque. In the case of a single vane, the torque was computed from a single moment of the aerodynamic force acting on the vane; however in the case of bi-vanes the torque is the sum of four moments resulting from two lift and two drag forces acting on the vane pair.

---

* The experimental values far exceed the predictions by theory, see Figure B3, p. 120.

The drag of bi-vanes also depends on the trim angle and incidence as shown in Figures 13 and 16. Generally, drag depends on trim angle for low incidences; hence low drag is experienced with low trim angle and vice versa. However, with increasing incidence the difference between the drag curves gradually diminishes and from sixteen degrees upward, there appears no significant difference between the curves. It is also of interest to note that at low incidences the drag of the lower trim angles (ϕ = 0, 5, 10) increases, but this is not the case with the higher trim angles (ϕ = 15, 20) when the drag slightly decreases first with increasing incidence. The results are substantially equal for both positive and negative trim angles.

The moment coefficients of bi-vanes represent a more complex pattern as it obviously includes both lift and drag forces. For positive trim, Figure 14 (a), the rate of increase for ten degrees is the largest and for 20 degrees is almost zero. At about eight degrees of incidence there appears a change and the roles reverse, inasmuch as the zero trim angle curve begins to increase more markedly while the ten degree curve tapers off. The 15 degree curve, which appears first perfectly linear with incidence, has the highest moment at ten degrees incidence and also above 20 degrees. (This may be of importance when considering its high damping characteristics.) Between 18 and 20 degree incidence the curves of the lower trim flatten out while the curves of ϕ = 10, 15 and 20 degrees show increasing moment with incidence.

The results on moments markedly differ for negative trim angles (Fig. 15(b)). Here zero moment occurs for $\phi = -20°$ at about 10 degrees of incidence, thus locating the "hang-up" position. The $\phi = -5°$ trim produces markedly lower moments than the $\phi = +5°$ trim while the higher trim angles produce remarkably poor results. Clearly, the negative trim configuration is wholly unsatisfactory for bi-vanes with variable distance between the vanes.

Results on moments of bi-vanes with constant distance show similar results (Fig. 17), notably, that negative trim angles produce results inferior to positive angles. However, both the plus and the minus 20 degree trim show "hang-ups" (the $\phi = +20°$ at about 4 degrees, $\phi = -20°$ at about 24 degrees of incidence), which leaves $\phi = +10°$ that produces satisfactory moment.

Results on lift for conical vanes (Figs. 18(a) and (b)) show satisfactory values for ±5° divergence as compared with zero divergence and with the AR = 2.5 flat plate. However, for higher positive divergence (10 and 15 degrees), the lift falls off considerably and for negative 10 and 15 degree cone angles "hang-ups" occur.

Results on drag for conical vanes (Figs. 19(a) and (b)) show results similar to those obtained for bi-vanes with the curves converging at higher incidences and with the drag being about proportional to the cone angle at low incidence.

Results on moments (Figs. 20(a) and (b)) are most satisfactory for zero divergence, but gradually fall off and at 10 and 15 degrees divergence the values are too small to restore equilibrium at low incidences.

Results pertaining to various "cruciform" configurations indicated satisfactory lift and low drag for lower incidences as shown in Figures 21 and 22. The moment increased with incidence for swept, trapezoid, and delta planforms, but was found rather flat for the rectangular model as shown in Figure 23. Since "cruciform" models were made of two conventional planforms intersecting at right angles at their axis of symmetry, the results obtained for lift, drag, and moment are expected to generally be about the same value as if they were for single plates. Experiments proved this to be correct even when the intersecting plates were rotated by 45 degrees from a standing cross + to a tilted cross x orientation.

Damping and Frequency

For the various single vane models, the results for constant arm length are presented in Figure 24, where damping ratio, ξ, is plotted against initial offset angle, β_0, in the upper half, and against air velocity in the lower half of the page.

Similar experiments were repeated for the No. 1 model, using different arm lengths ranging from 1 in. (.025 m) to 5 in. (.127 m) as shown in Figure 25. Additional experiments were performed using arm length from 7 in. (.178 m) to 18 in. (.456 m), including the effects of counter weight size and shaft length on damping; these results are shown in Figure 26.

The results for arm length less than 5 in. (.127 m) indicate a relatively large scattering of the experimental damping ratio, while the calculated

damping is presented as a single horizontal line because of its independence of air speed and initial offset angle. The large scatter at low damping was caused by the difficulty in obtaining accurate readings due to the slow decrease in the amplitude of the oscillations.

Generally, the experimentally obtained damping ratio was found to be higher than the theoretical prediction and at times the discrepancy between the two exceeds 100%. In isolated instances, however, some experimental points do fall near the calculated lines. As indicated in Figure 26, the predicted values move closer to the experimental results with less scattering as the arm length increases and will even become equal at a certain armlength. At this length the experimental and theoretical (calculated) curves intersect and with further increasing arms the experimental results fall slightly below the calculated values. This discrepancy could possibly be attributed to the bending of the rod at the larger armlength. The reason for the increasing discrepancy between theory and experiment for short armlength is not fully understood but is probably caused by the assumption of a single force acting on the vane at the aerodynamic center. This assumption apparently holds well for a long arm, but may fail for a short arm. Experiments show that for very short arms the theory underestimates damping by a factor of almost four.

Of the single vanes tested models No. 1 and No. 12 yielded the best average damping characteristics for a fixed armlength as shown in Table II(a).

Damping of bi-vanes increases with trim angles up to $\phi = 15°$ and, to some extent, improves with decreasing armlength, as shown in Figure 27. Results on bi-vanes with different vane thickness is shown in Figure 28 where armlength is replaced by arm angle (see Appendix B, Fig. B2). It appears that for both vane thicknesses optimum condition occurs at arm angle, $\gamma = 40°$ and trim angle, $\phi = +15°$. Average damping values for bi-vanes are presented in Table II(b). The vane with lesser thickness (inertia), however, produces the higher damping as may be anticipated from theory. Since damping obtained by bi-vanes was found to be much higher than that of single vanes, their application may be well worth consideration.

The results of damping for the box vane and various cone vanes with two different armlengths are presented in Table II(c). It appears that damping

ratio increases with divergence angle but remains substantially constant for negative divergence (convergence) with best damping obtained at the 15 degree angle at the longer armlength.

The damping of cruciform vanes is listed in Table II(d) and the results clearly indicate that a negligible difference exists between the two possible orientation marked + and x. The results show that highest damping was experienced with model 27A.

Frequencies were recorded for all experiments and were found to be in accordance with theory which predicts a direct linear relation with air speed and an inverse relation with armlength. Since all results show similar characteristics, a sample result only is presented in Figure 29, while all other results are listed in Table II. It is noted that no attempts were made to predict frequency by theory.

Time Response

Since damping increases and frequency decreases with increasing armlength, designers may face the problem which variable (or parameter) to choose as their basis for design from the two alternative courses available. They may find it impractical to design a vane that satisfies the demand for both high damping and high frequency.

The present study shows that the third alternative, namely the time response of the vane, which combines the frequency and the damping into a single parameter, may be a satisfactory basis for design, especially for fast response requirements.

It is shown [see Appendix A, Eq. A(15)], that the time required for a vane to return to some specified fraction of its original offset is inversely proportional to the frequency-damping product, and that the response time thus becomes inversely proportional to airspeed. The plotted results appear fairly consistent at all speeds as shown in Figures 30, 31 and 32. It appears that a particular vane configuration which yields at some speed a certain response time will also maintain its relation relative to other vanes and the curves run consistently parallel or near parallel with each other.

For single vanes the effects of armlength and airspeed for No. 1 model are clearly demonstrating the decreasing time response with increasing airspeed

and decreasing armlength, as shown in Figure 30. For constant armlength, Figure 31 shows the effect of planform on time response revealing a considerably faster response for the higher and medium aspect ratio rectangular wings (models No. 1 and 4).

Conveniently, rectangular wings can also be attached directly to an axis of rotation* (like the "Richardson" vane; see Ref. [20]), hence its armlength may be reduced to an absolute minimum which incidentally is the distance between leading edge and AC. Therefore rectangular planforms may be selected, from practical considerations, as probably the best choice. And while the high aspect ratio wing has better time response the low aspect ratio wing (AR = 1 or 1/2) has the practical advantage of having the shorter side attached to the pivotal shaft of oscillations (Ref. [20]).

For bi-vanes there appears a marked decrease of time response with increasing trim up to $\phi = 15°$ and arm angle as shown in Figure 32. Here the top four curves show the improvement in time response with increasing trim for a constant 10-degree arm angle, while the remaining curves show the improvement with increasing arm angle for the constant 15-degree trim. These results are again represented in Figure 33 where time response is plotted against arm angle for various airspeeds. These curves appear to have minima which all occur at approximately 40 degrees arm angle. These results are considered satisfactory and could be even further improved by varying the aspect ratio or the distance or both between the vanes. Such efforts, however, were considered beyond the scope of the present study.

Response characteristics of box and cone vanes as well as the remaining cruciform configurations are summarized in Table II where the results of all vanes are also shown for convenience. The reason for this may be attributed to the experience gained with single and bi-vanes which indicates that much of the results can be effectively and indeed conveniently presented in tabular form. More particularly the table also shows response length (last column) which is defined as velocity times response time (see Eq. 5b). This is a convenient parameter being independent of airspeed.

It appears from Table II(c) that response length for the above models also decreases with decreasing armlength. For the cone vane the optimum response length was attained with the 5-degree divergence angle for the long arm.

---

* The axis of rotation is also the centerline of the shaft of oscillations.

but with the 10-degree divergence angle for the short arm. For cruciform vane configurations the best results were attained with model 27A for both the short and long arm, followed by Model No. 26.

As predicted by theory the results indicate that the A.C. was indeed found at a distance of quarter chord for some models, while for other planforms it was found at different location generally at a greater distance from the leading edge, as shown in Figure 34. The results also show for most vanes an increase of this distance with increasing incidence. Note that the location of A.C. is a fraction of the mean chord $\bar{c}$ given by the expression $\bar{c} = S/b$.

CONCLUSIONS

1. The experimentally obtained damping ratio for single vanes was found generally higher than the values predicted from existing theory where experimentally obtained lift-curve slope results were employed for the calculations.

2. Damping proved to be independent of airspeed and dependent on armlength, in accordance with theory. However, the discrepancy found between the experimentally obtained damping and calculated values appear to be strongly influenced by armlength and for short arms the theory fails altogether. This conclusion suggests a revision of the existing theory.

3. The tests show that rectangular single vanes with high aspect ratio planforms and having long arm, and also swept or delta planforms, produce high damping.

4. Natural frequency proved to increase consistently and linearly with air speed and decrease with increasing armlength, in accordance with theory. The frequency ratio was found highest for the high aspect ratio planforms (model 1 and 9) for the same armlength and the lowest for the low aspect ratio vane.

5. Since damping increases and frequency decreases with armlength it would be impractical to design a vane that satisfies the demand for both high damping and high frequency. Instead, to predict the most suitable design, a single parameter embodying the combined effects of frequency and damping is proposed either in the form of time response or response length. For single vanes the fastest time response was recorded for the high and medium aspect ratio rectangular planforms; in addition to these two, short response was also

obtained in models 9, 10 and 14. Since response increases with armlength, for fast response best results can be possibly obtained with the shortest arm.

6. Bi-vanes were found to produce high damping ratios and values well in excess of single vanes were measured during the tests. However, performance of bi-vanes was found to be critically dependent on trim angle as well as of armlength (or arm angle) and optimum results, including response length, were obtained with positive 15-degree trim and 40-degree arm angle (short arm but not the shortest). Above 15-degree trim angle the bi-vane has a tendency to "hang-up," that is to settle into a different equilibrium position from the original prior to oscillations. Bi-vanes setup with negative trim angle proved rather unsatisfactory.

7. Experiments showed that cone and box vanes were particularly sensitive to divergence angle. Positive divergence produced satisfactory damping and response length at the positive 15-degree divergence but negative divergence (convergence) was found, as in the case of bi-vanes, unsatisfactory. Also for these models response length decreased with decreasing armlength.

8. Results on damping of cruciform vanes indicate no substantial difference between the orientation + or x. For the long arm the highest damping and shortest response length was obtained with a "trapezoidal" configuration (model 27A) constructed with No. 11 planform. For the shorter arm only a slight improvement for the response length was noticeable.

9. Both damping and time response can be further improved by employing light materials and/or by keeping the thickness of the vanes at a minimum. Since stiffness of the vanes is also critical, there appears a conceivable trade-off by employing such planforms which more effectively resist bending (like a delta wing) although their response length might be somewhat less favorable.

REFERENCES

1. Arakawa, H.; "On Wind-vane of the R. A. E. Pattern," Geophysical Magazine, Vol. 4, 1931, pp. 53-59.

2. Barthelt, H. P. und Ruppersberg, G. H., "Die mechanische Windfahne, eine theoretische und experimentelle Untersuchung," Flugwissentschaftliche Forschungsanstalt FFM-Bericht No. 14 and 25, 1957.

3. Camp, Dennis W. and Turner, Robert E., "Response Tests of Cup, Vane, and Propeller Wind Sensors," Journal of Geophysical Research, Vol. 75, No. 27, Sept. 20, 1970, pp. 5265-5270.

4. Clink, W. L.; Bannister, N. A.; Styles, K. F., "Description and Test of an Electrically-Recording Gustiness Bi-Vane," Suffield Technical Note No. 32, Suffield Experimental Station, Ralston, Alberta, pp. 1-9.

5. Friedman, G. J., "Frequency Response Analysis of the Vane-Type Angle of Attack Transducer," Aero/Space Engineering, March 1959, pp. 69-75.

6. Garbell, Maurice A., "Fins for Aerological Instruments," Journal of Meteorology, pp. 82-90.

7. Lenschow, D. H., "Vanes for Sensing Incidence Angles of the Air from an Aircraft," Journal of Applied Meteorology, Vol. 10, December 1971, pp. 1339-1343.

8. MacCready, Jr., Jex, Henry R., "Response Characteristics and Meteorological Utilization of Propeller and Vane Wind Sensors," Journal of Applied Meteorology, Vol. 3, April 1964, pp. 182-193.

9. Pinsker, W. J. G., "The Static and Dynamic Response Properties of Incidence Vanes with Aerodynamic and Internal Viscous Damping," U. D. C. No. 629.13.052.42: 533.6.013.423: 533.6.013.6, C. P. No. 652, August 1962, pp. 1-24.

10. Richardson, Norman R., "Dynamic and Static Wind-Tunnel Tests of a Flow-Direction Vane," NASA TN D-6193, April 1971, pp. 1-21.

11. Rijkoort, P. J. and Wieringa, J., "Wind Information for Landing and Take-Off and Siting of Instruments," Aeronautical Meteorology, Proc. of the WMO Sci. & Tech. Conf. on Aeronautical Meteorology, March 1968, N69-31576, pp. 158-166.

12. Rijkoort, P. J.; Schmidt, F. H.; Velds, C. A. and Wieringa, J., "A Meteorological 80-m Tower Near Rotterdam," Boundary-Layer Meteorology 1, 1970, 5-17.

13. Sachdev, R. H. and Rajan, K. K., "An Electronic Computing Wind Vane for Turbulence Studies," J. of Applied Meteorology, Vol. 10, December 1971, pp. 1331-1338.

14. Sanuki, M.; Kimura, S. and Hayashi, H., "A Proposed Wind Vane with Practically No Overshoot," Meteorology & Geophysics, Tokyo, Vol. 16, No. 2, 1965, pp. 84-89.

15. Sanuki, M.; Kumura, S. and Hayashi, H., "Wind Vane with Extremely Small Moment of Inertia and Its Possible Application," Meteorology & Geophysics, Vol. 17, No. 1, Oct. 1966, pp. 46-50.

16. Sanuki, M.; "Studies on Biplane Wind Vanes, Ventilator Tubes and Cup Anemometers (I)," Papers in Meteorology & Geophysics, Tokyo, Vol. 1, No. 1, Oct. 1950, pp. 81-132.

17. Wieringa, J., and Van Lindert, F. X. C. M., "Application Limits of Double-Fin and Coupled Wind Vanes," J. of Applied Meteorology, Vol. 10, February 1971, pp. 137-145.

18. Wieringa, J., "Evaluation and Design of Wind Vanes," J. Applied Meteorology, Vol. 6, Dec. 1967, pp. 1114-1122.

19. Wieringa, J., "Gust Factors Over Open Water and Built-Up Country," Boundary-Layer Meteorology, Vol. 3, No. 4, March 1973, pp. 424-441.

20. Barna, P. S.; and Crossman, G. R., "Fast Response Vanes for sensing Flow Patterns in Helicopter Rotor Environment," Contractors Report NASA CR-132545, 1974.

TABLE I

COMPARISON BETWEEN THEORETICAL AND EXPERIMENTAL LIFT-CURVE SLOPES ($dC_L/d\alpha$)

Model Number	Aspect Ratio	$2\pi \frac{AR}{2 + AR}$ Uncorrected $dC_L/d\alpha$	$E = \frac{Perim.}{2b}$	$2\pi \frac{AR}{2 + (E)AR}$ Corrected $dC_L/d\alpha$	Experimentally Obtained		Mean for 8° Correlated With:	
					Initial Lift Curve $(dC_L/d\alpha)_o$	Mean for 8°	$2\pi \frac{AR}{2 + AR}$	$2\pi \frac{AR}{2 + (E)AR}$
1	5	4.48	1.2	3.927	5.15, 4.81 5.27, 4.75 4.995	5.04, 4.87 5.04, 4.93 4.97	Fair	Poor
2	5	4.48	1.2	3.927	4.06, 4.01 4.035	5.04, 4.01 4.52	Good	Poor
3	1	2.09	2.0	1.571	1.72	2.12	Good	Poor
4	2.5	3.49	1.4	2.856	3.03	3.67, 3.61 3.64	Fair	Very Poor
5	1	2.09	2.414	1.423	2.63, 2.12 2.37	2.23, 2.29 2.26	Fair	Very Poor
6	2.5	3.49	1.814	2.403	2.98, 3.49 3.25	3.66, 3.66 3.66	Fair	Very Poor
7	5	4.48	1.614	3.119	4.01, 3.49 3.75	4.29, 4.29 4.29	Fair	Very Poor
8	.5	2.50	3	1.79	2.52, 2.40 2.46	2.18, 2.06 2.12	Poor	Poor
9	5	4.48	1.076	4.25	3.49, 4.35 3.92	5.15, 4.64 4.89	Fair	Poor
10	2.23	3.31	1.499	2.623	1.78, 1.83 1.81	2.92, 2.75 2.83	Poor	Fair

TABLE I (contd)

Model Number	Aspect Ratio	$2\pi \frac{AR}{2 + AR}$ Uncorrected $dC_L/d\alpha$	$E = \frac{Perim.}{2b}$	$2\pi \frac{AR}{2 + (E)AR}$ Corrected $dC_L/d\alpha$	Experimentally Obtained		Mean for 8° Correlated With	
					Initial Lift Curve $(dC_L/d\alpha)_o$	Mean for 8°	$2\pi \frac{AR}{2 + AR}$	$2\pi \frac{AR}{2 + (E)AR}$
11	2.5	3.49	1.270	3.034	3.21, 3.20 3.20	3.38, 3.43 3.40	Good	Poor
12	1	2.09	2.561	1.378	1.54, 1.72 1.68	1.66, 1.54 1.60	Poor	Fair
13	1.27	2.36	1.571	1.997	1.54, 1.83 1.68	2.29, 2.18 2.23	Fair	Fair
14	5	4.48	1.38	3.528	3.72, 3.60 3.66	4.58, 4.46 4.52	Good	Very Poor

TABLE II

NATURAL FREQUENCY, DAMPING RATIO AND RESPONSE LENGTH OF VARIOUS VANES

(a) Single Vanes

Vane Model No.	Armlength, r_n(m)	Damping Ratio, ξ	Frequency Ratio f_n/U (cycles/m)	Response Length $U/f_n\xi$(m)
1	.127	.123	0.174	46.7
2	----	----	-----	----
3	.127	.098	0.109	93.6
4	.127	.112	0.160	55.8
5	.127	.111	0.114	79.0
6	.127	.098	0.154	66.3
7	.127	.102	0.170	57.7
8	.127	.084	0.120	99.2
9	.127	.109	0.179	51.3
10	.127	.118	0.157	54.0
11	.127	.099	0.168	60.1
12	.127	.126	0.114	69.6
13	.127	.104	0.114	84.3
14	.127	.104	0.176	54.6
1	.051	.102	0.231	42.4
1	.076	.110	0.217	41.9
1	.102	.121	0.198	41.7
1	.203	.143	0.171	40.9
1	.229	.141	0.159	44.6
1	.305	.161	0.138	45.0
1	.381	.170	0.129	45.6
1	.406	.174	0.120	47.9
1	.457	.172	0.111	52.4
1	.533	.171	0.101	57.9
4	.376	.146	.1145	59.8
4	.251	.130	.1400	54.9
4	.190	.115	.1583	54.9

TABLE II (contd)

(a) Single Vanes (contd)

Vane Model No.	Armlength, r_n(m)	Damping Ratio, ξ	Frequency Ratio, f_n/U (cycles/m)	Response Length, $U/f_n\xi$(m)
4	.122	.099	.1915	52.7
4	.102	.094	.2098	50.7
4	.076	.093	.2326	46.2
4	.058	.091	.2474	44.4

TABLE II (contd)

(b) Bi-vanes, Const. Vane Distance (Model #18) 1.6 mm Thick

Vane Trim Angle, ϕ (°)	Armlength r_n(m)	Damping Ratio, ξ	Frequency Ratio, f_n/U (cycles/m)	Response Length, $U/f_n\xi$(m)
0	.376	.119	.0917	91.6
5	.376	.126	.0975	81.4
10	.376	.149	.0934	71.9
15	.376	.220	.0640	71.0
0	.251	.104	.1118	86.0
5	.251	.121	.1195	69.2
10	.251	.132	.1149	65.9
15	.251	.198	.0841	60.1
0	.190	.097	.1315	78.4
5	.190	.105	.1422	67.0
10	.190	.126	.1436	55.3
15	.190	.224	.1092	40.9
0	.122	.078	.1628	78.8
5	.122	.091	.1745	63.0
10	.122	.118	.1825	46.4
15	.122	.233	.1458	29.4
0	.102	.070	.1821	78.4
5	.102	.087	.1923	59.8
10	.102	.125	.2022	39.6
15	.102	.250	.1655	24.2
0	.076	.044	.1637	138.8
5	.076	.061	.1843	88.9
10	.076	.084	.1995	59.7
15	.076	.208	.1678	28.7

TABLE II (contd)

(b) Bi-Vanes (contd) (Model #18A) 1 mm Thick

Vane Trim Angle ϕ (°)	Armlength r_n(m)	Damping Ratio, ξ	Frequency Ratio, f_n/U (cycles/m)	Response Length, $U/f_n\xi$(m)
0	.251	.131	.1423	53.6
5	.251	.142	.1494	47.1
10	.251	.167	.1507	39.7
15	.251	.251	.0837	47.6
0	.190	.120	.1620	51.4
5	.190	.129	.1713	45.3
10	.190	.149	.1861	36.1
15	.190	.241	.1195	34.7
0	.122	.092	.2058	52.8
5	.122	.103	.2197	44.2
10	.122	.147	.2282	29.8
15	.122	.283	.1673	21.1
0	.102	.086	.2326	50.0
5	.102	.092	.2380	45.7
10	.102	.140	.2608	27.4
15	.102	.302	.2304	14.4
0	.076	.052	.1852	103.8
5	.076	.067	.2286	65.3
10	.076	.109	.2487	36.9
15	.076	.262	.2112	18.1

TABLE II (contd)

(c) Box (Model #20) and Cone (Models #19A, 21, 22, 23) Vanes

Vane Model No.	Trim Angle, ϕ (°)	Armlength r_n(m)	Damping Ratio, ξ	Frequency Ratio, f_n/U (cycles/m)	Response Length, $U/f_n\xi$(m)
20	(0)	.251	.115	.125	69.5
	(-15)	.251	.157	.076	83.8
20	(0)	.071	.046	.203	107.1
	(-15)	.071	.155	.125	51.6
23	(0)	.251	.106	.1159	81.4
21	(5)	.251	.123	.1226	66.3
22	(10)	.251	.120	.0868	96.0
19A	(15)	.251	.174	.0649	88.6
21	(-5)	.251	.096	.1073	97.1
22	(-10)	.251	.065	.0550	279.7
19A	(-15)	.251	.099	.0403	250.6
23	(0)	.071	.060	.1982	84.1
21	(5)	.071	.090	.2170	51.2
22	(10)	.071	.138	.1512	47.9
19A	(15)	.071	.128	.1557	50.2
21	(-5)	.071	.076	.1946	67.6
22	(-10)	.071	.071	.1266	111.3
19A	(-15)	.071	.100	.0796	125.6

TABLE II (concld)

(d) Cruciform Vanes (Model #24, 25, 26, 27, 27A)

Vane Model No.	Armlength r_n(m)	Damping Ratio, ξ	Frequency Ratio, f_n/U (cycles/m)	Response Length, $U/f_n\xi$(m)
24 +	.251	.105	.1266	75.2
24 x	.251	.102	.1186	82.7
25 +	.251	.108	.1150	80.5
25 x	.251	.104	.1087	88.5
26 +	.251	.119	.1311	64.1
26 x	.251	.121	.1243	66.5
27 +	.251	.129	.1288	60.2
27 x	.251	.126	.1212	65.5
27A +	.251	.132	.1302	58.2
27A x	.251	.129	.1198	64.7
24 +	.094	.075	.1892	70.5
24 x	.094	.075	.1848	72.2
25 +	.056	.078	.1860	68.9
25 x	.056	.071	.1776	79.3
26 +	.122	.102	.1946	50.4
26 x	.122	.102	.1821	53.8
27 +	.086	.097	.1812	56.9
27 x	.086	.092	.1803	60.3
27A +	.068	.096	.2045	50.9
27A x	.068	.093	.1960	54.9

NOTE: Symbol + or x shows relative orientation of vane surfaces.

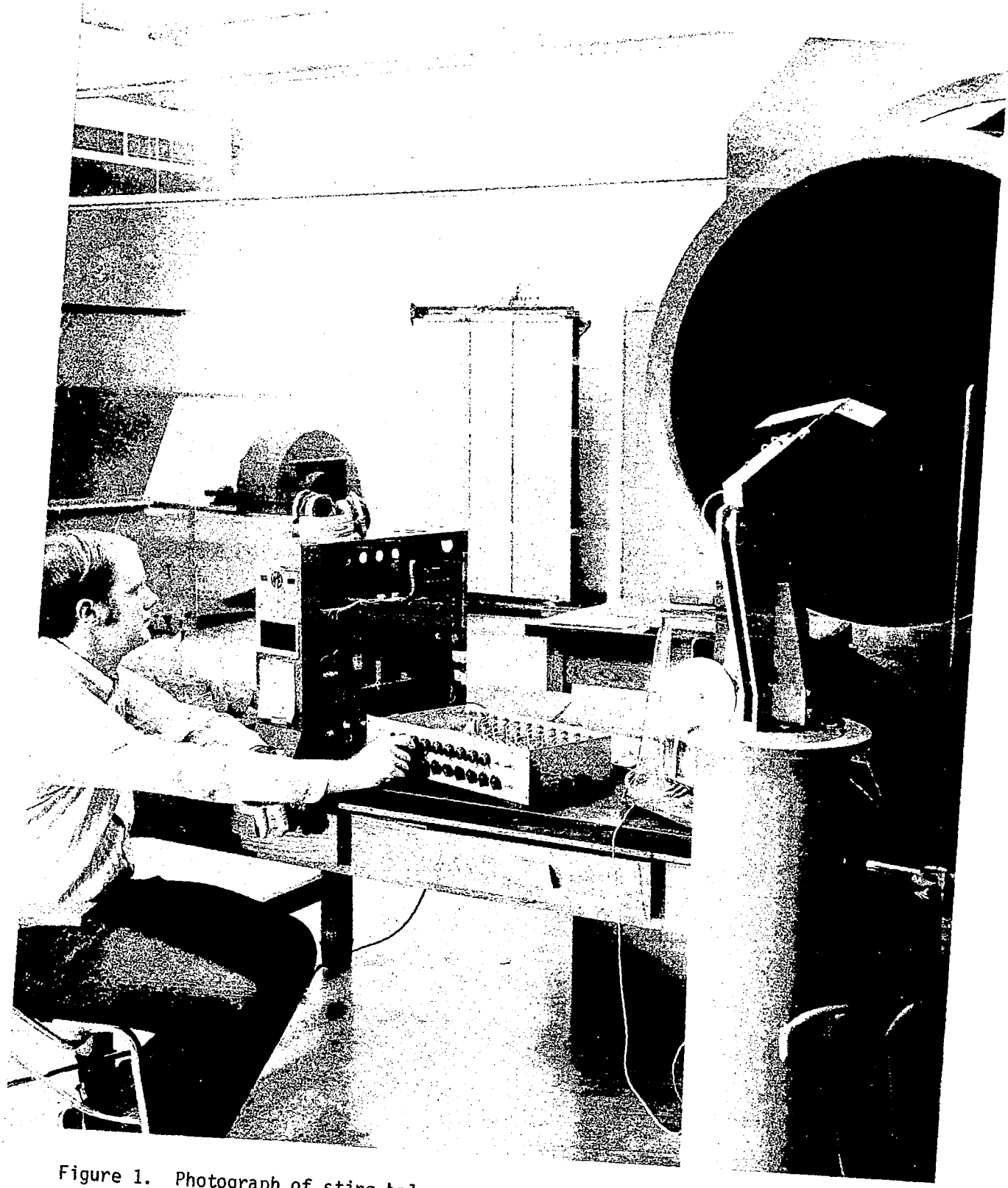

Figure 1. Photograph of sting-balance support-system set up to measure lift and drag located in front of open end wind tunnel.

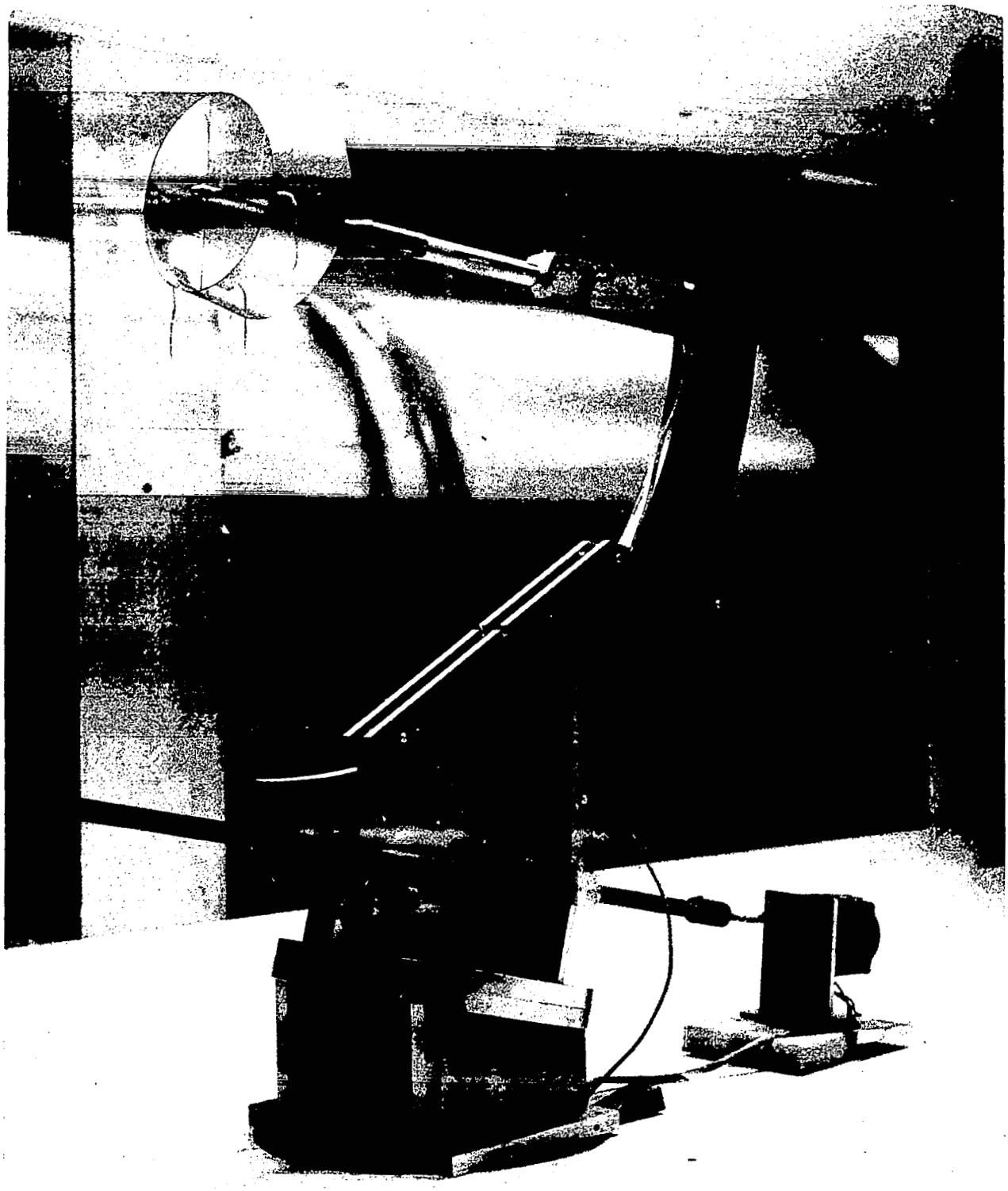

Figure 2. Sting balance located inside 3' x 4' closed wind tunnel.

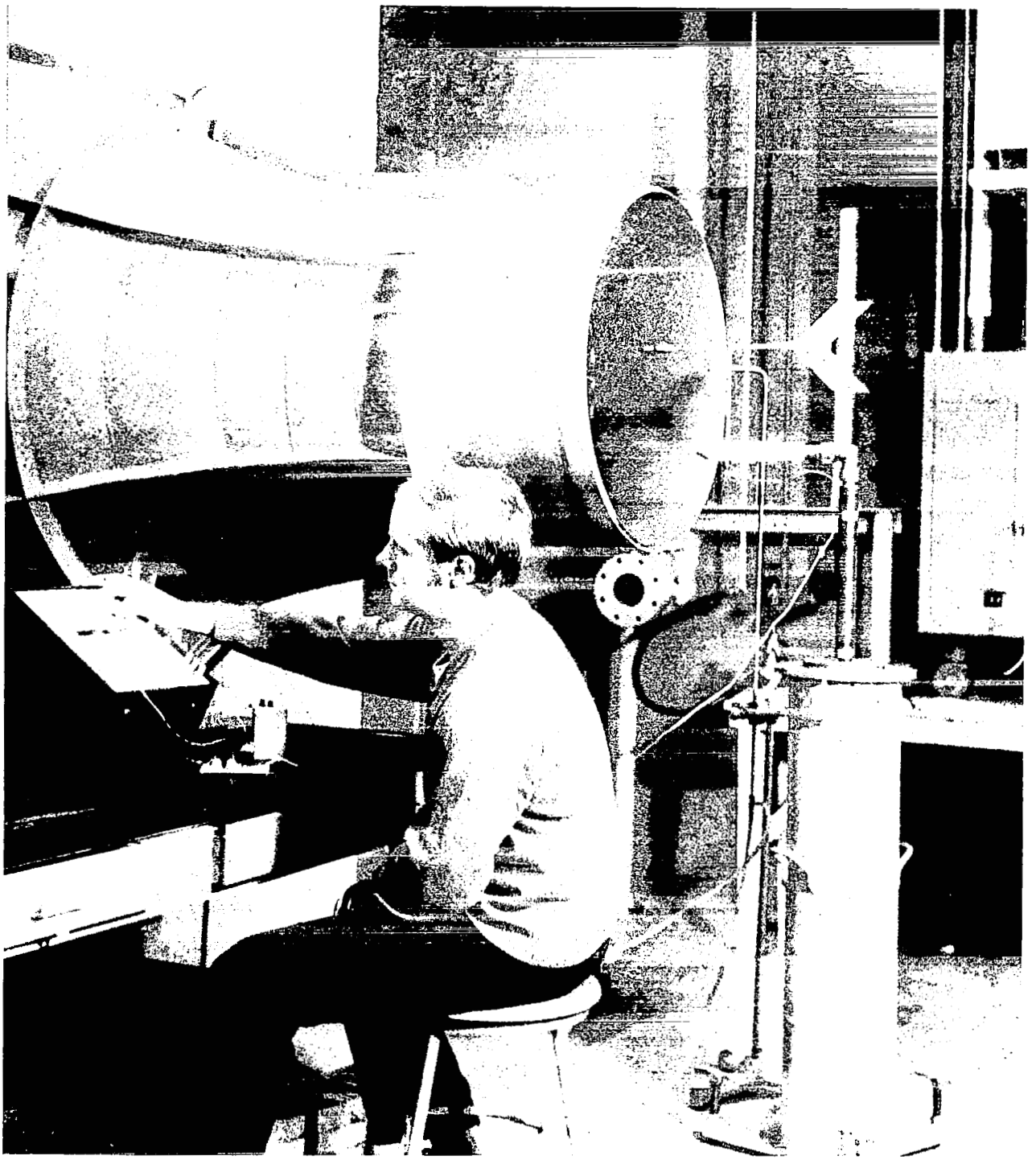

Figure 3. Apparatus set-up for measuring damping and frequency.

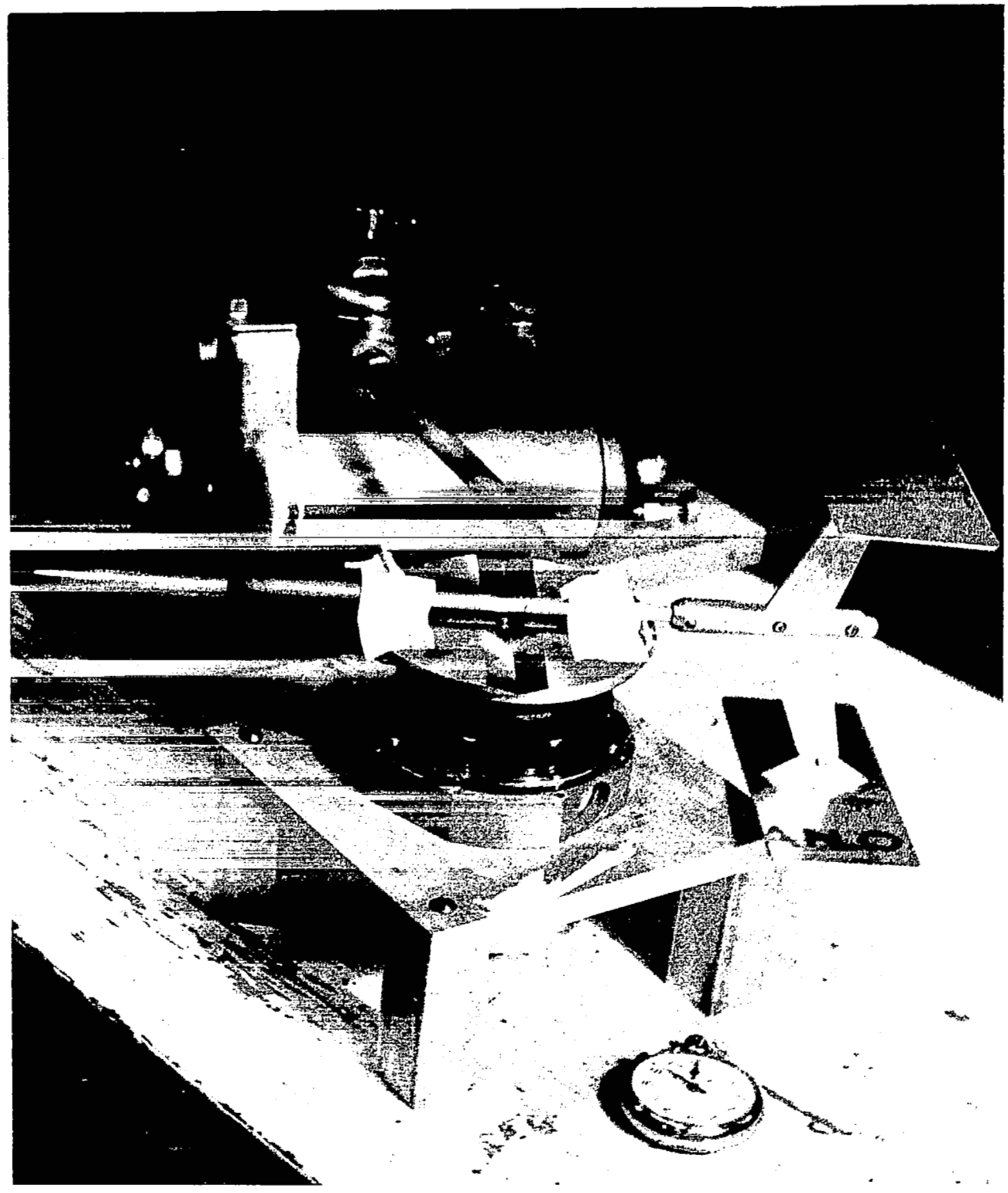

Figure 4. Oscillating turntable set-up for measuring moment of inertia.

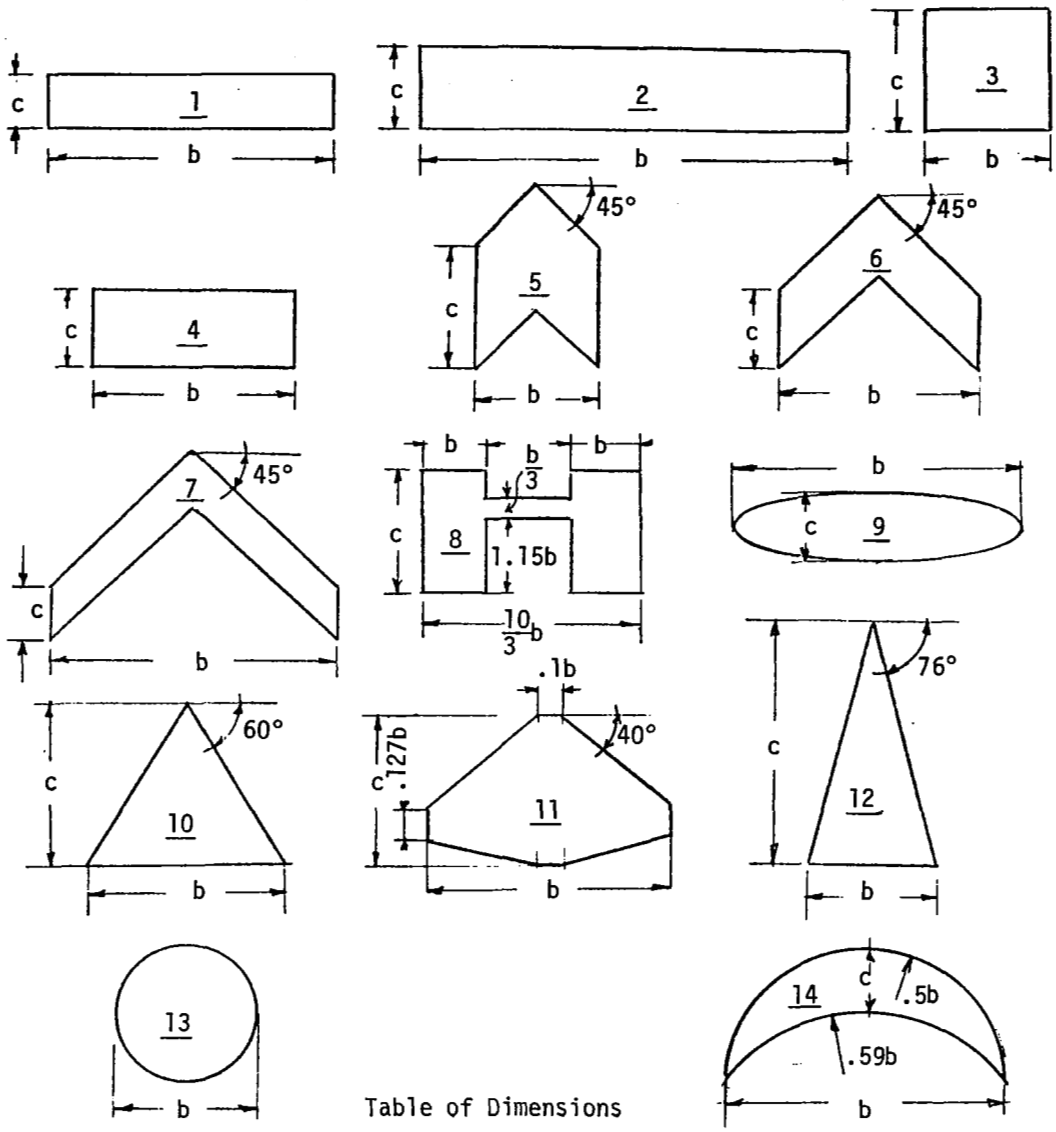

Table of Dimensions

Model	1	2	3	4	5	6	7	8	9	10	11	12	13	14
b ins	10	15	4.47	7.07	4.47	7.07	10	2.25	10	6.8	7.1	4.47	5.02	10
m	.254	.381	.113	.179	.113	.179	.254	.057	.254	.172	.180	.113	.127	.254
c ins	2	3	4.47	2.83	4.47	2.83	2	4.5	2.55	5.88	4.45	8.94	5.02	2.25
m	.051	.076	.113	.072	.113	.072	.051	.114	.065	.149	.113	.227	.127	.057
$\bar{c}$ ins	2	3	4.47	2.83	4.47	2.83	2	4.5	2.00	2.94	2.85	4.47	2.00	1.976
m	.051	.076	.113	.072	.113	.072	.051	.114	.051	.0747	.0725	.113	.051	.0503
AR	5	5	1	2.5	1	2.5	5	.5	5	2.23	2.5	1	1.27	5

(a) Numbers underlined inside configurations refer to the model numbers.

Figure 5. Test Wing Planforms of Flat Plates

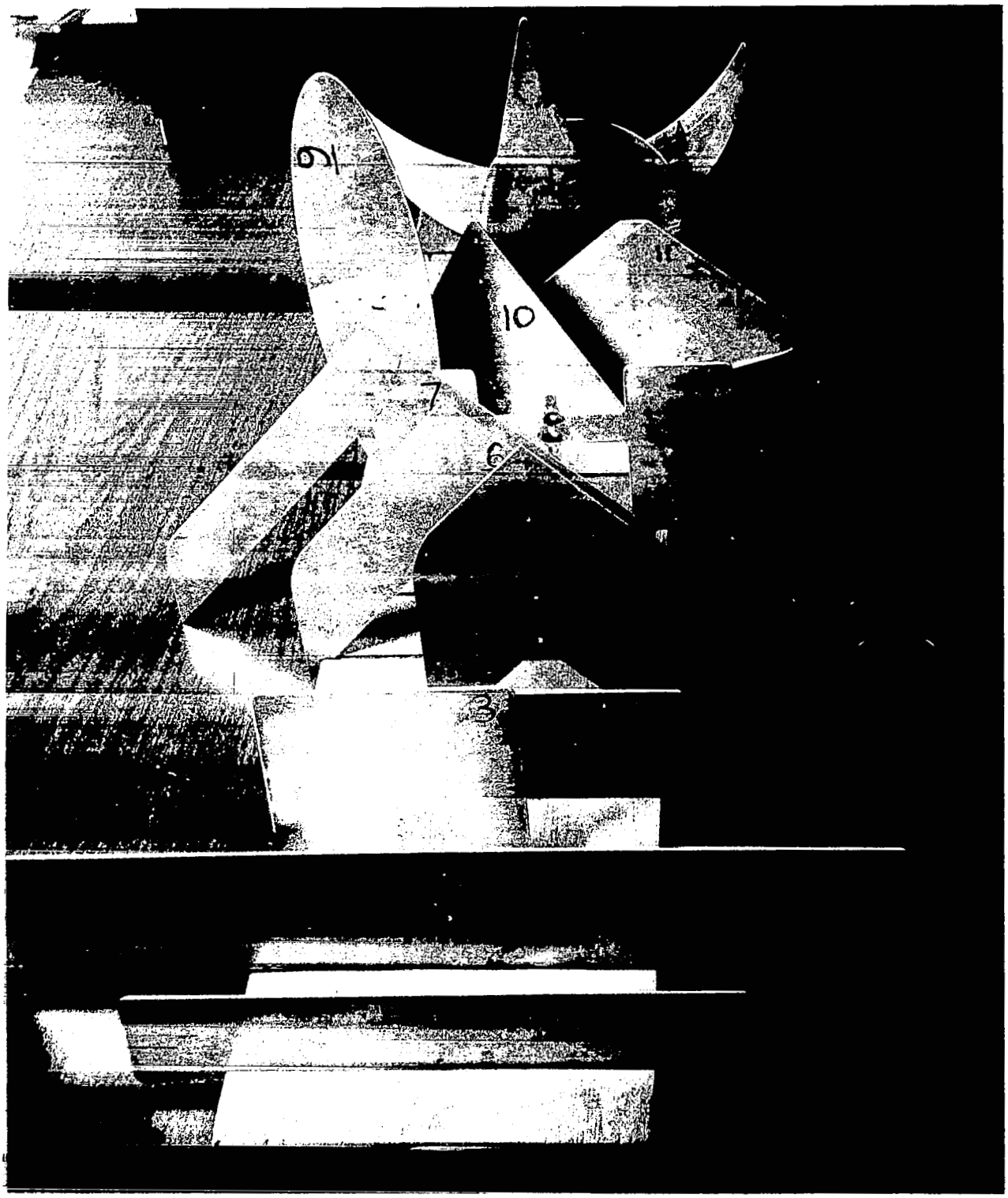

Figure 5(b). Photographs of flat plate vanes.

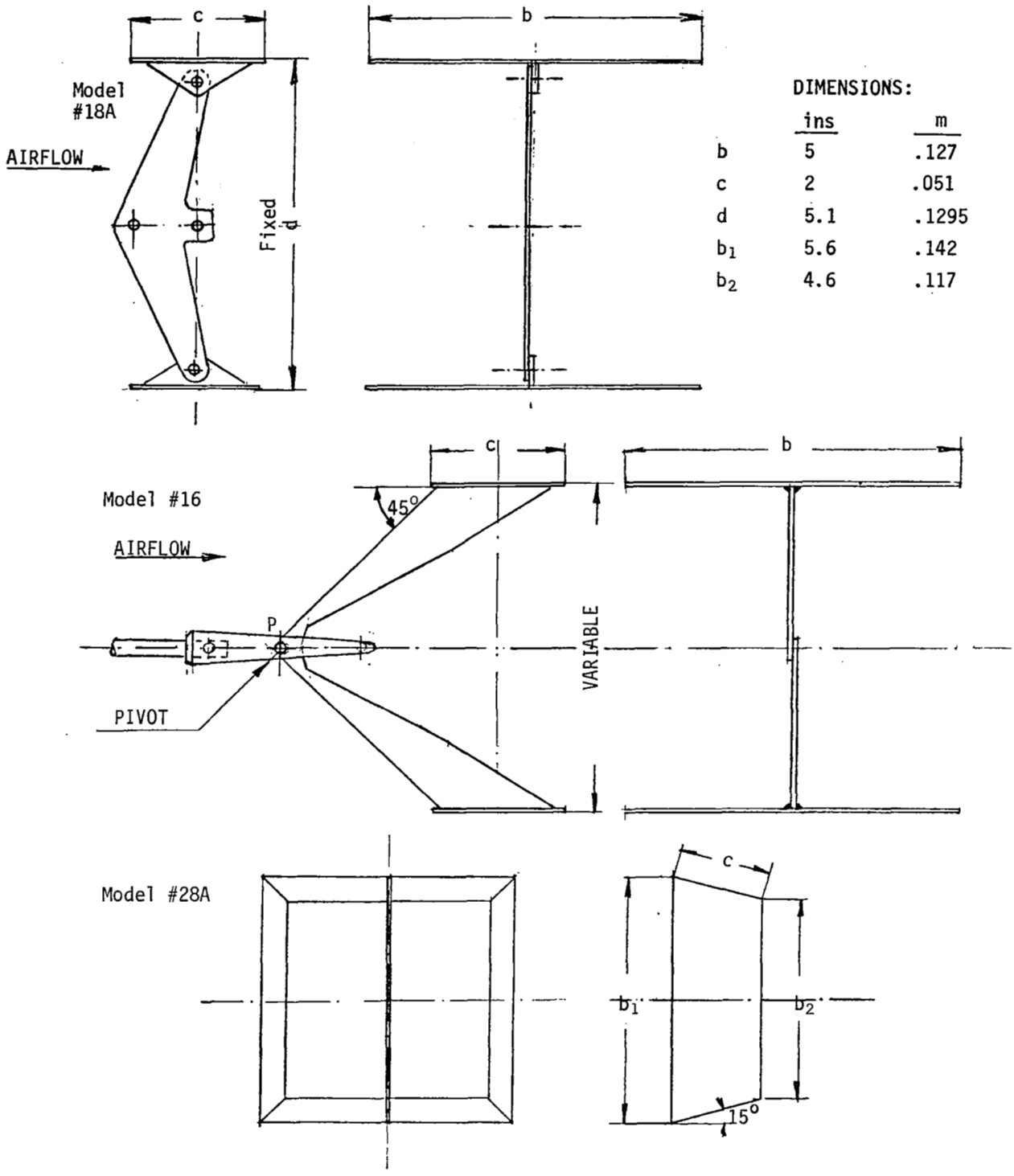

(a) Model Specifications

Figure 6. Design details of bivanes (18A, 16) and of the boxvane (28A)

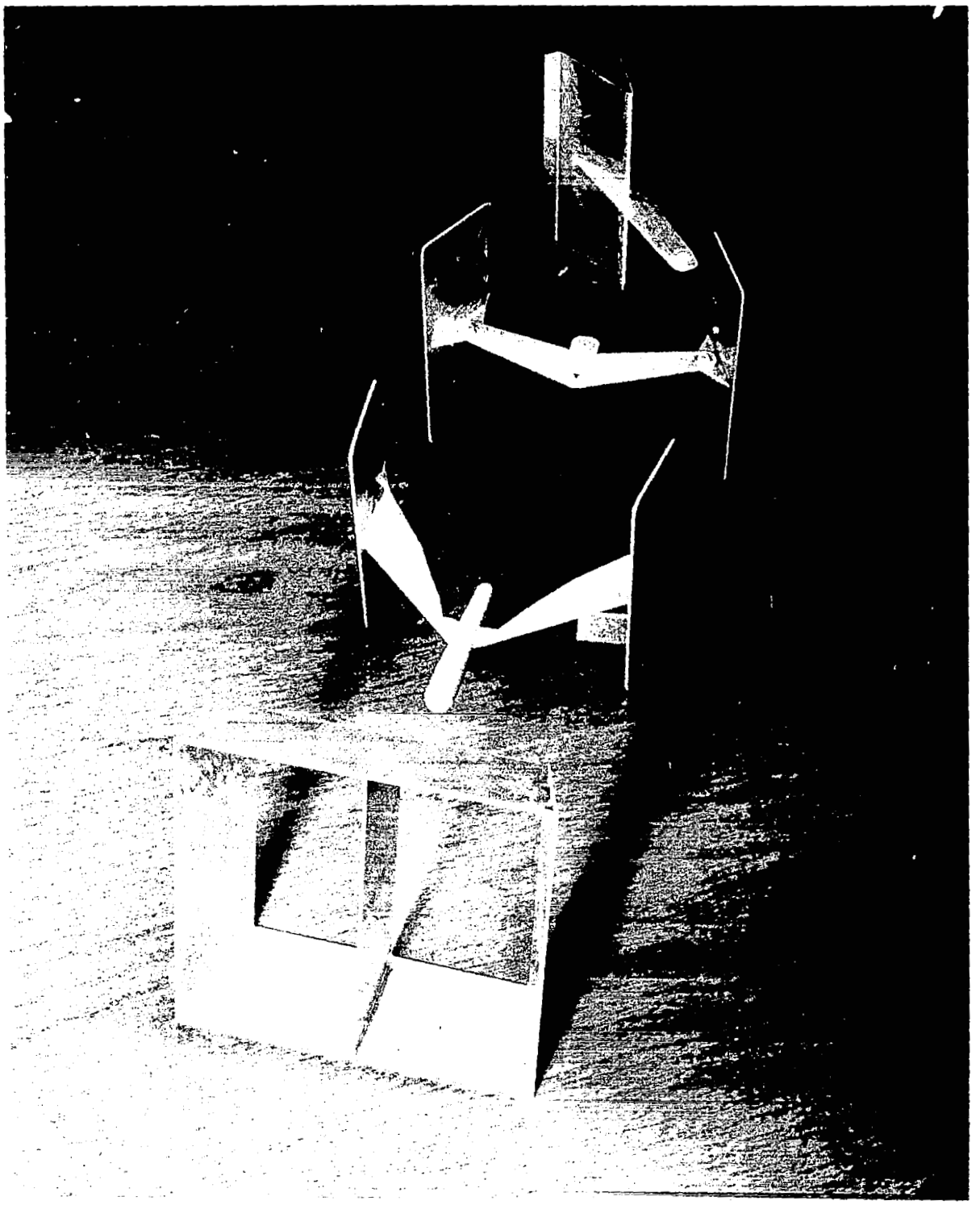

Figure 6(b). Photographic details of bivane models including a "V" vane and a "box" vane.

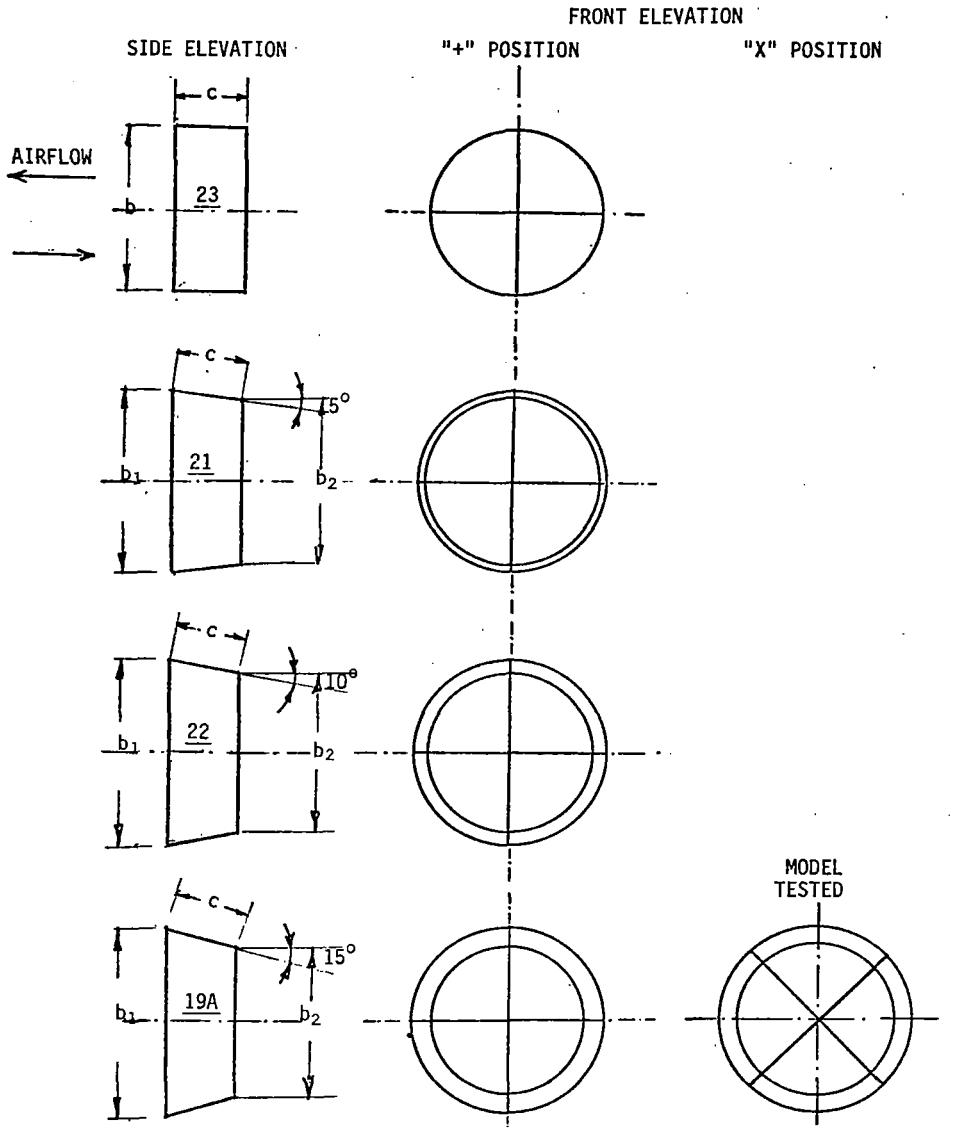

Model	23	21	22	19A
b_1 ins	5	5.4	5.5	5.5
m	.127	.137	.140	.140
b_2 ins	5	5	4.8	4.5
m	.127	.127	.122	.114

(a) Side and Front Elevation

Figure 7. Details of Cone-Vane Models.

Figure 7(b). Photographic details of cone vane models.

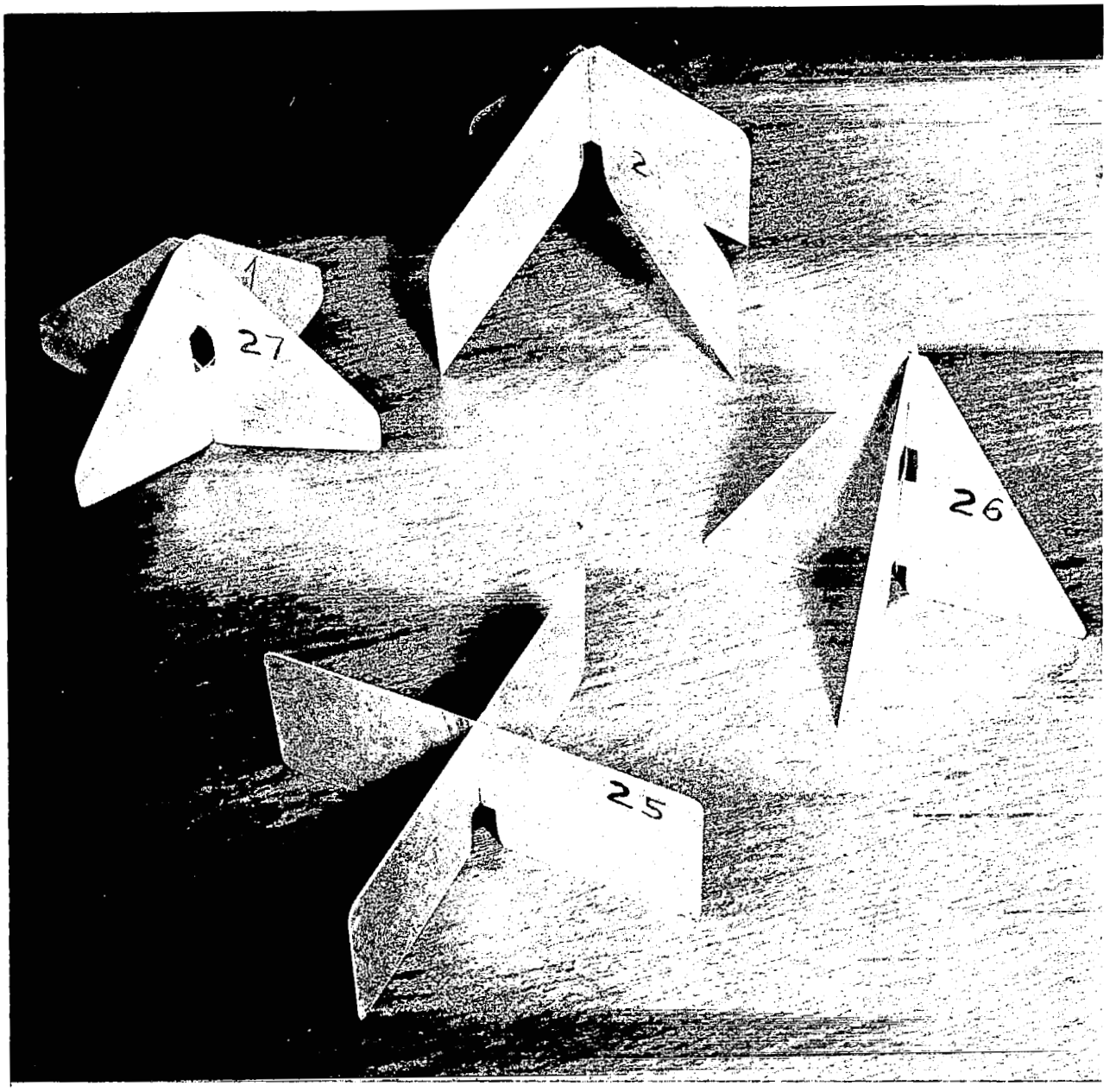

Figure 8. Photographs of cruciform vane models.

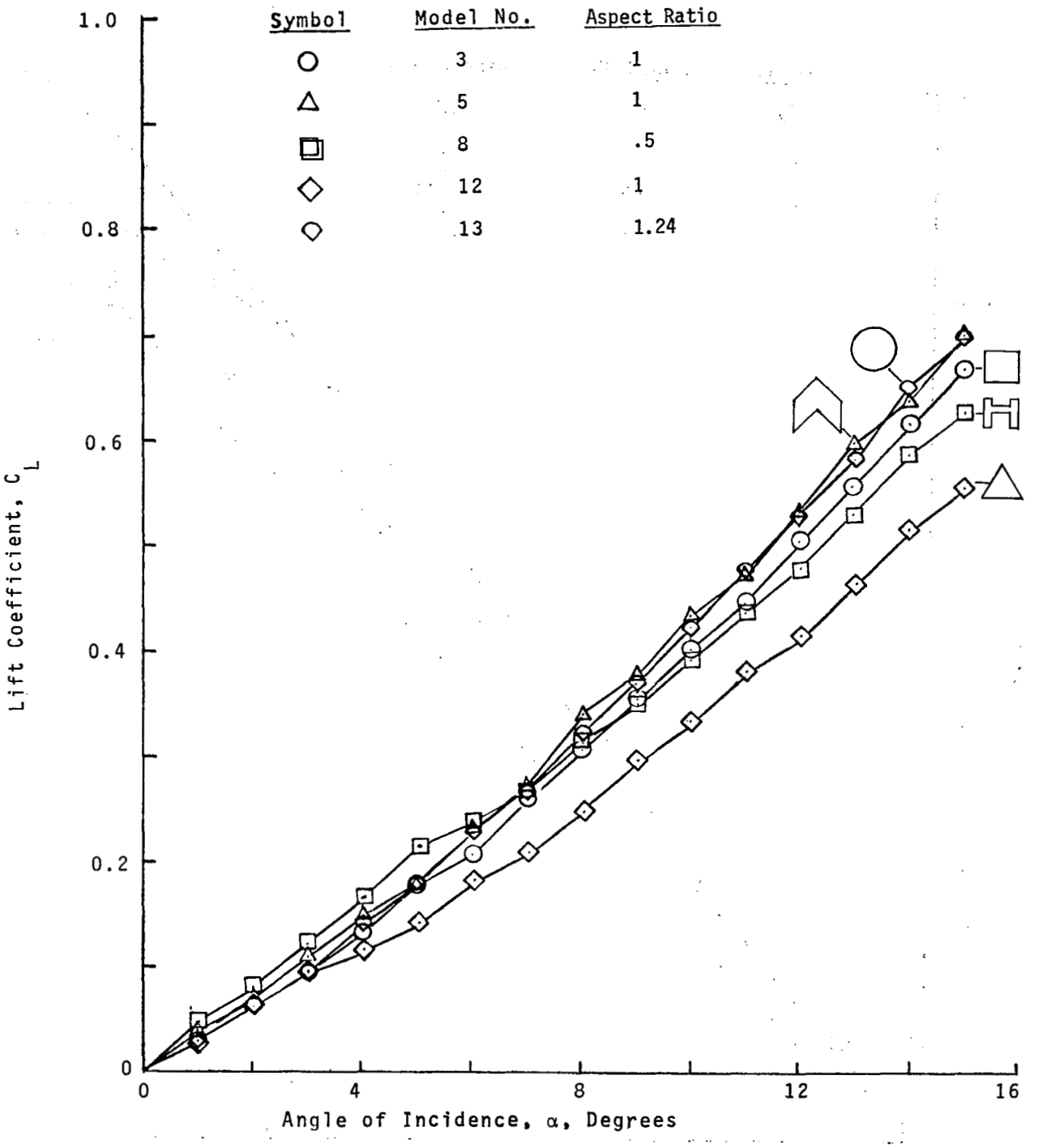

(a) Results on Models 3, 5, 8, 12, 13

Figure 9. - Variation of Lift with Incidence of Flat Plate Models

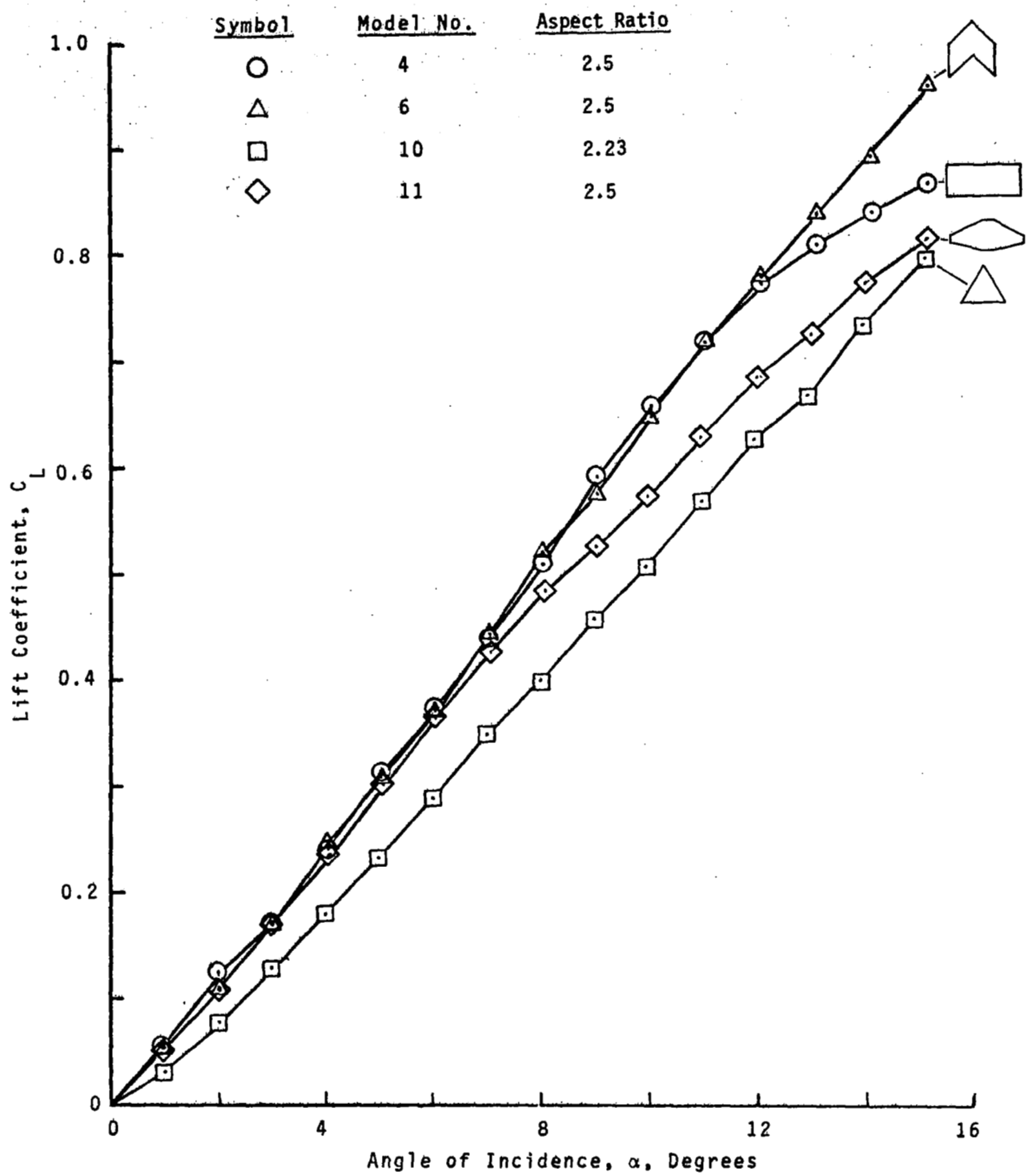

(b) Results of Models 4, 6, 10, 11

Figure 9. - Continued

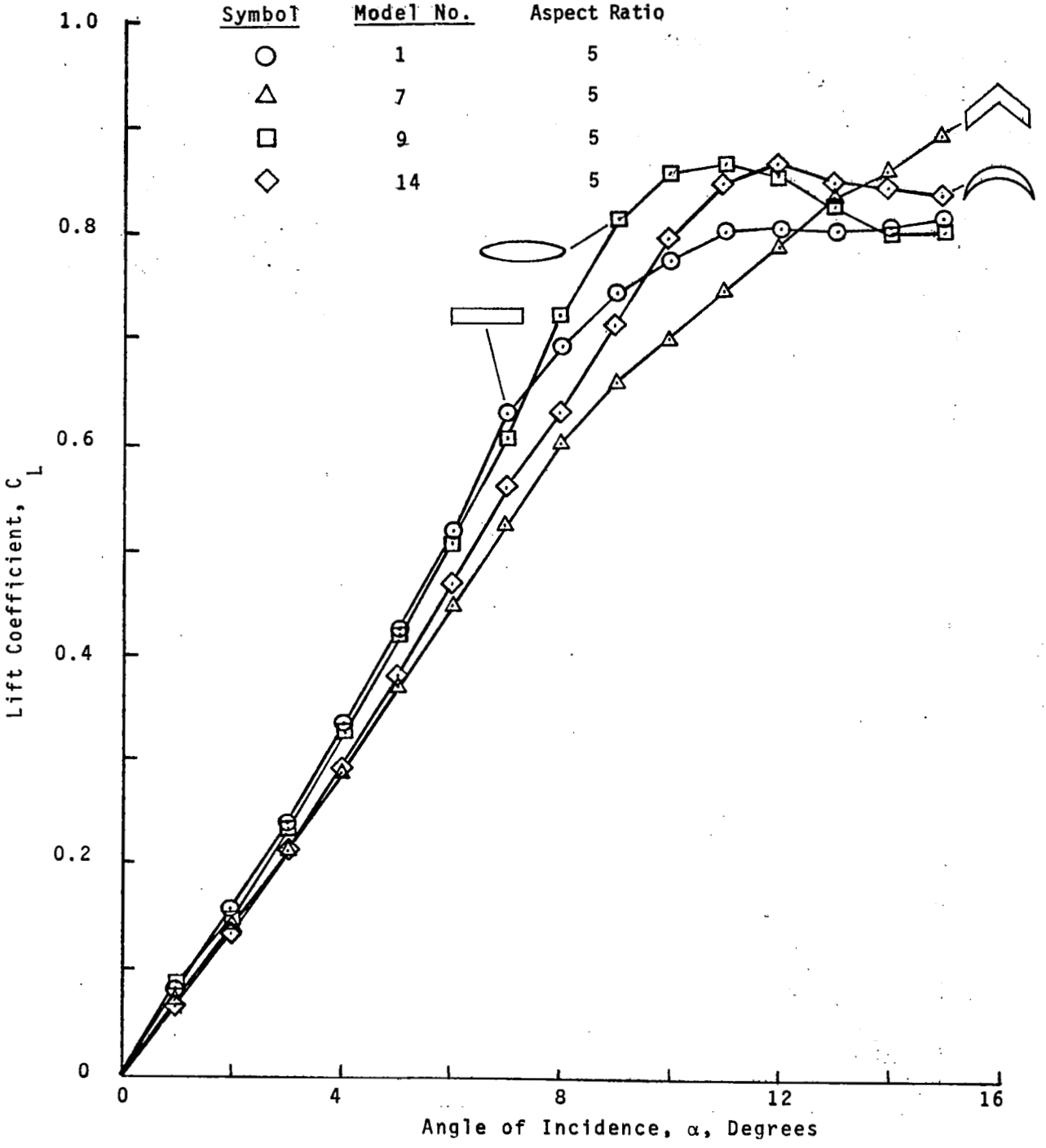

(c) Results on Models 1, 7, 9, 14

Figure 9. - Concluded

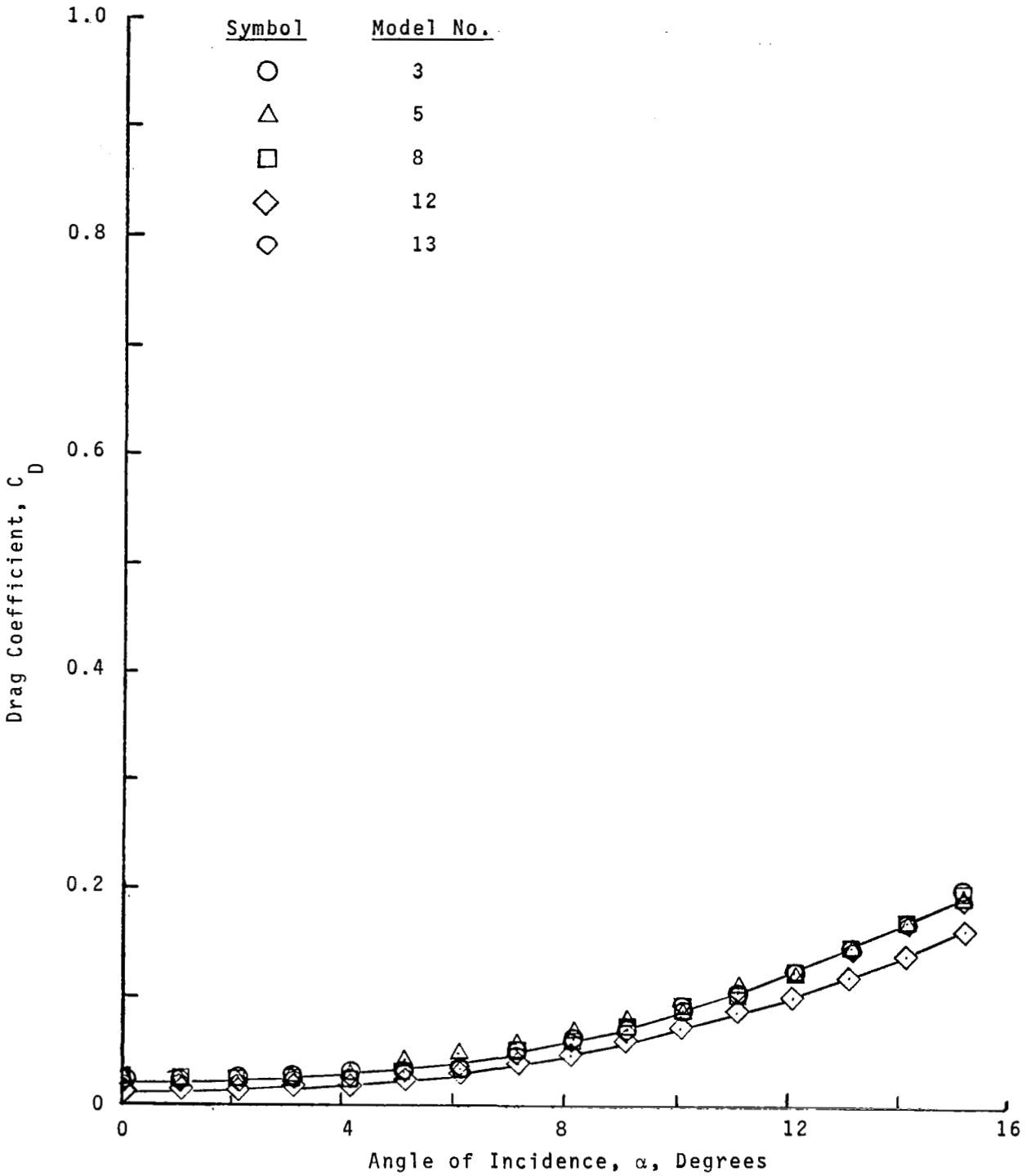

(a) Results on Models 3, 5, 8, 12, 13

Figure 10. - Variation of Drag with Incidence of Flat Plate Models

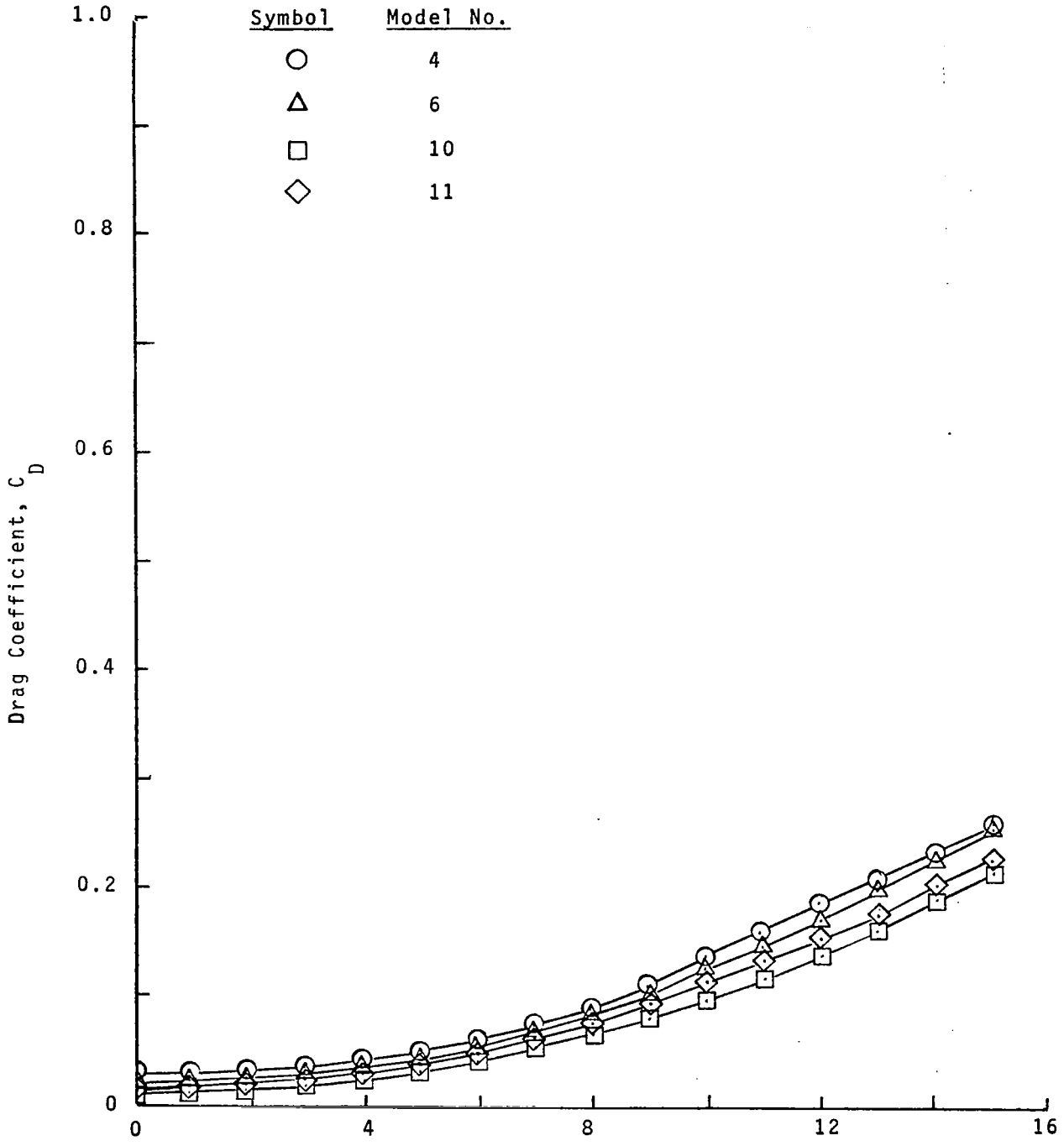

(b) Results on Models 4, 6, 10, 11

Figure 10. - Continued

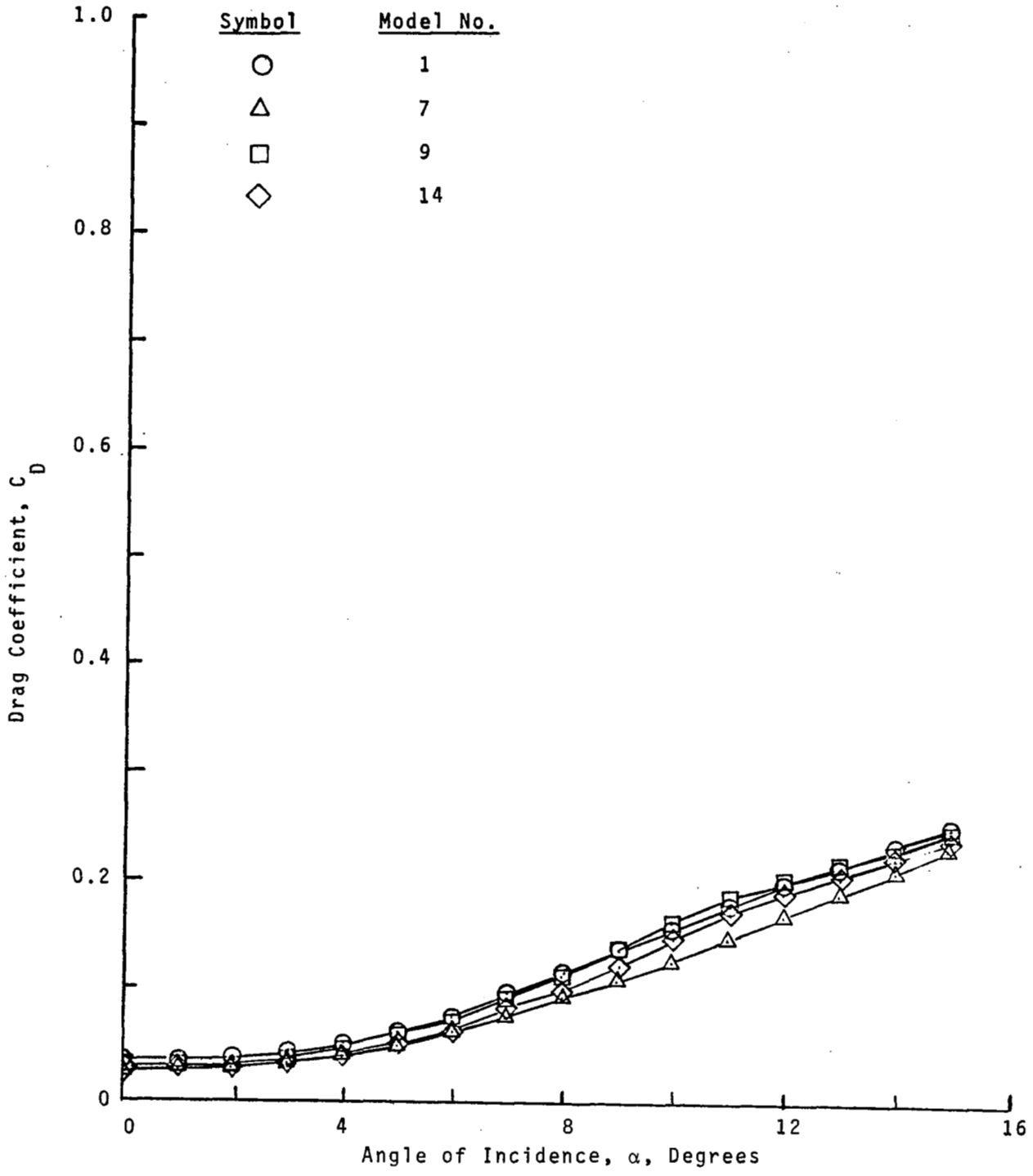

(c) Results on Models 1, 7, 9, 14

Figure 10. - Concluded

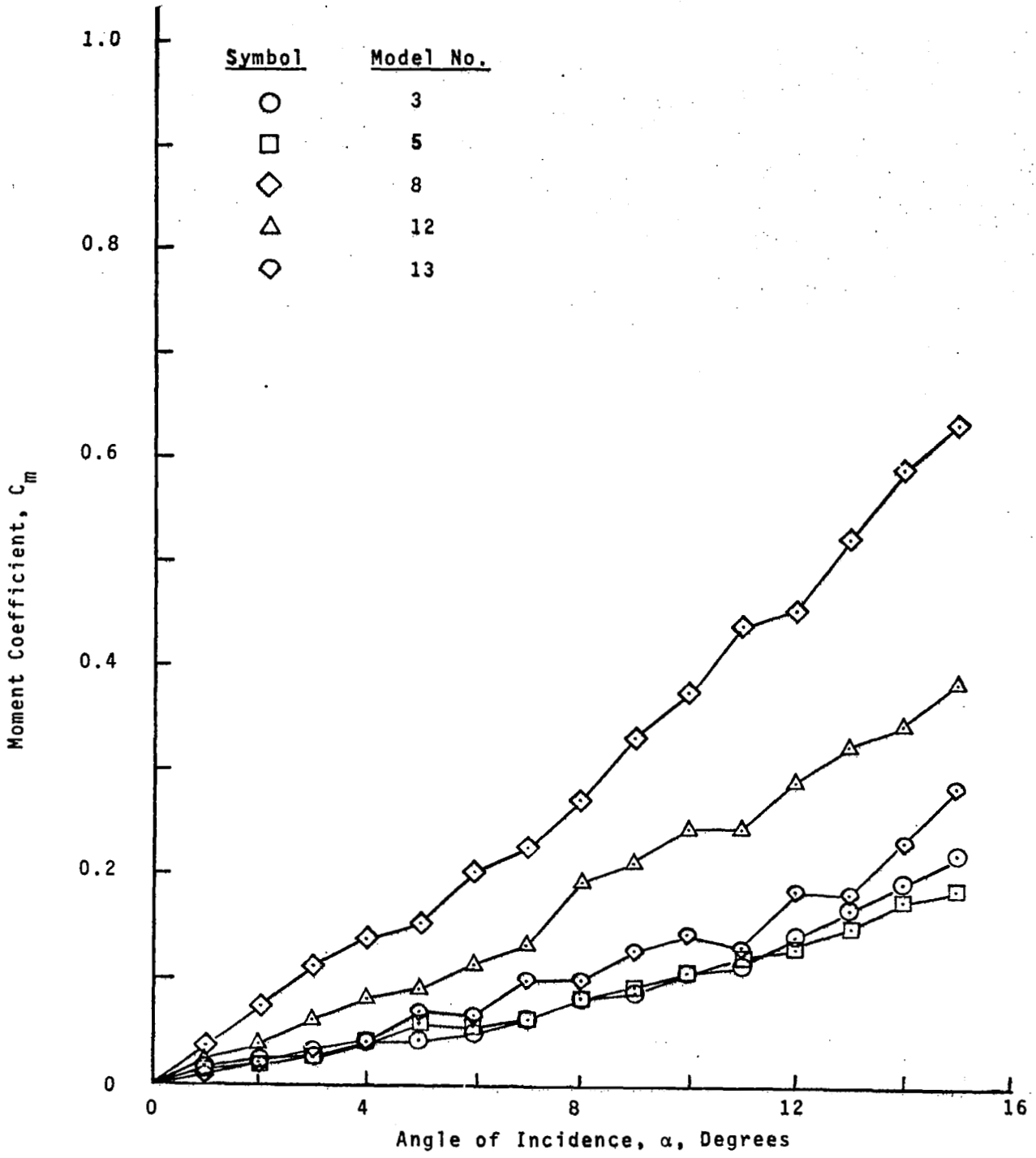

(a) Results on Models 3, 5, 8, 12, 13

Figure 11. - Variation of Moment Coefficient with Incidence for Flat Plate Models

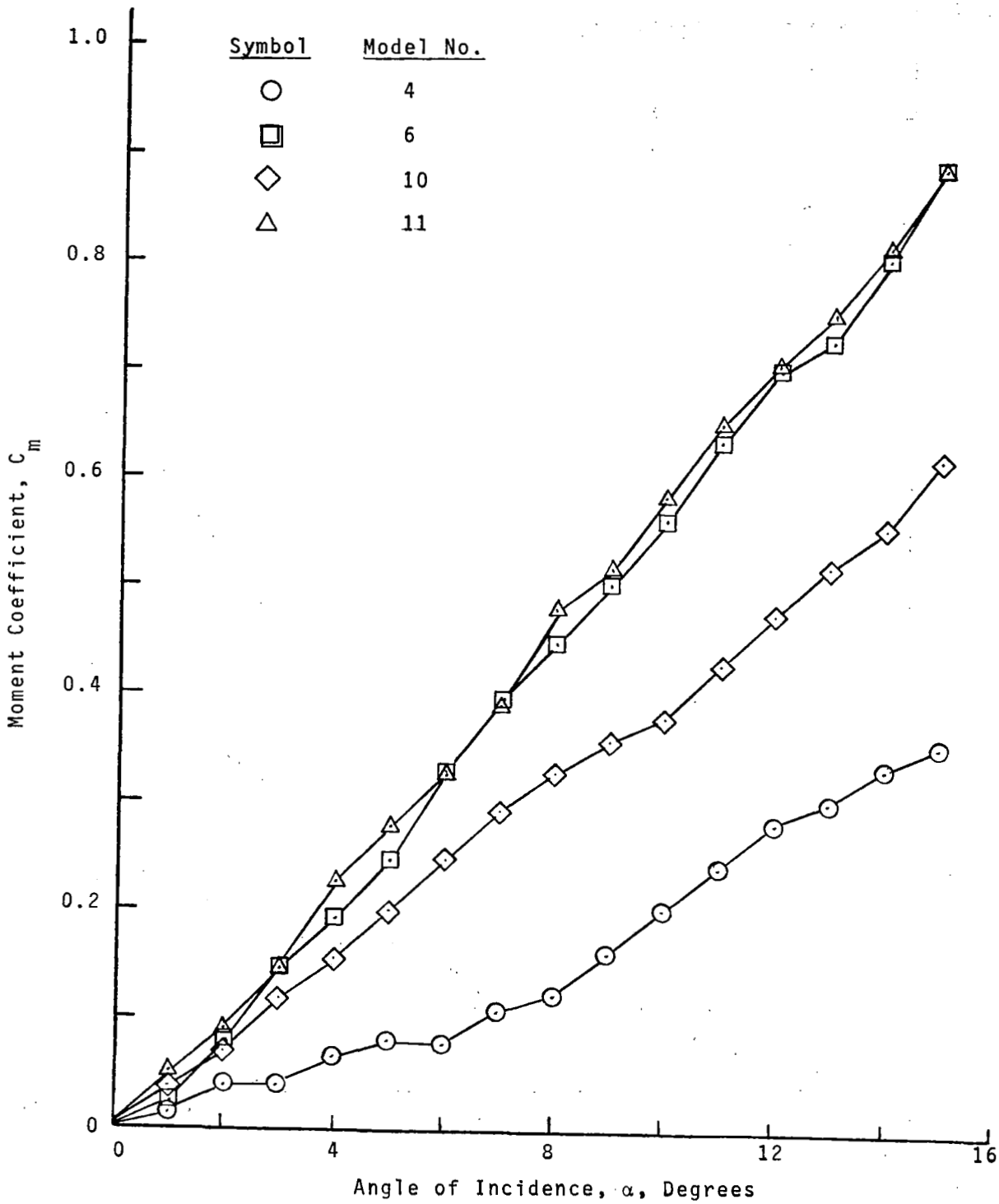

(b) Results on Models 4, 6, 10, 11

Figure 11. - Continued

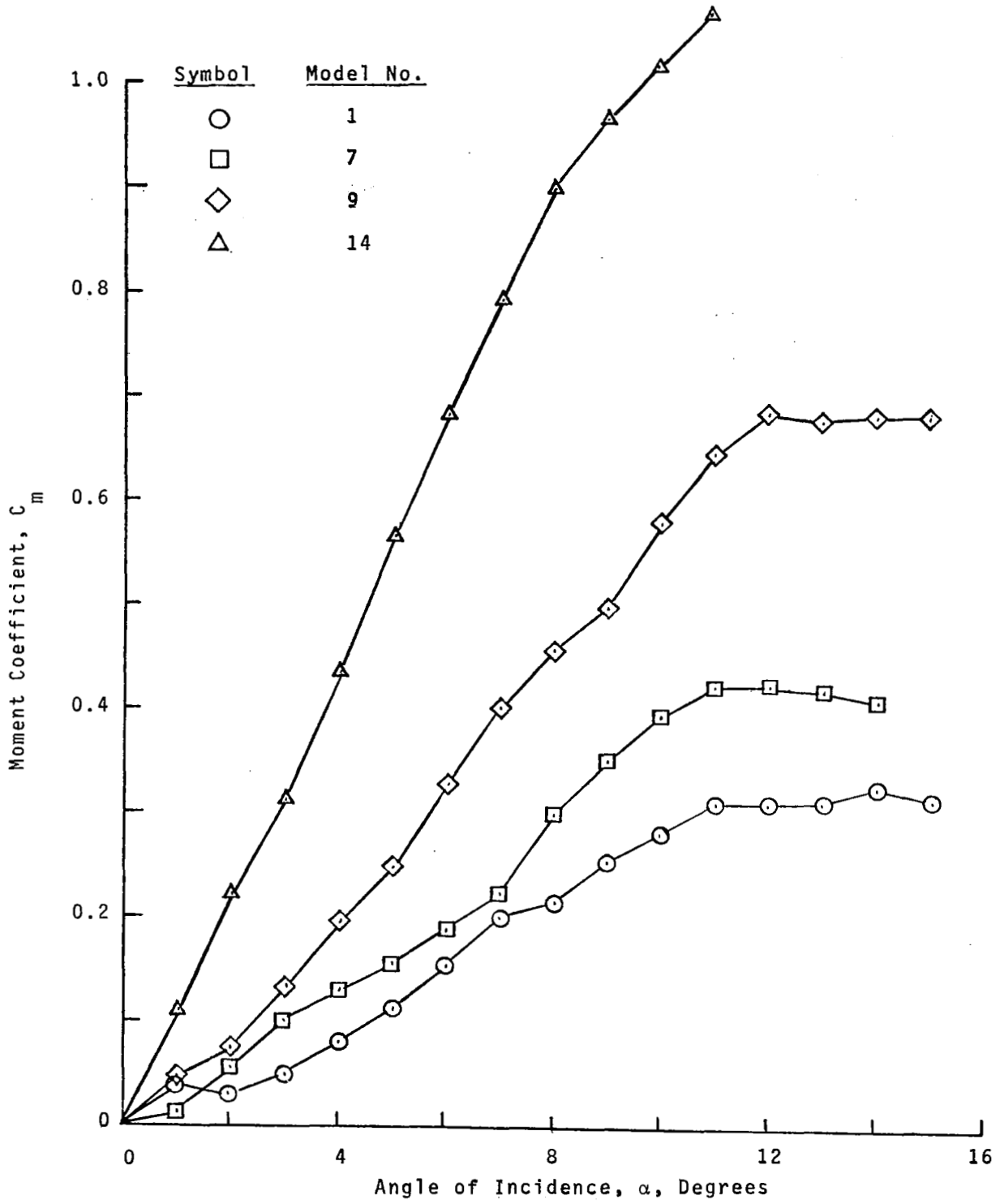

(c) Results on Models 1, 7, 9, 14

Figure 11. - Concluded

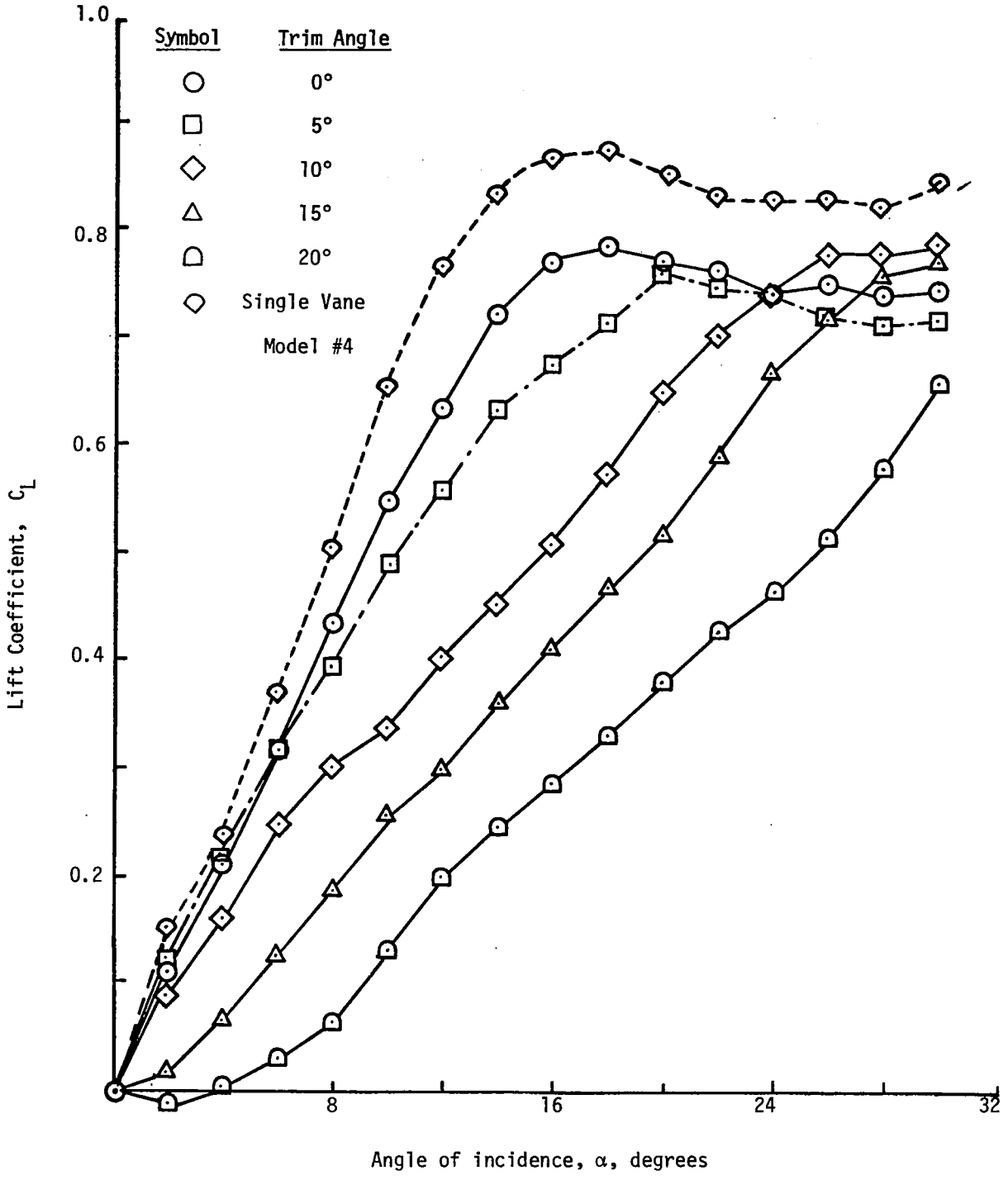

(a) Positive trim angle $+\phi$

Figure 12. Variation of lift with incidence and trim angle for bivanes with variable distance between vanes. Model 16.

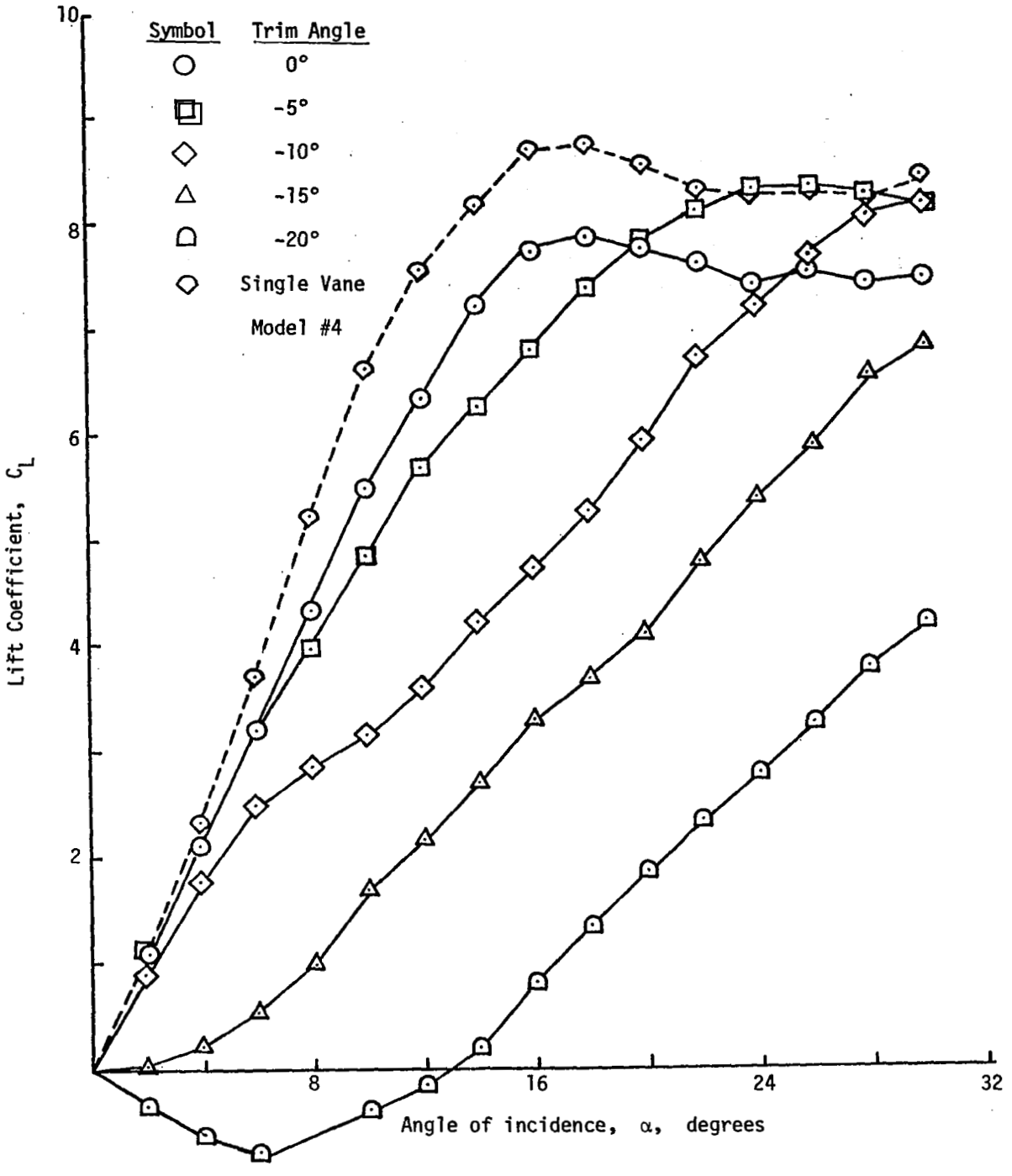

(b) Negative trim angle - ϕ

Figure 12. - Concluded

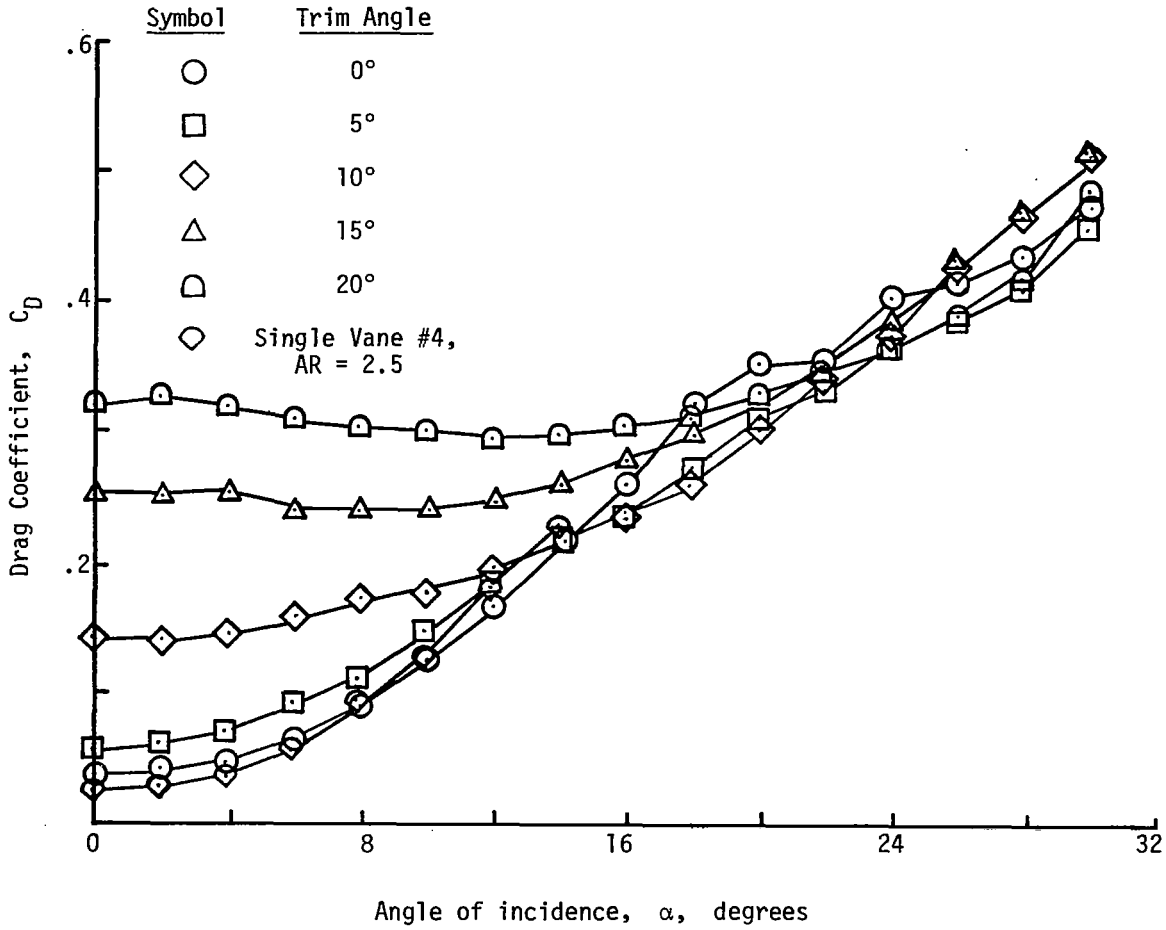

(a) Positive trim angle $+\phi$

Figure 13. Variation of drag with incidence and trim angle for bivanes with variable distance between vanes. Model 16.

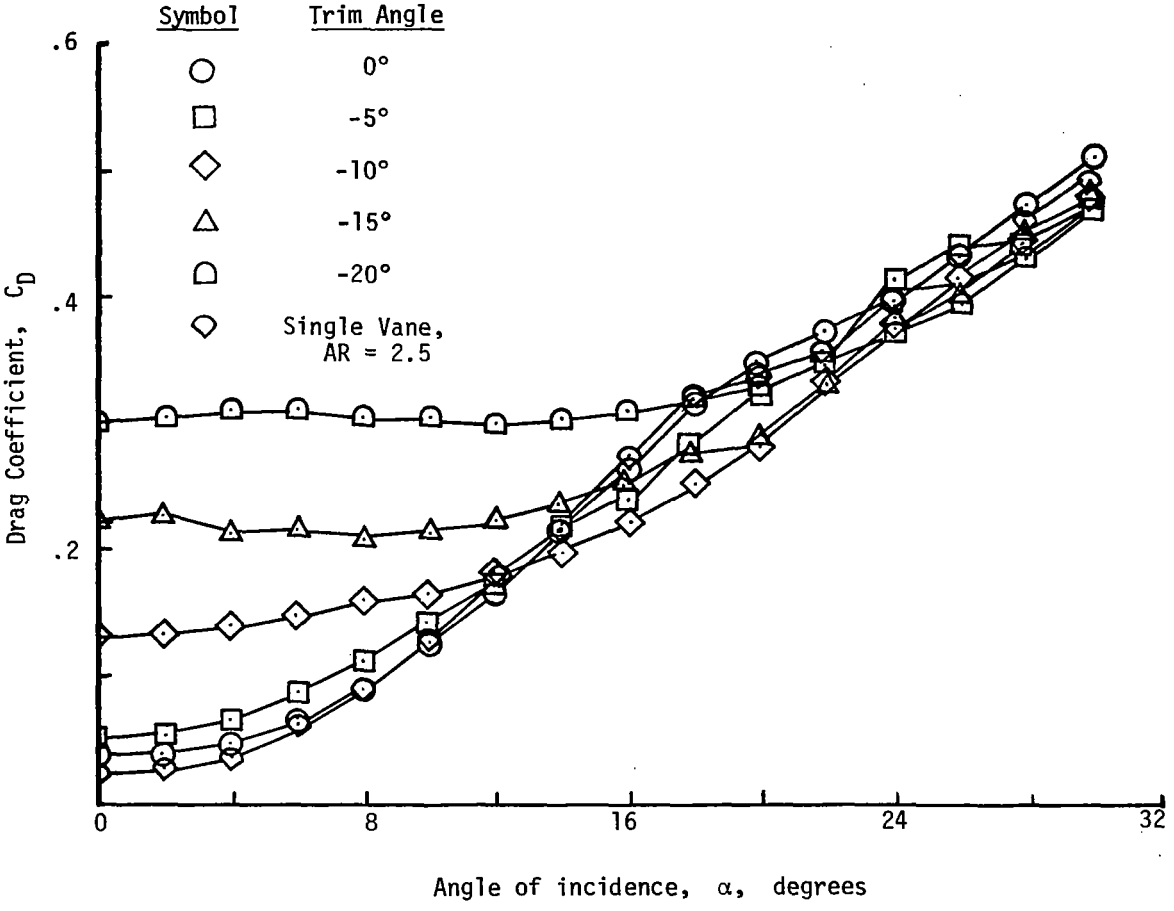

(b) Negative Trim angle $-\phi$

Figure 13. - Concluded

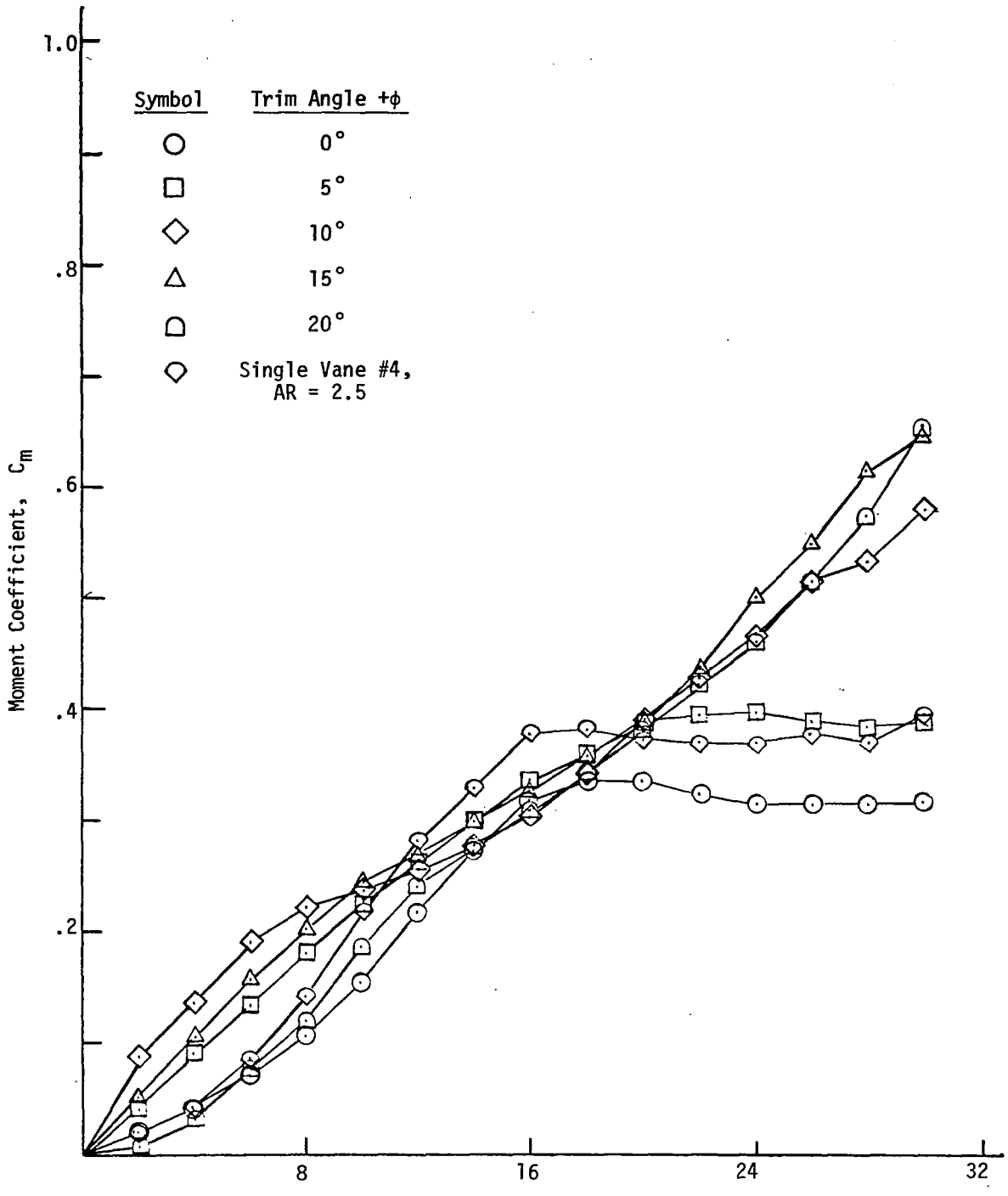

(a) Positive trim angle

Figure 14. Variation of moment coefficient with incidence and trim angle for bivanes with variable distance between vanes. Model 16.

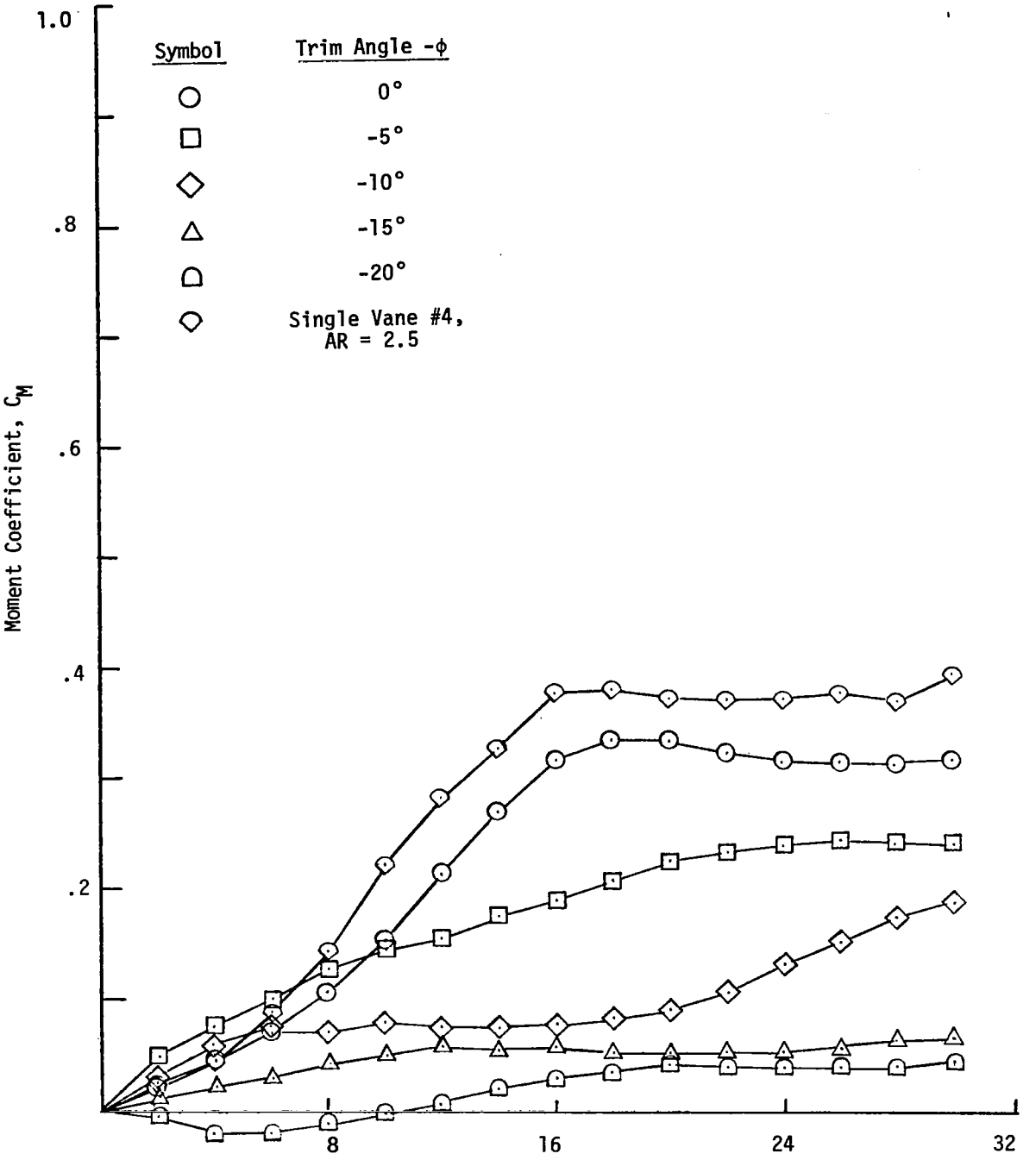

(b) Negative trim angle -ϕ

Figure 14. - Concluded

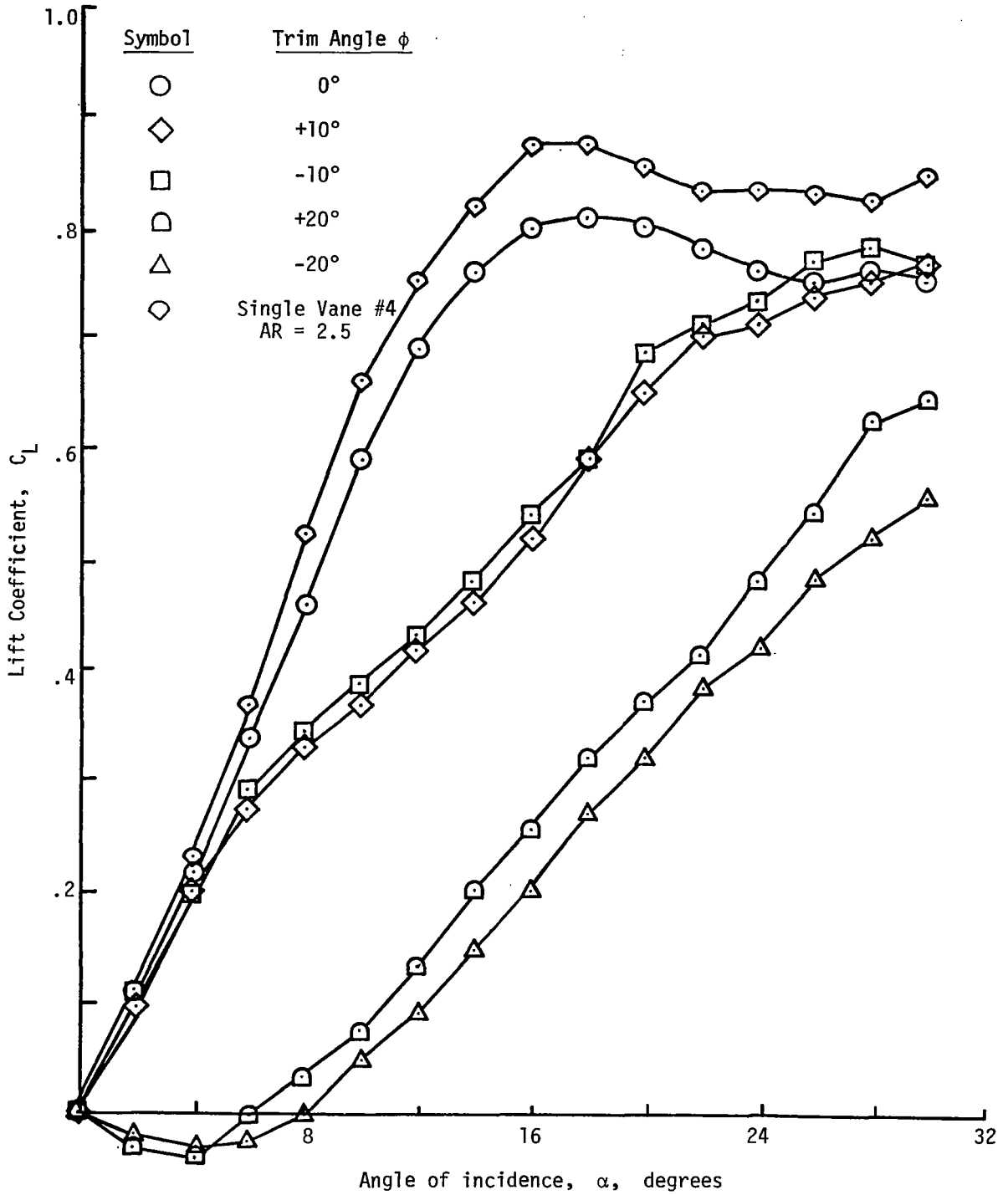

Comparative curves for positive and negative trim angles

Figure 15. Variation of lift with incidence and trim angle for bivanes with constant distance between vanes. Model 18.

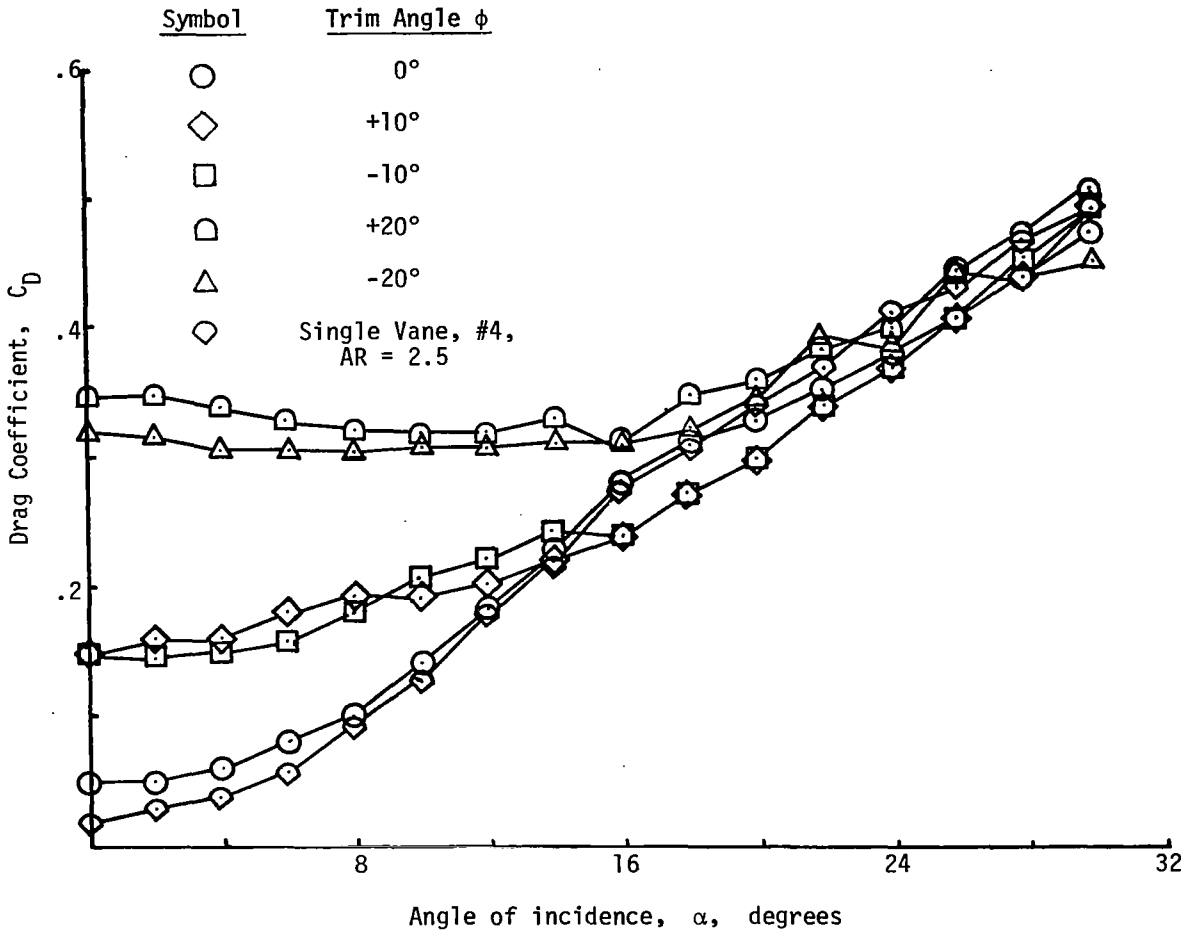

Comparative curves for positive and negative trim angles

Figure 16. Variation of drag with incidence and trim angle for bivanes with constant distance between vanes. Model 18.

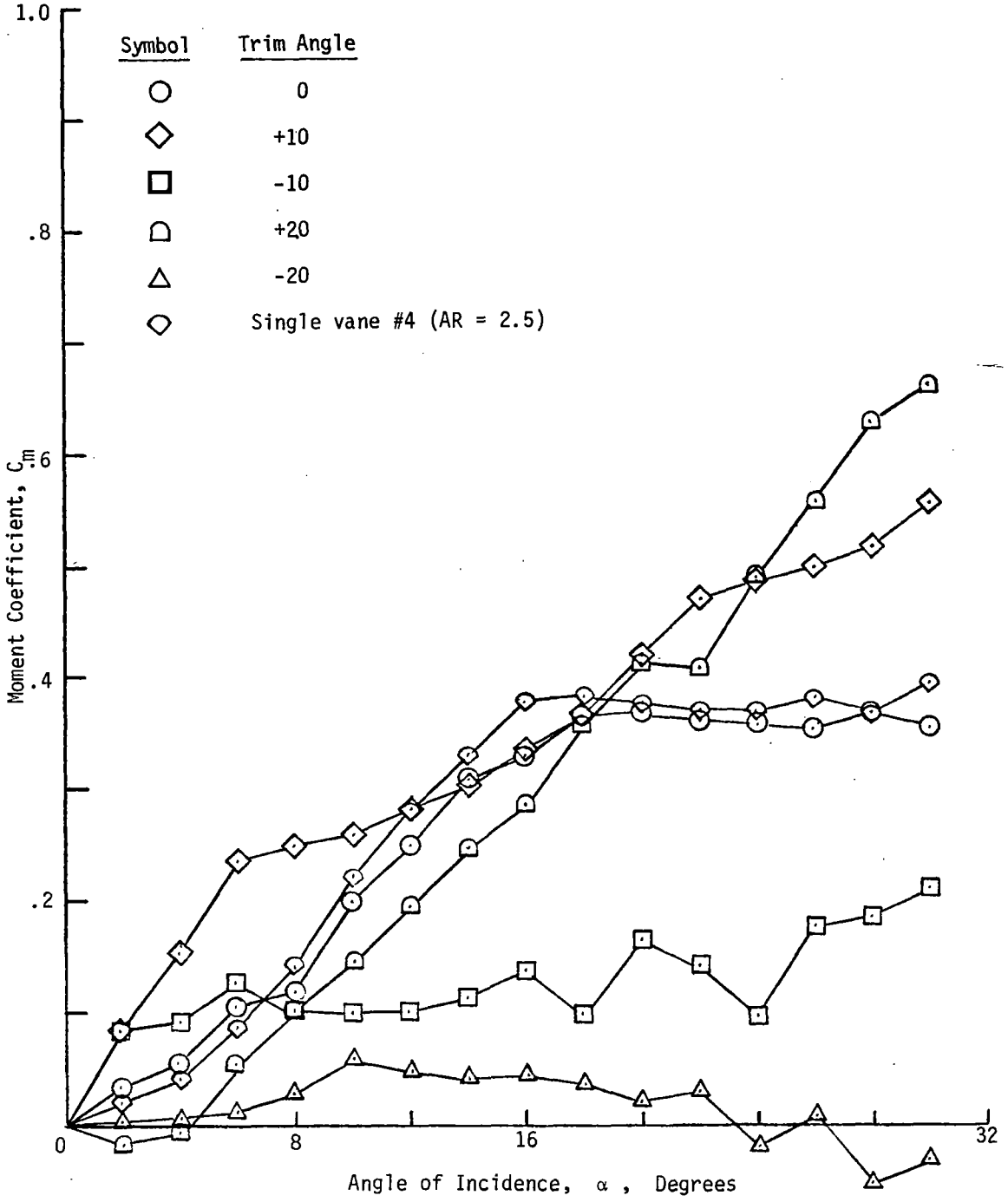

Figure 17. Variation of moment coefficient with incidence and trim angle for bivanes with constant distance between vanes. Model 18.

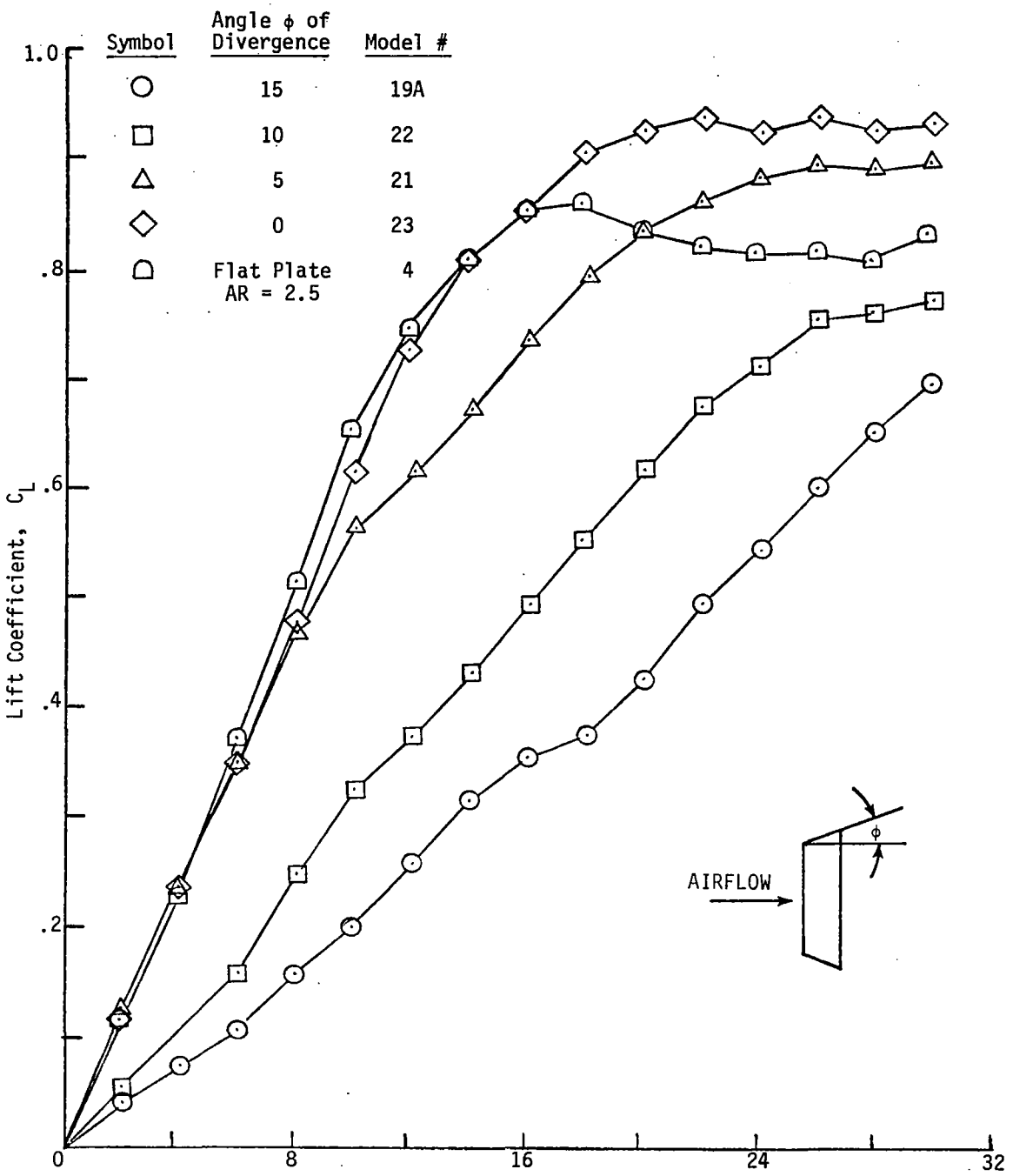

(a) Diverging Cones

Figure 18. Variation of lift with incidence and angle of divergence for conical vanes.

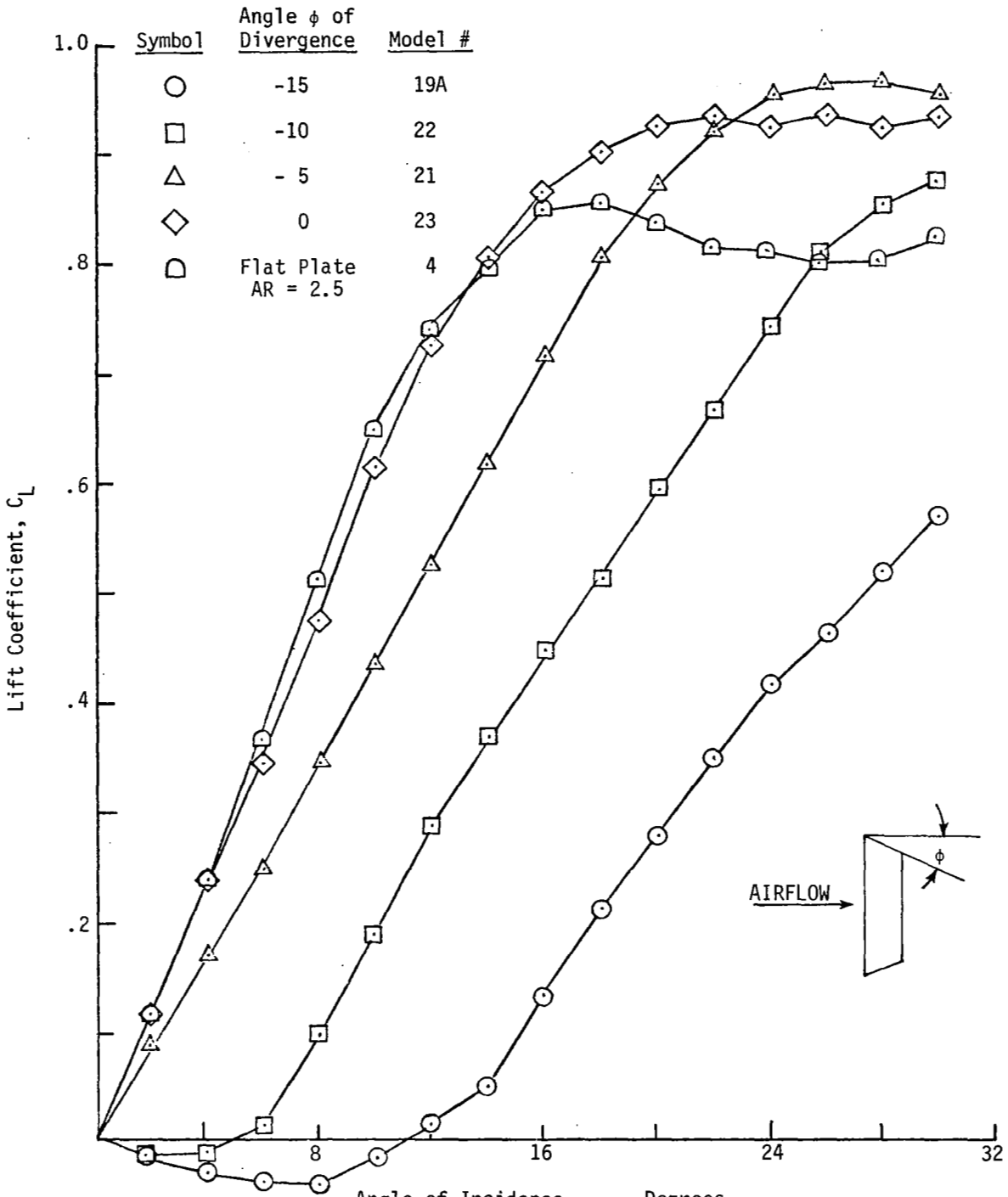

(b) Converging Cones

Figure 18. - Concluded

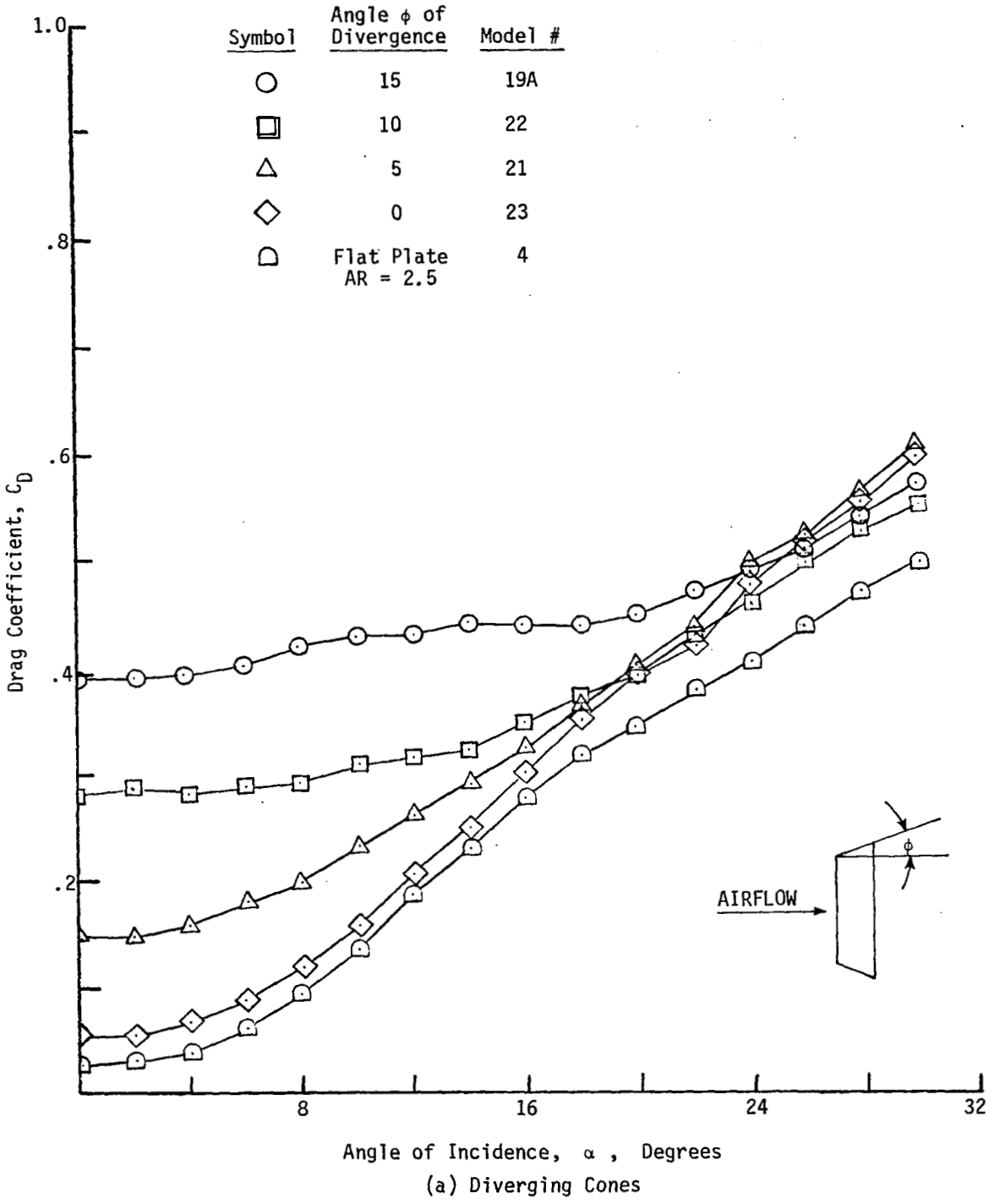

Figure 19. Variation of drag with incidence and angle of divergence for conical vanes.

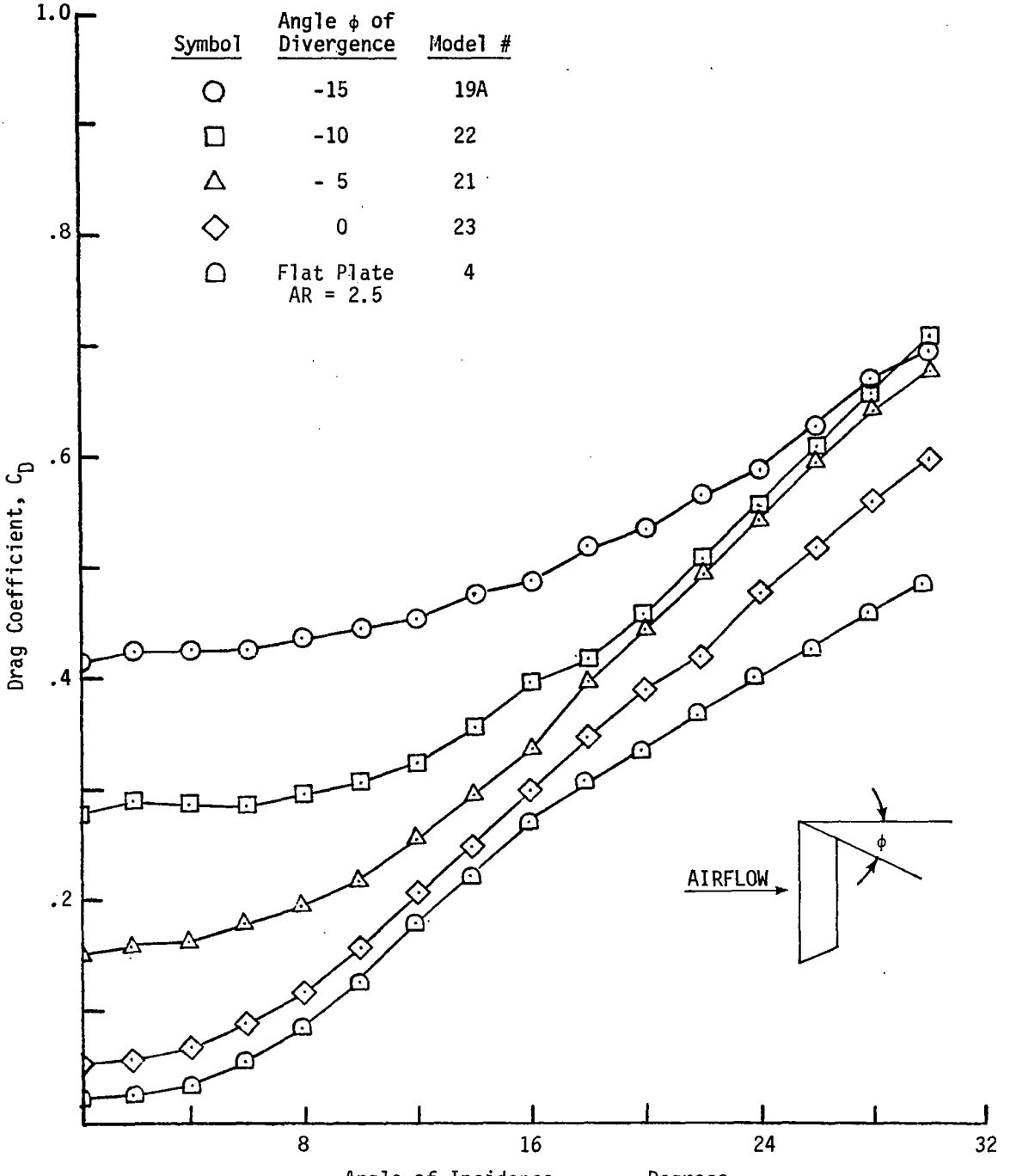

(b) Converging Cones

Figure 19. - Concluded

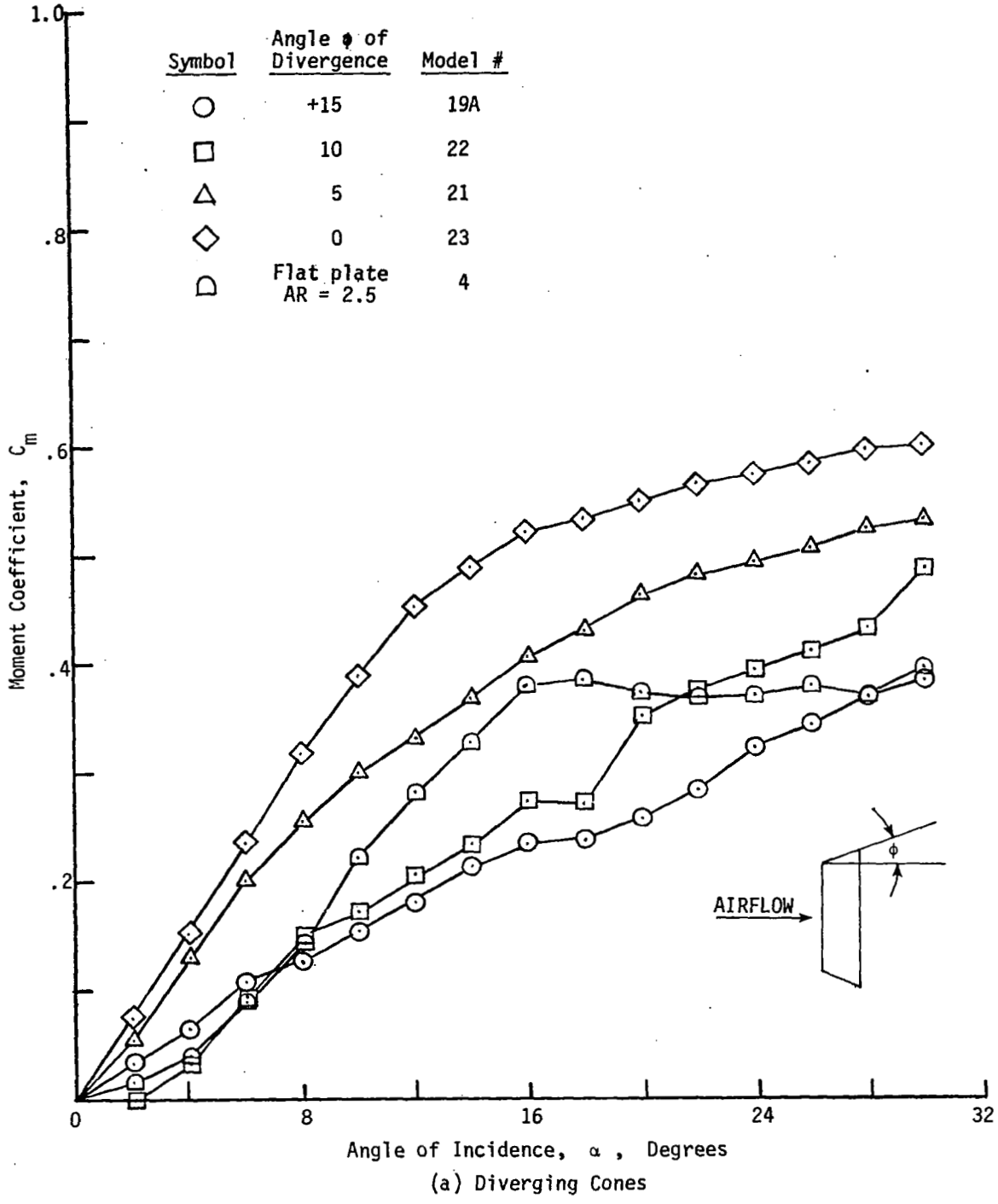

(a) Diverging Cones

Figure 20. Variation of moment with incidence and angle of divergence for conical vanes.

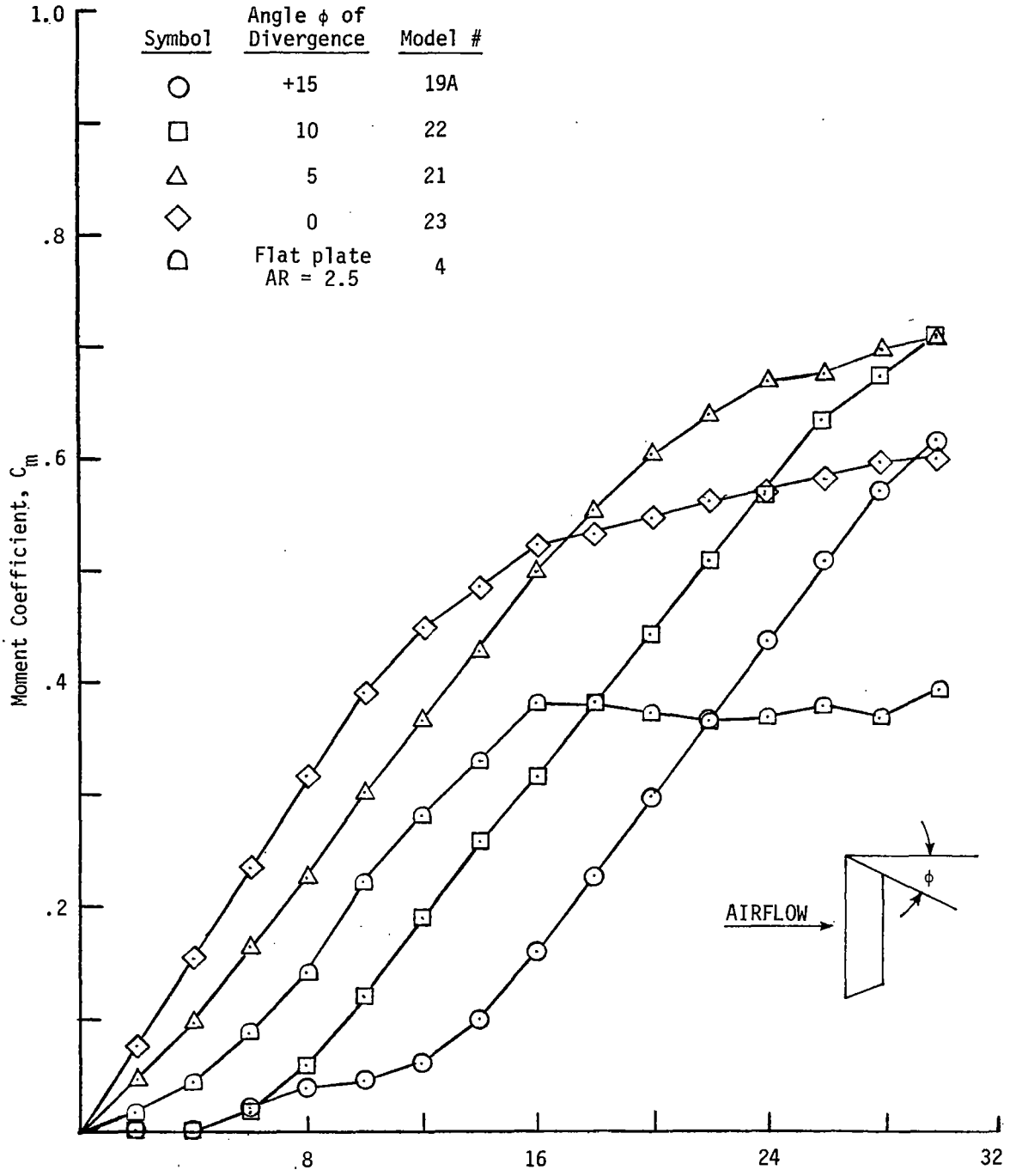

(b) Converging Cones

Figure 20. - Concluded

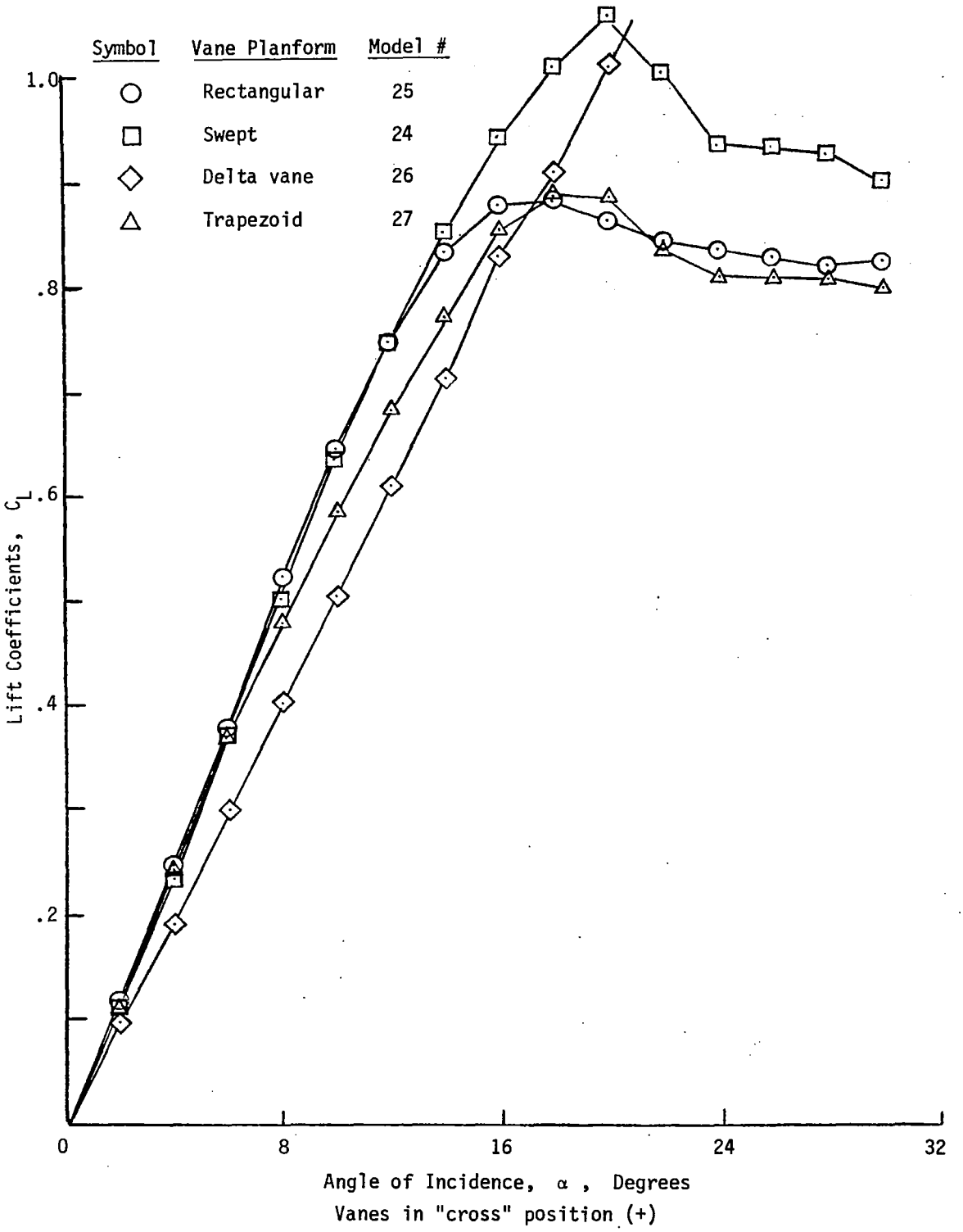

Figure 21. Variation of lift with incidence of cruciform vane configurations.

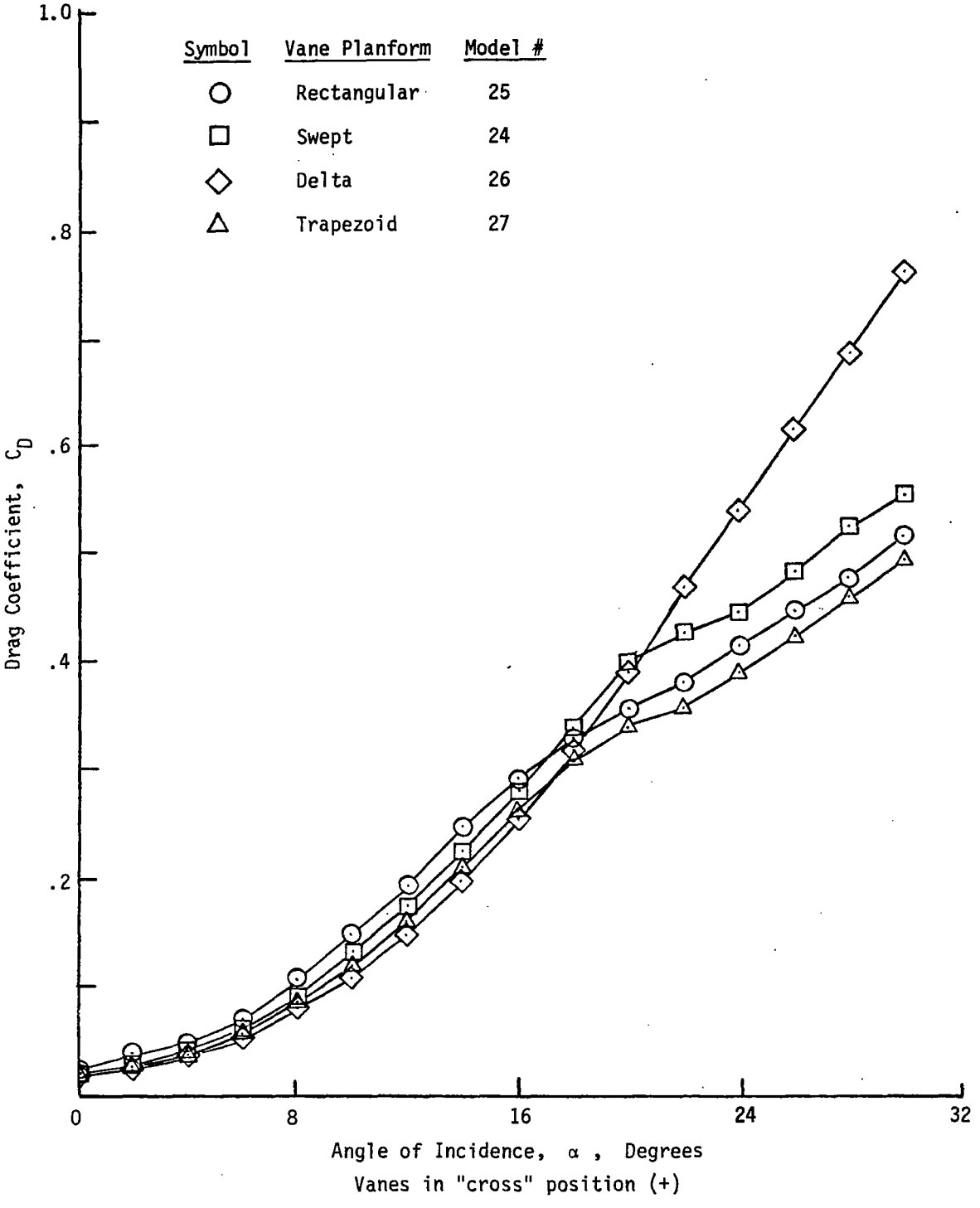

Figure 22. Variation of drag with incidence of cruciform vane configurations.

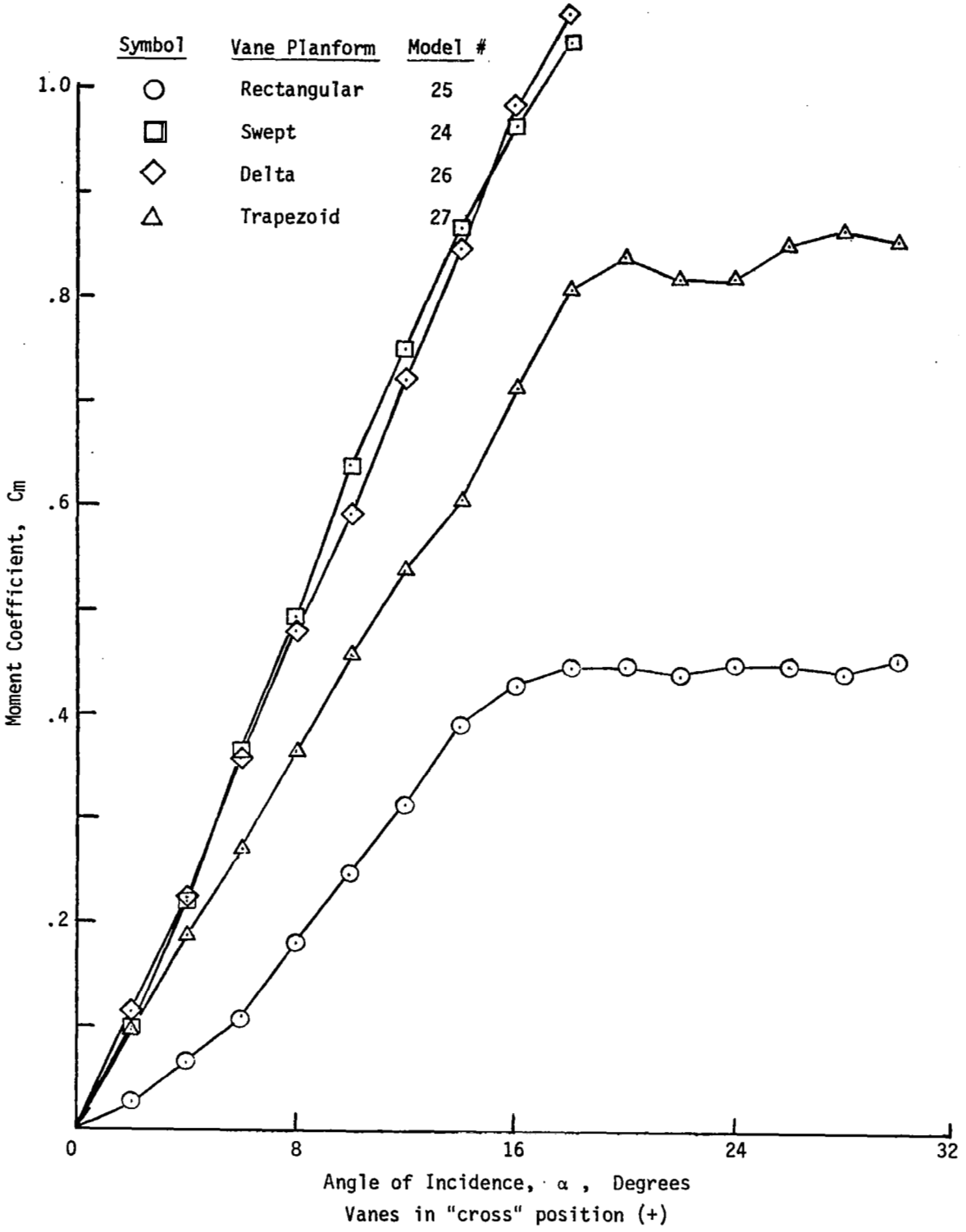

Figure 23. Variation of moment with incidence of cruciform vane configurations.

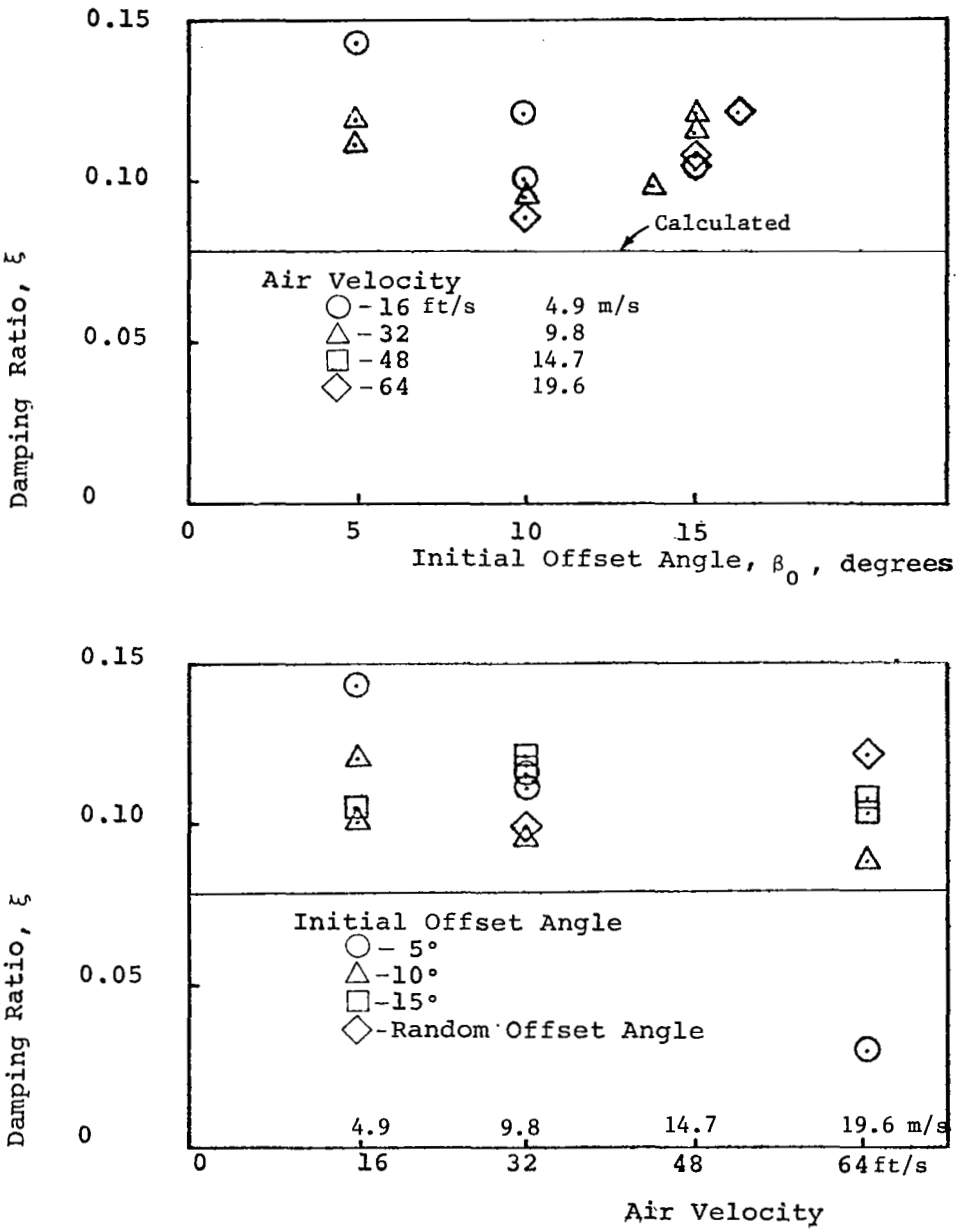

(a) Model 1, AR=5

Figure 24. Variation of Damping Ratio With Initial Offset Angle and Air Velocity. All models tested with constant arm length r_n = 5 ins (.127 m) except as stated otherwise.

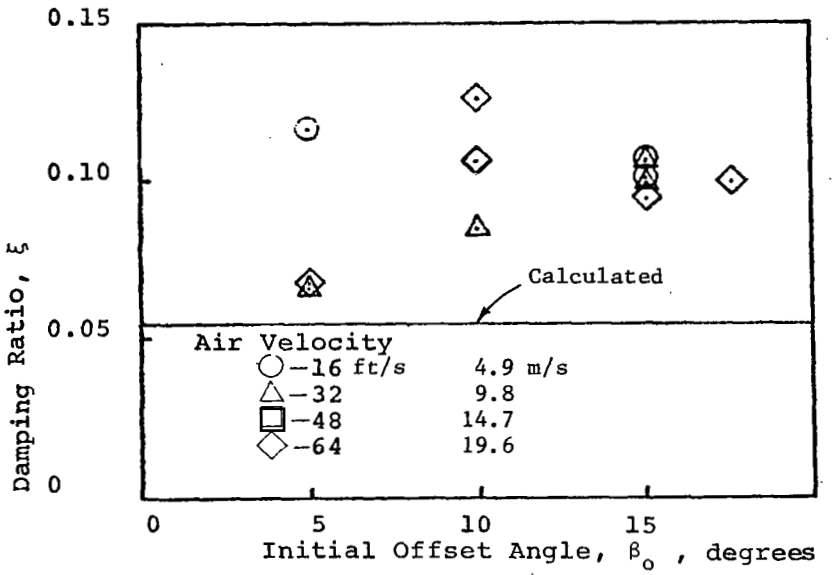

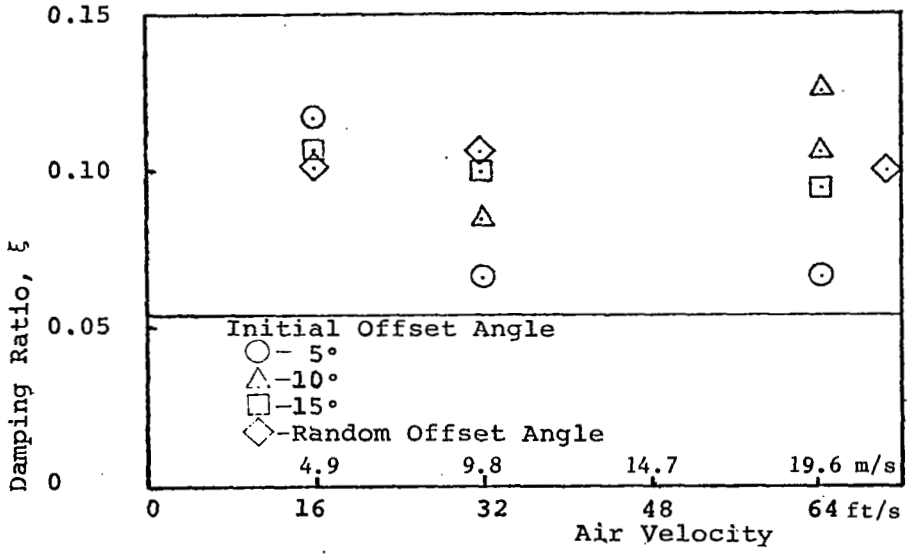

(b) Model 3, AR=1

Figure 24. Continued.

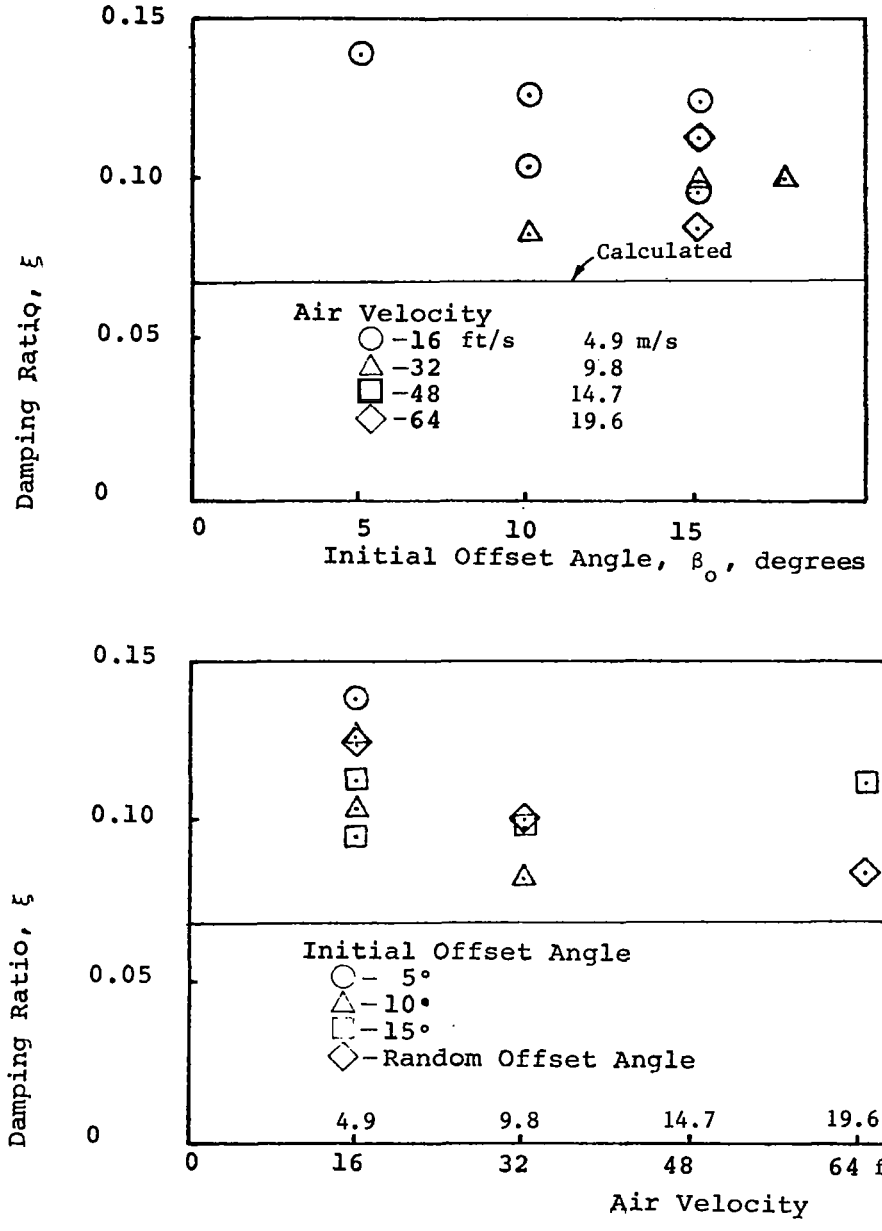

(c) Model 4, AR=2.5

Figure 24. Continued.

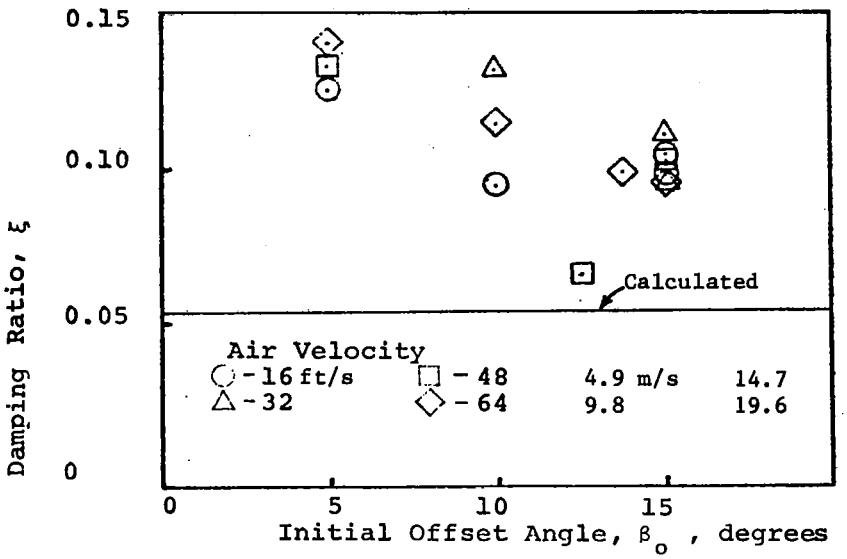

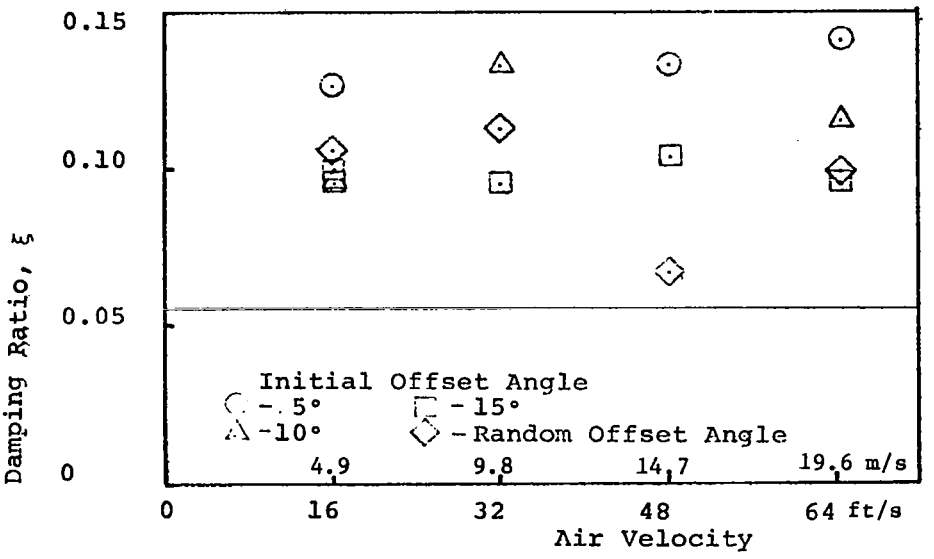

(d) Model 5, AR=1

Figure 24. Continued.

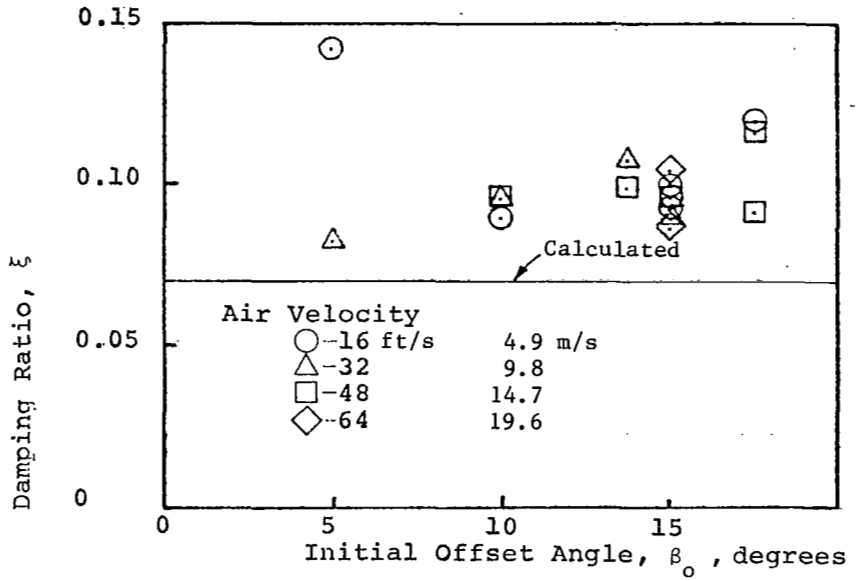

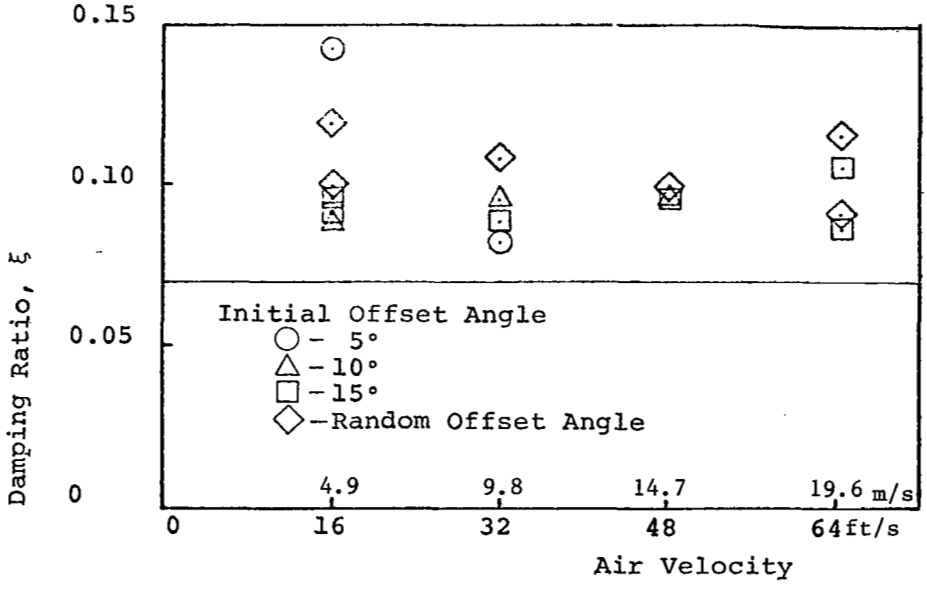

(e) Model 6, AR=2.5

Figure 24. Continued.

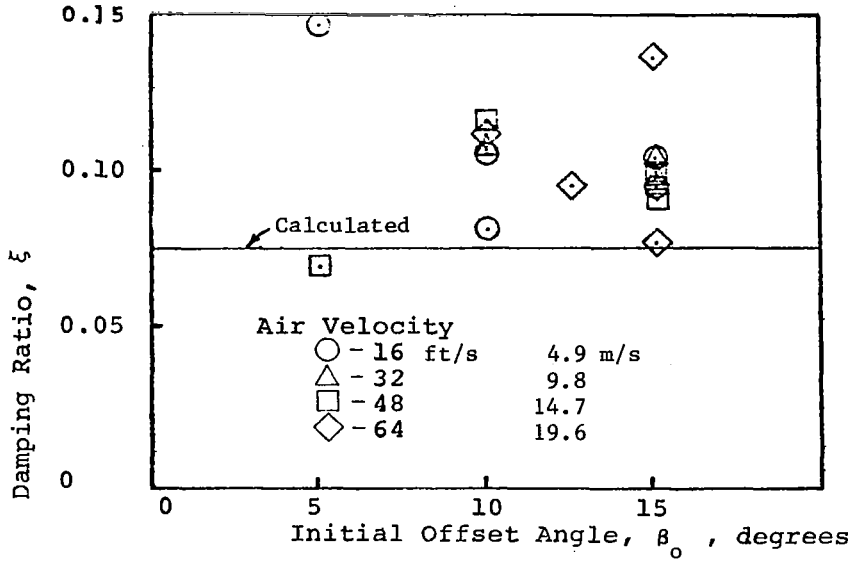

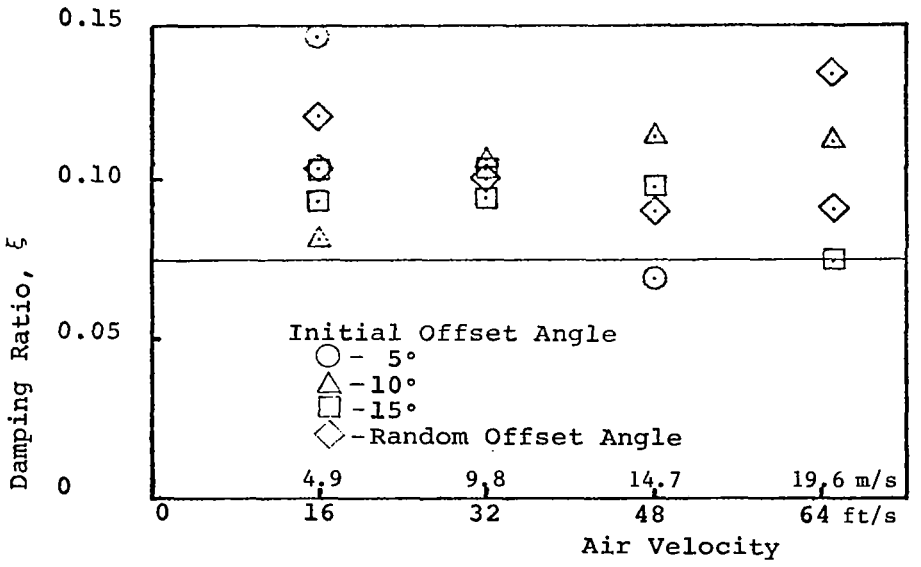

(f) Model 7, AR=5

Figure 24. Continued.

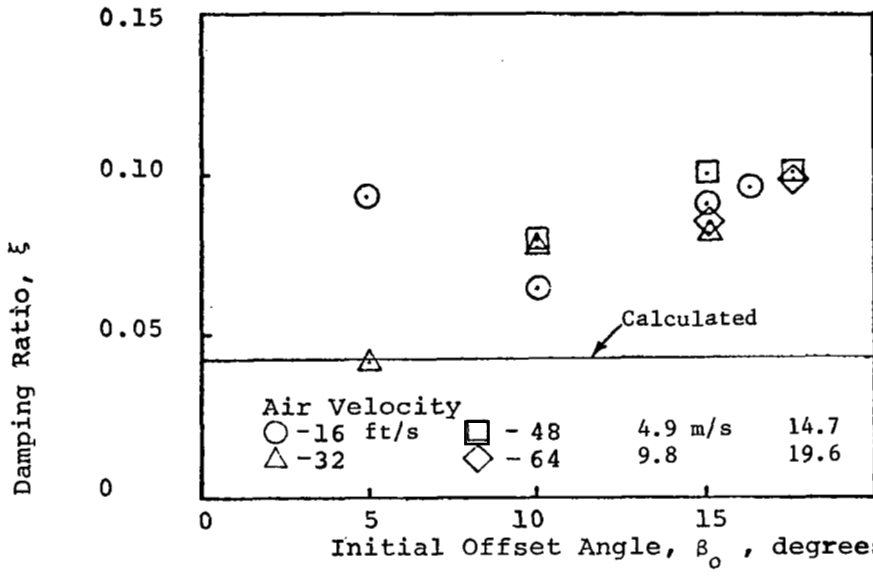

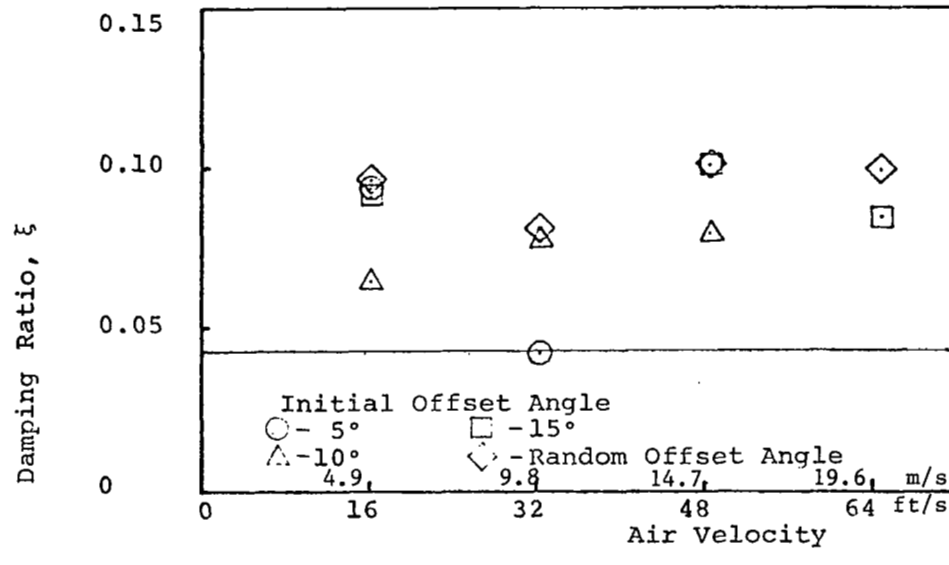

(g) Model 8, AR=$\frac{1}{2}$, r_n =4.7

Figure 24. Continued.

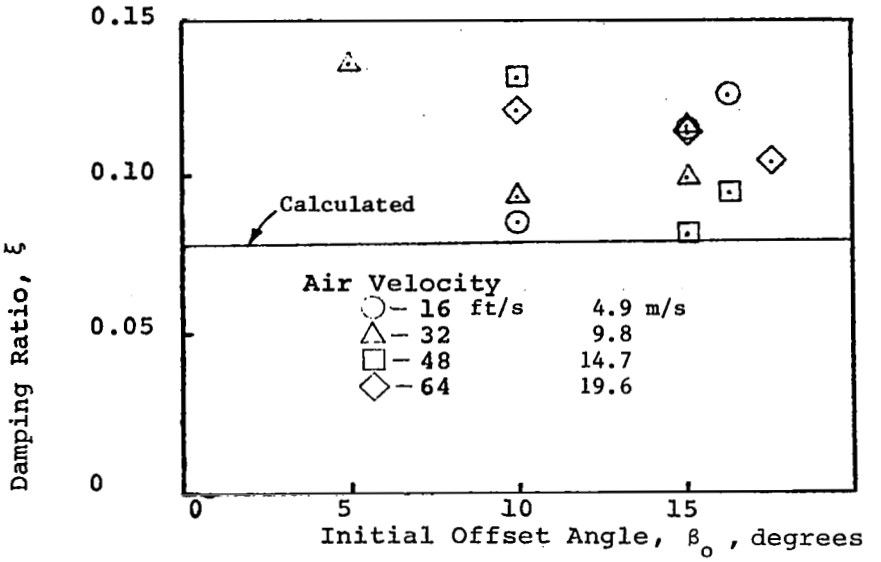

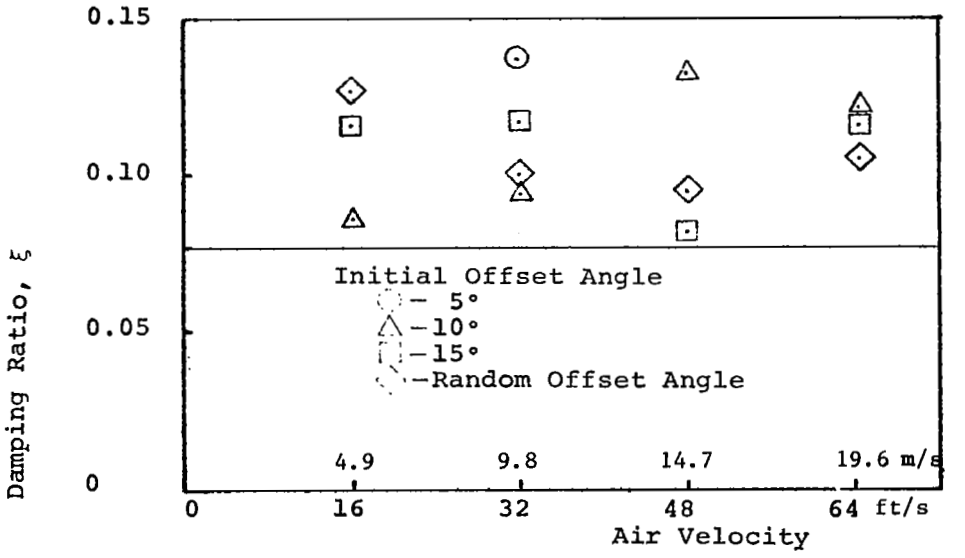

(h) Model 9, AR=5

Figure 24. Continued.

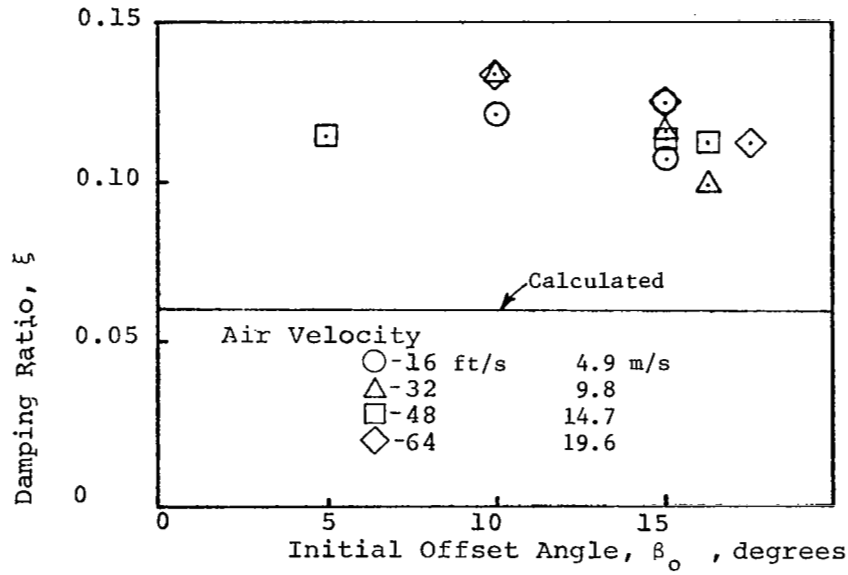

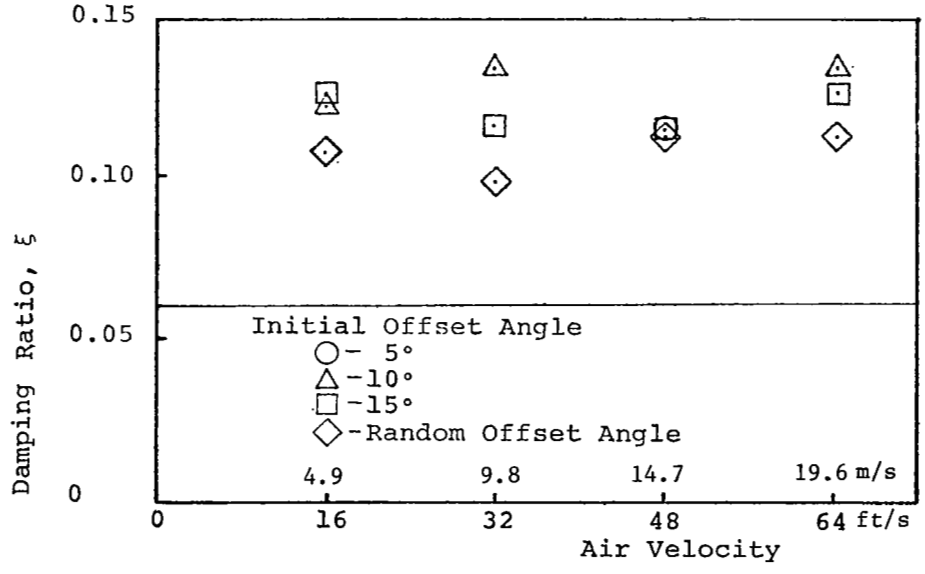

(i) Model 10, AR = 2.24

Figure 24. Continued.

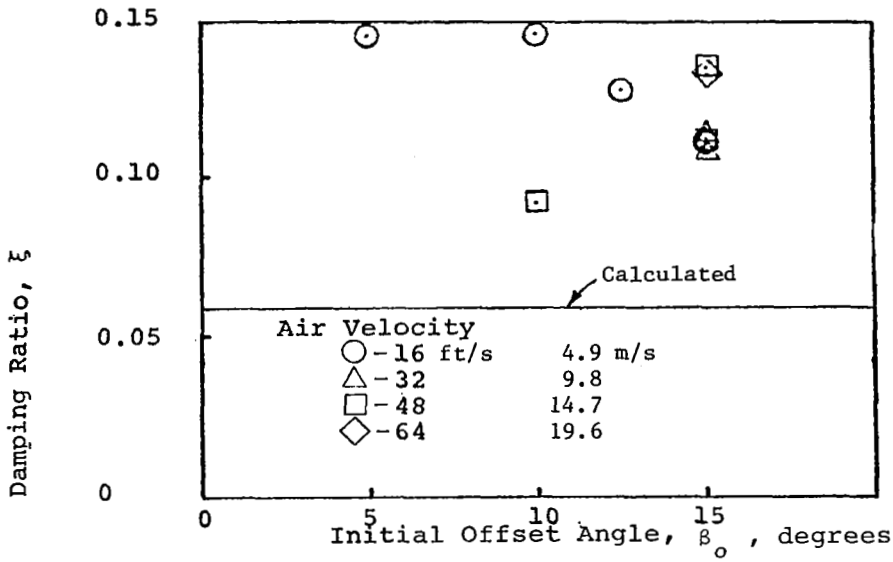

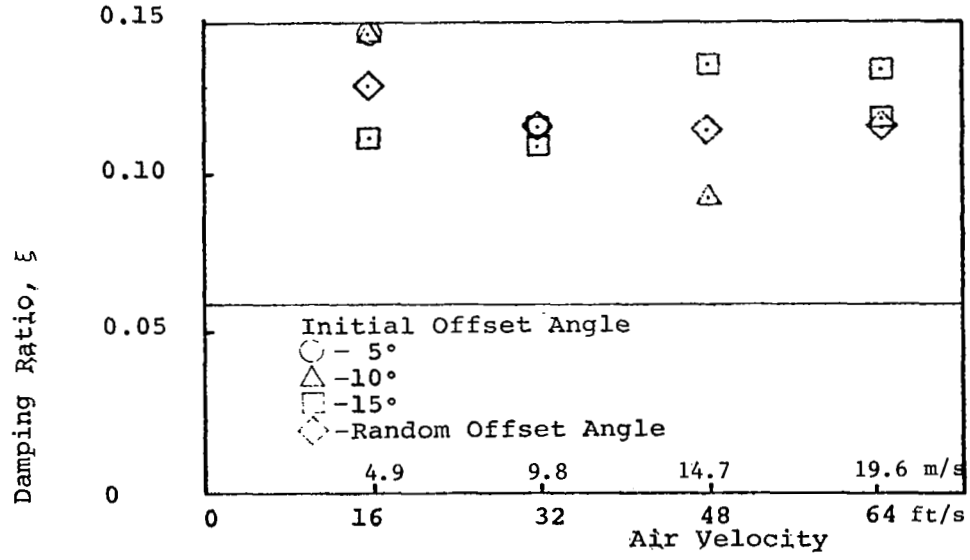

(j) Model 12, AR=1, r_n=5.85

Figure 24. Continued.

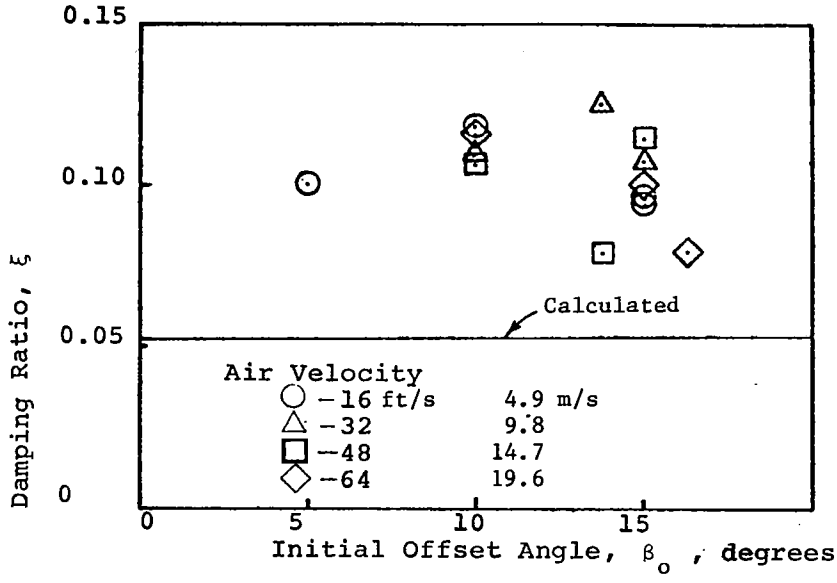

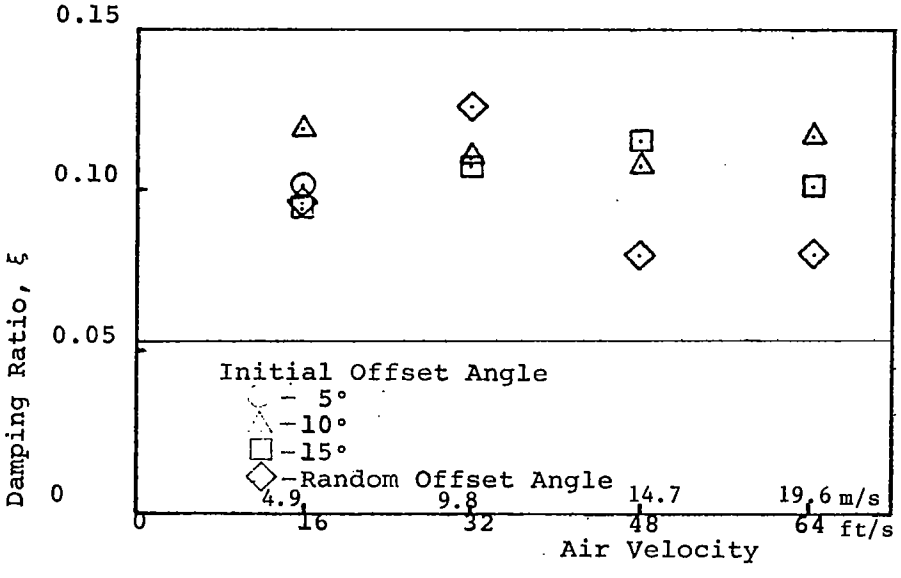

(k) Model 13, AR=1.27

Figure 24. Continued.

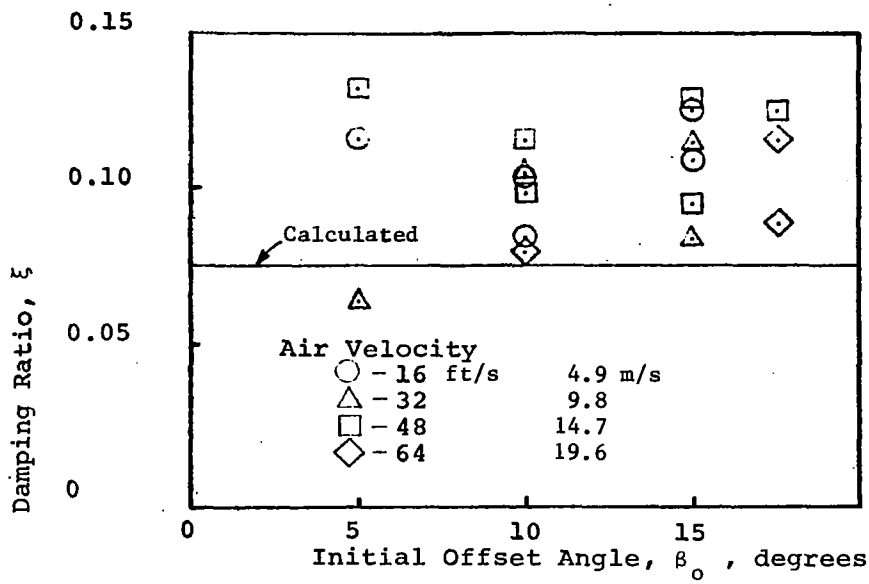

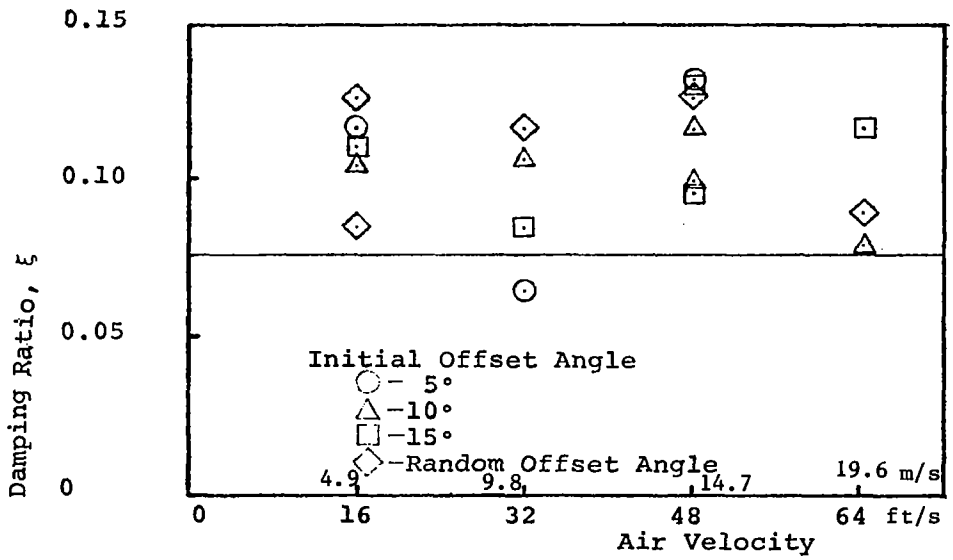

(1) Model 14, AR=5

Figure 24. Concluded.

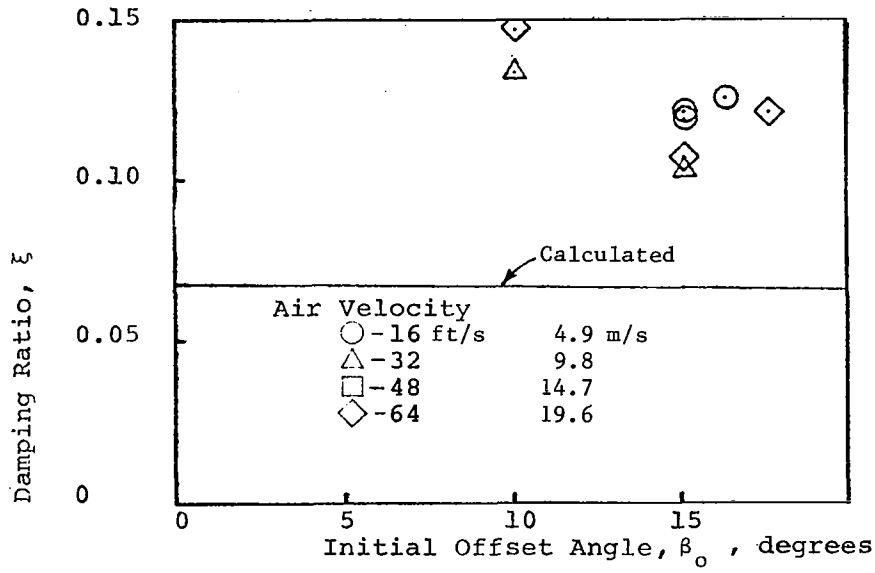

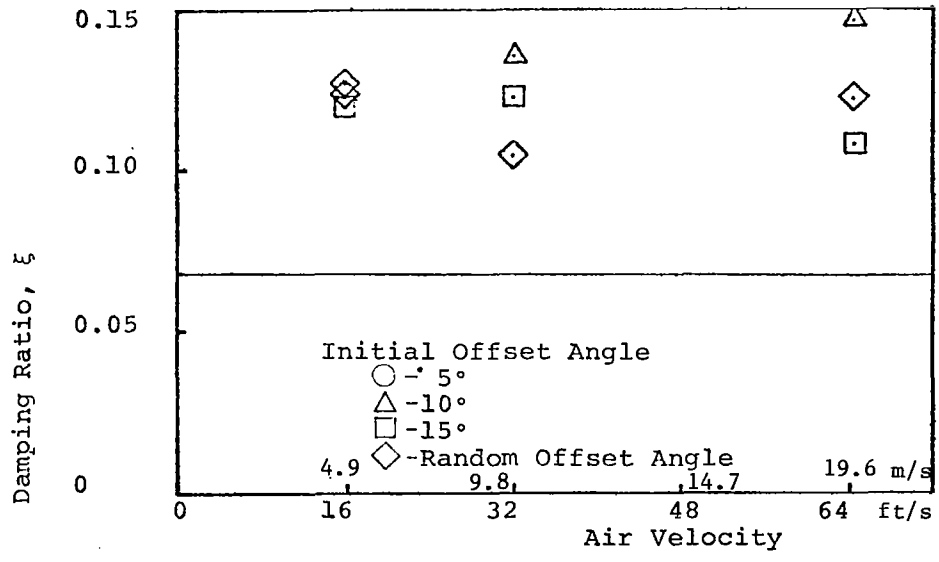

(a) Armlength r_n = 4 ins (.1015 m)

Figure 25. Variation of damping ratio with initial offset angle and air velocity for Model No. 1 for various armlength.

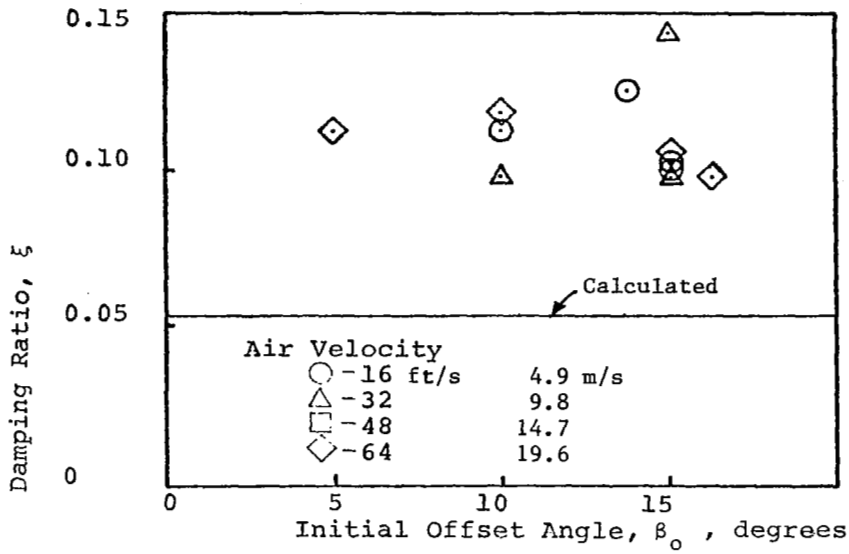

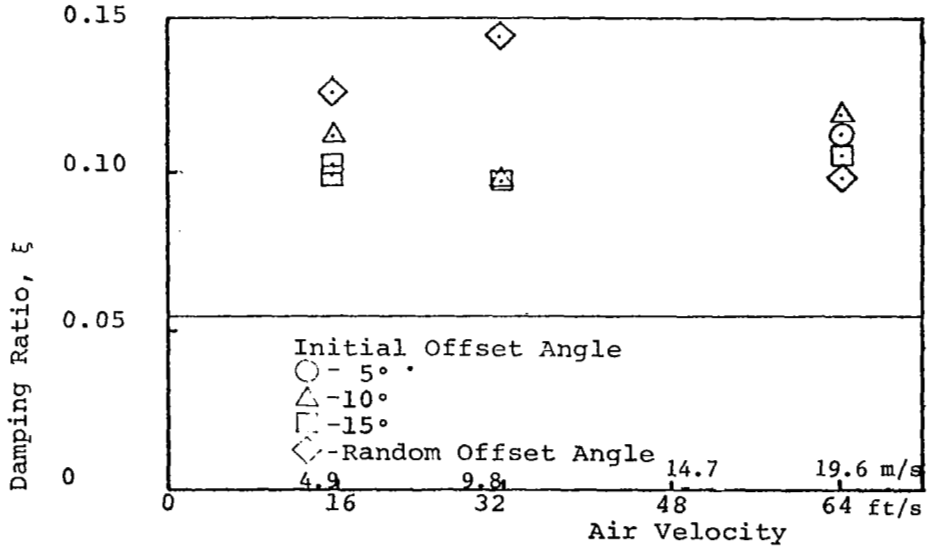

(b) Armlength r_n = 3 ins (.0762 m)

Figure 25. Continued.

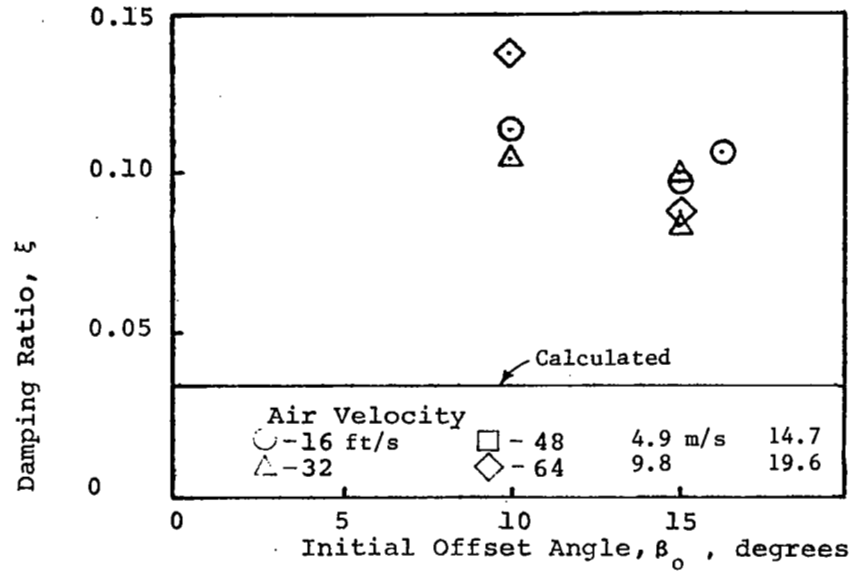

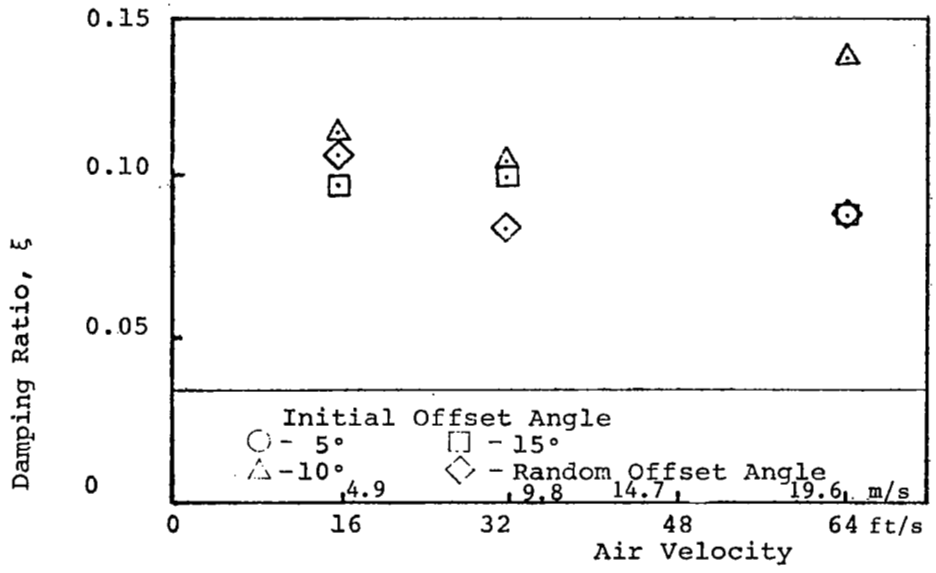

(c) Armlength r_n = 2 ins (.058 m)

Figure 25. Concluded.

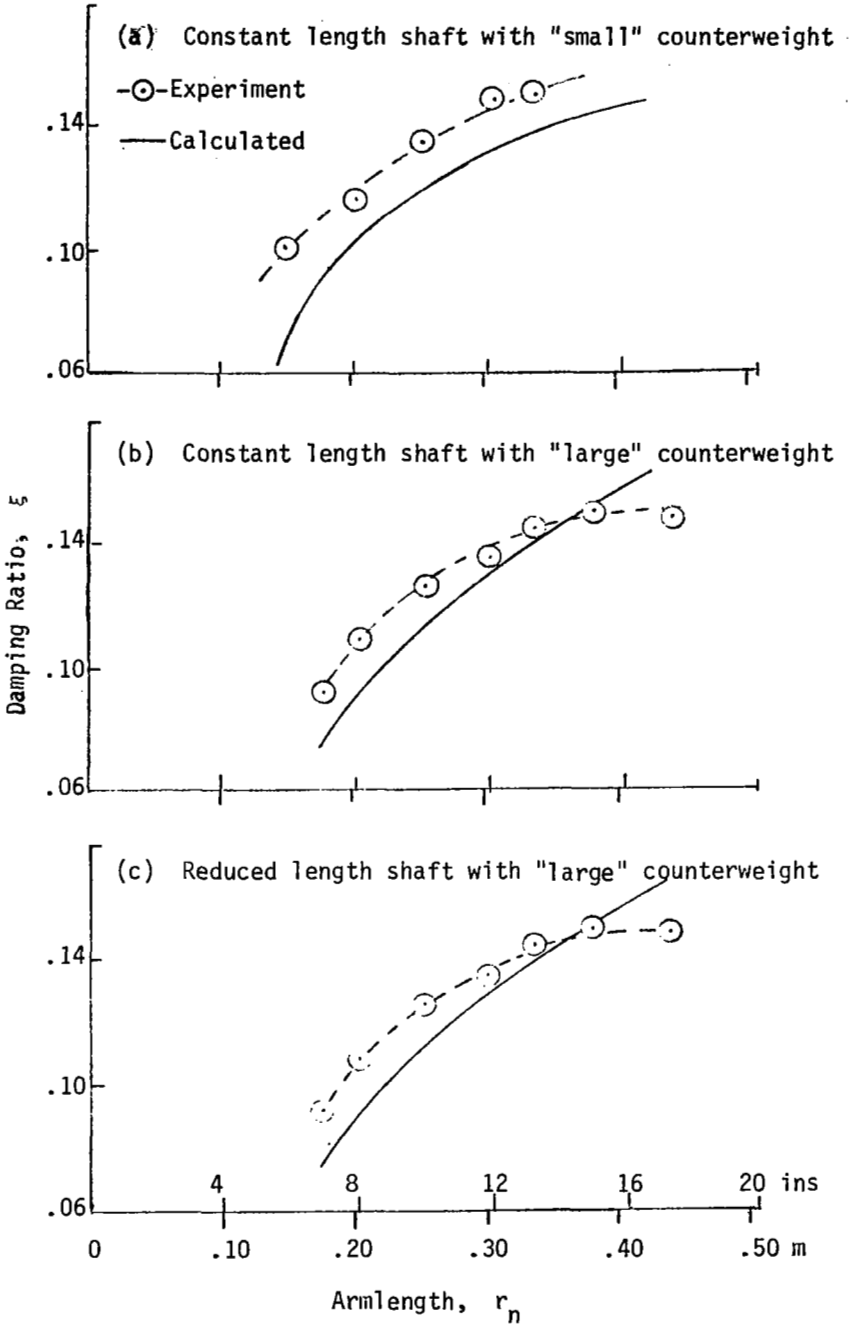

Small counterweight .0507 kg
Large counterweight .1014 kg

Figure 26. Variation of damping with armlength averaged for four airspeeds. Comparison between calculated and experimental values of Model No. 1.

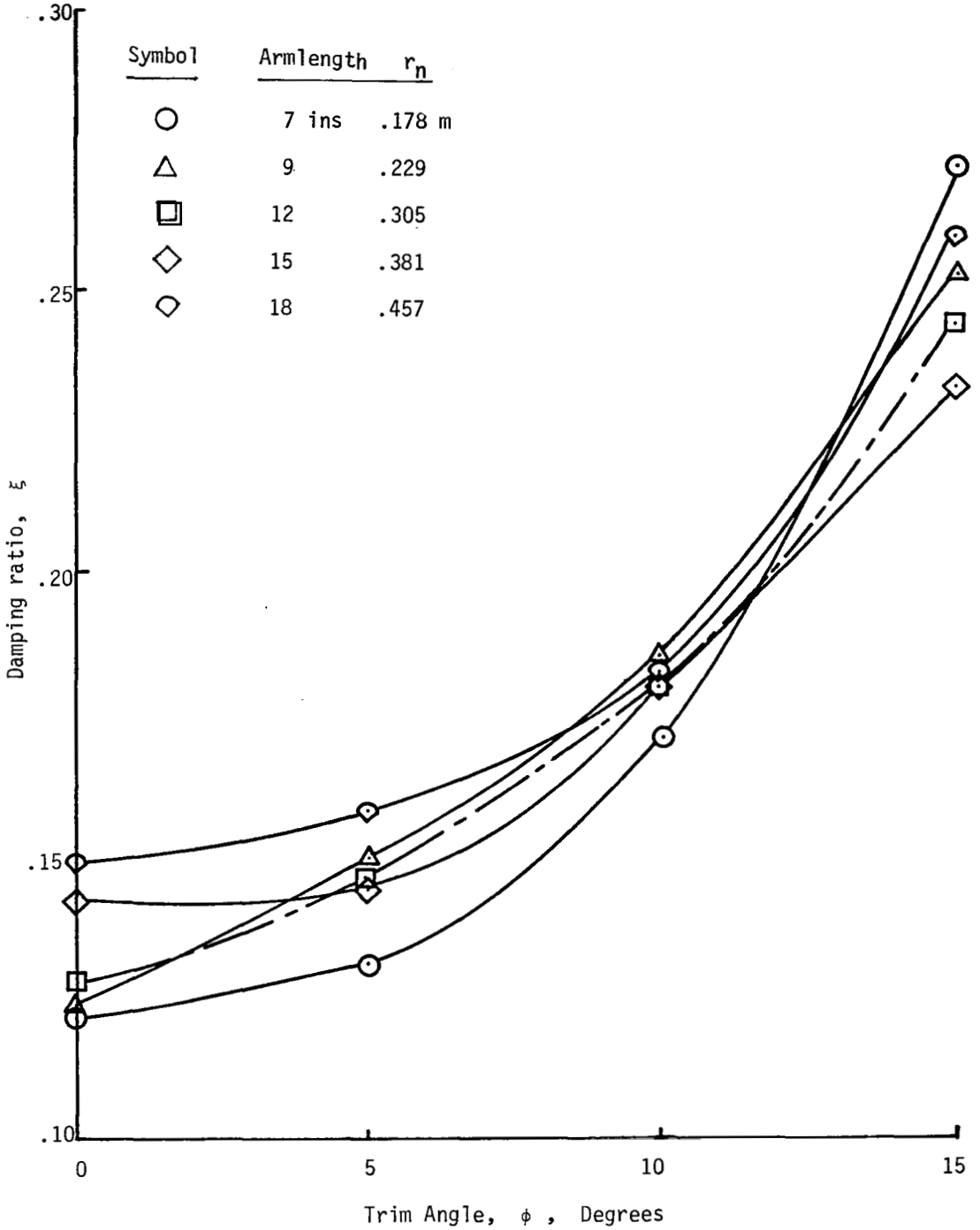

(a) Positive (ϕ+) Trim Angle Only

Figure 27. Variation of damping ratio of Bi-Vanes with trim angle ϕ for various armlengths.

VARIABLE VANE DISTANCE

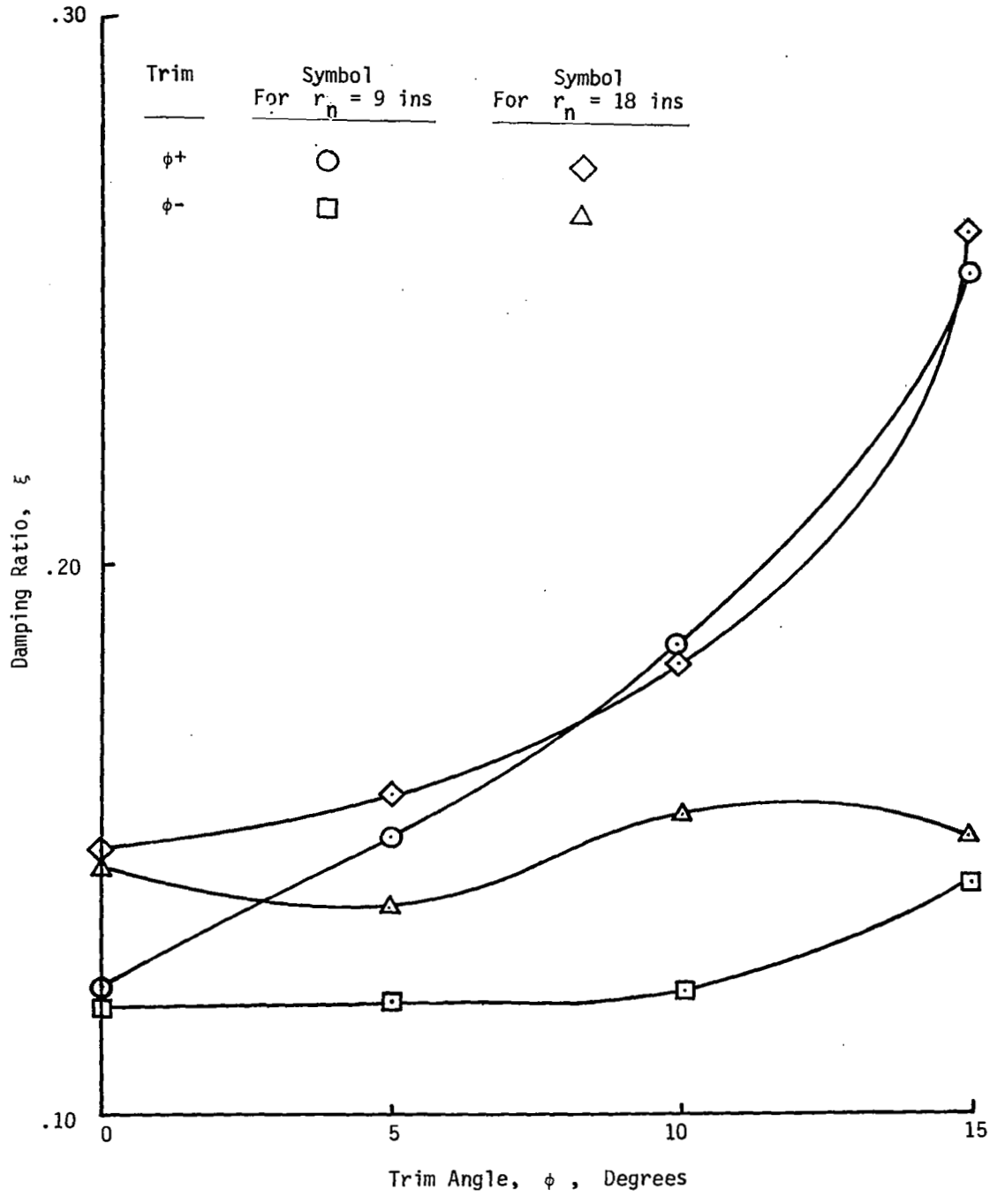

(b) Positive (ϕ+) and negative (ϕ-) trim angle (comparison)

Figure 27. Concluded.

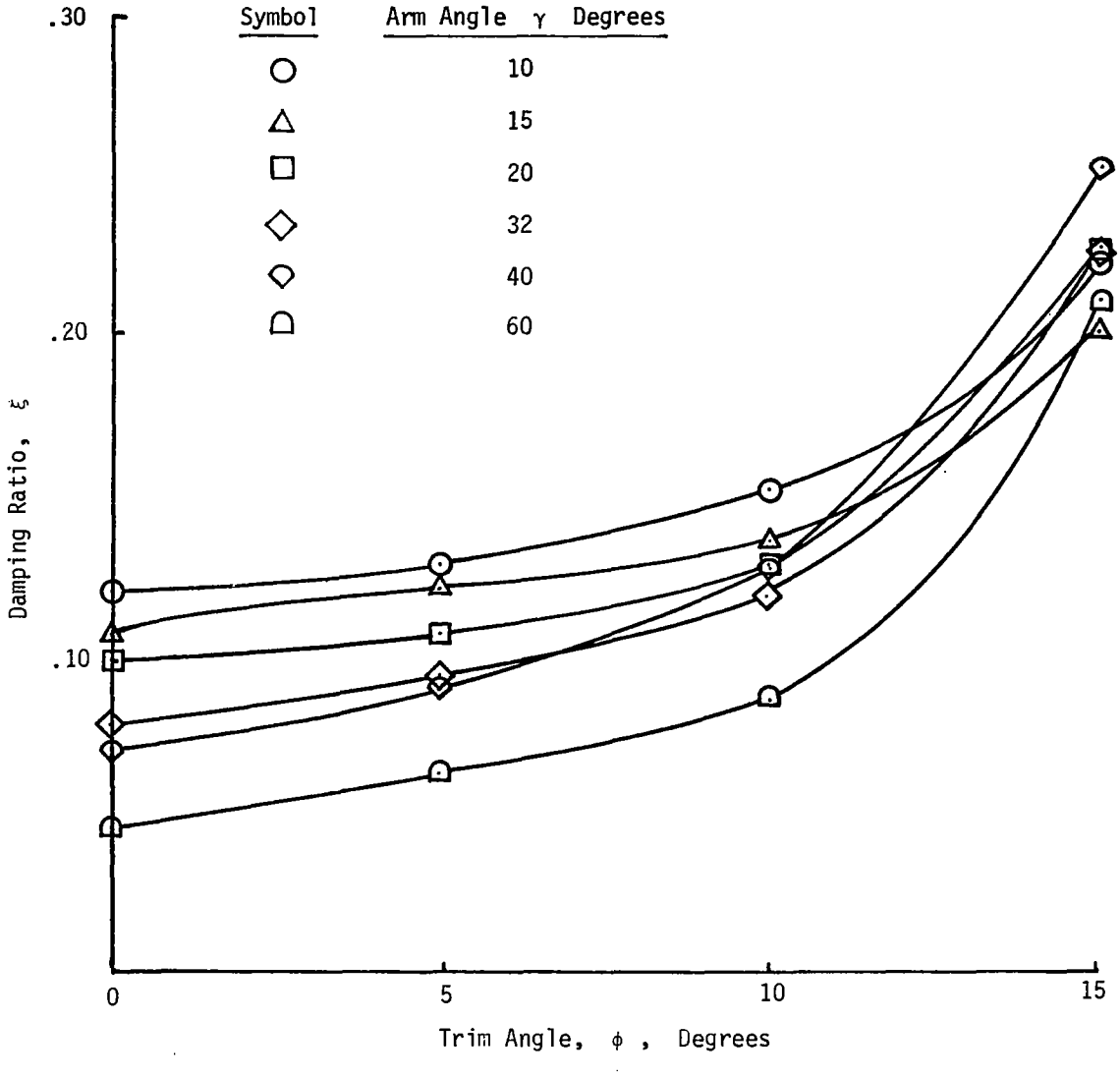

(a) Thick vane t = 0.0625 ins (.0016 m)

Figure 28. Variation of damping ratio of Bi-Vanes with trim angle for various arm angles (γ).

FIXED VANE DISTANCE

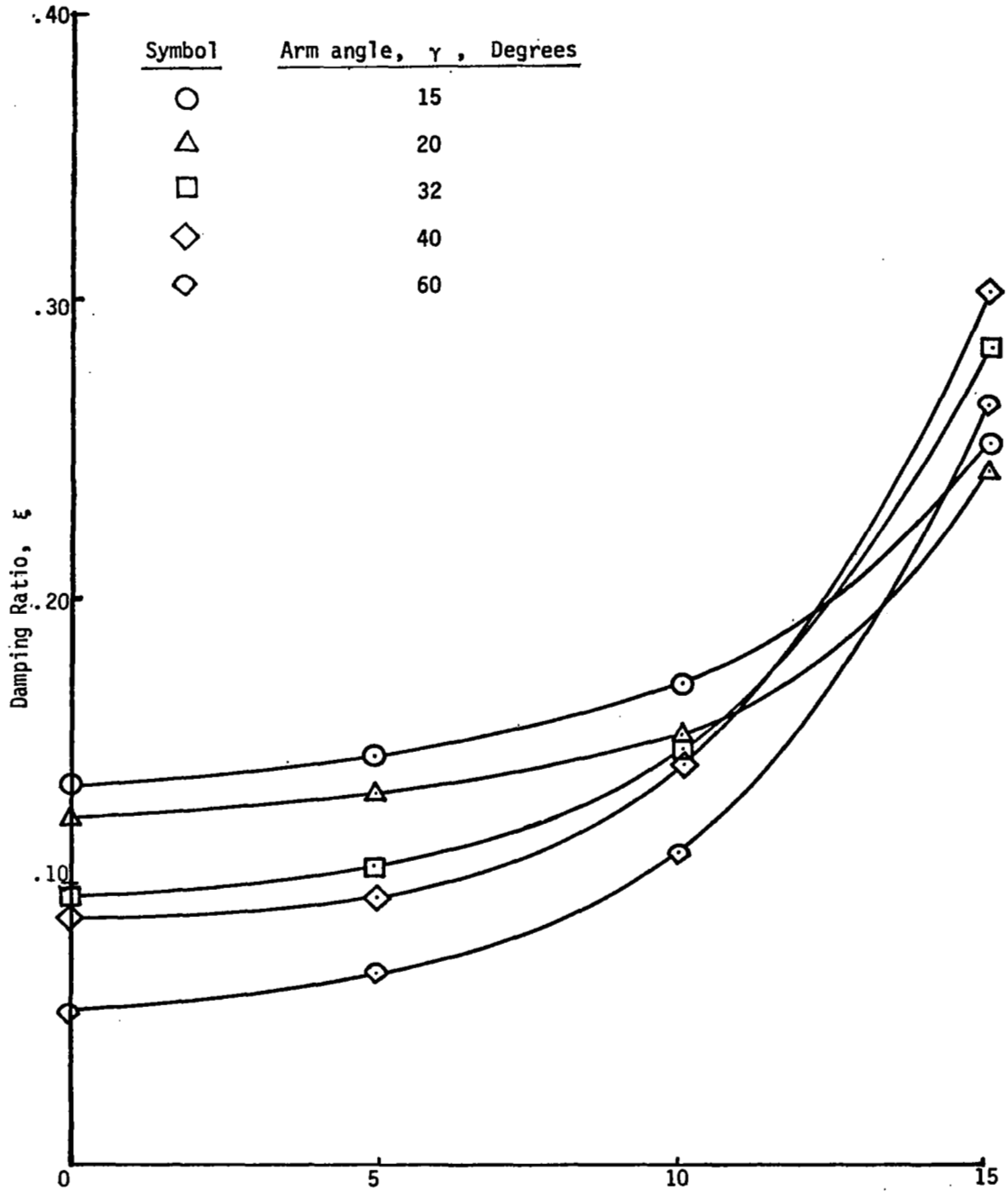

(b) Thin vane, t = .04 ins (.001 m)

Figure 28. Concluded.

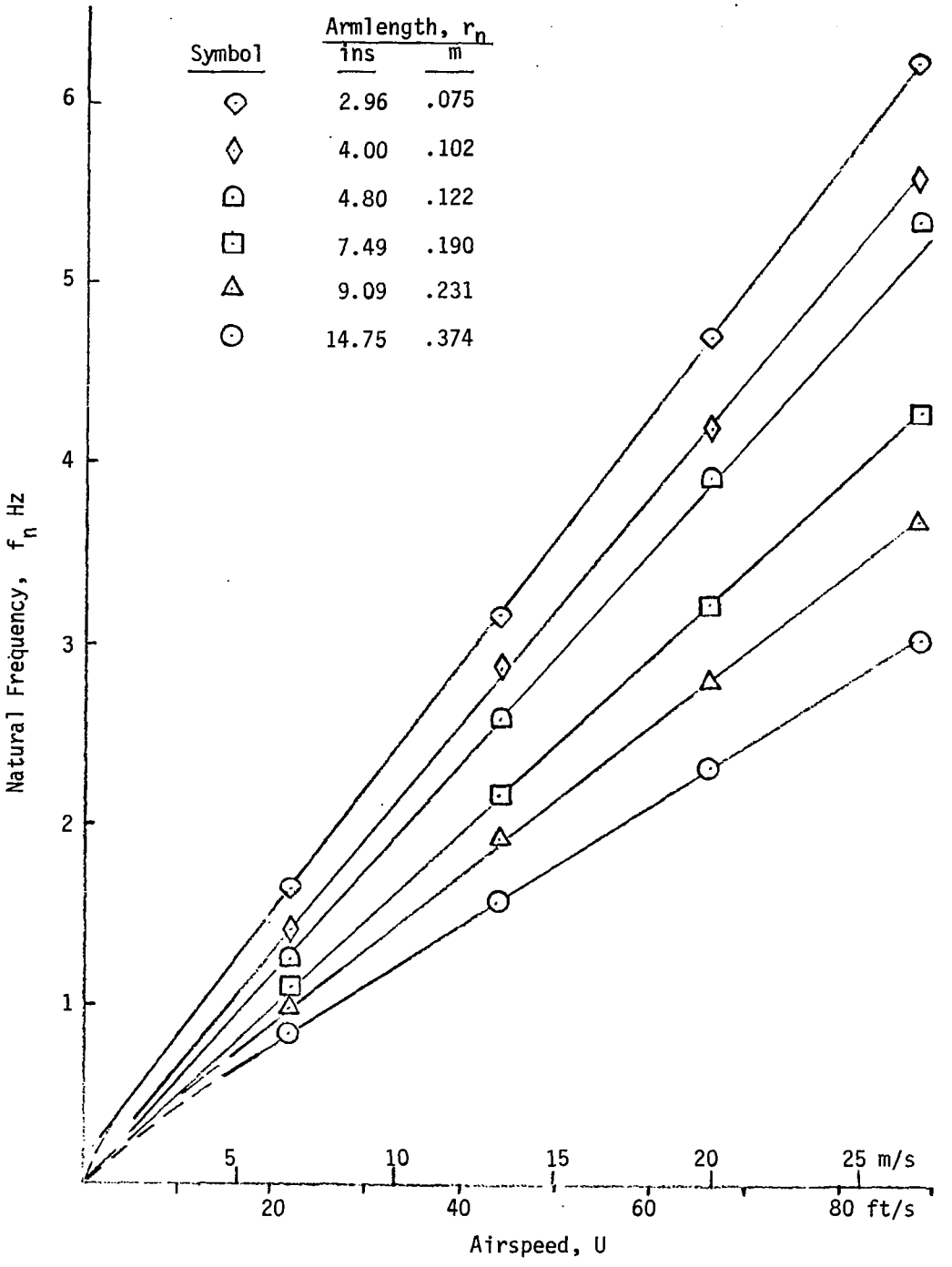

Figure 29. Variation of natural frequency of a single vane with AR = 2.5 with airspeed as affected by armlength.

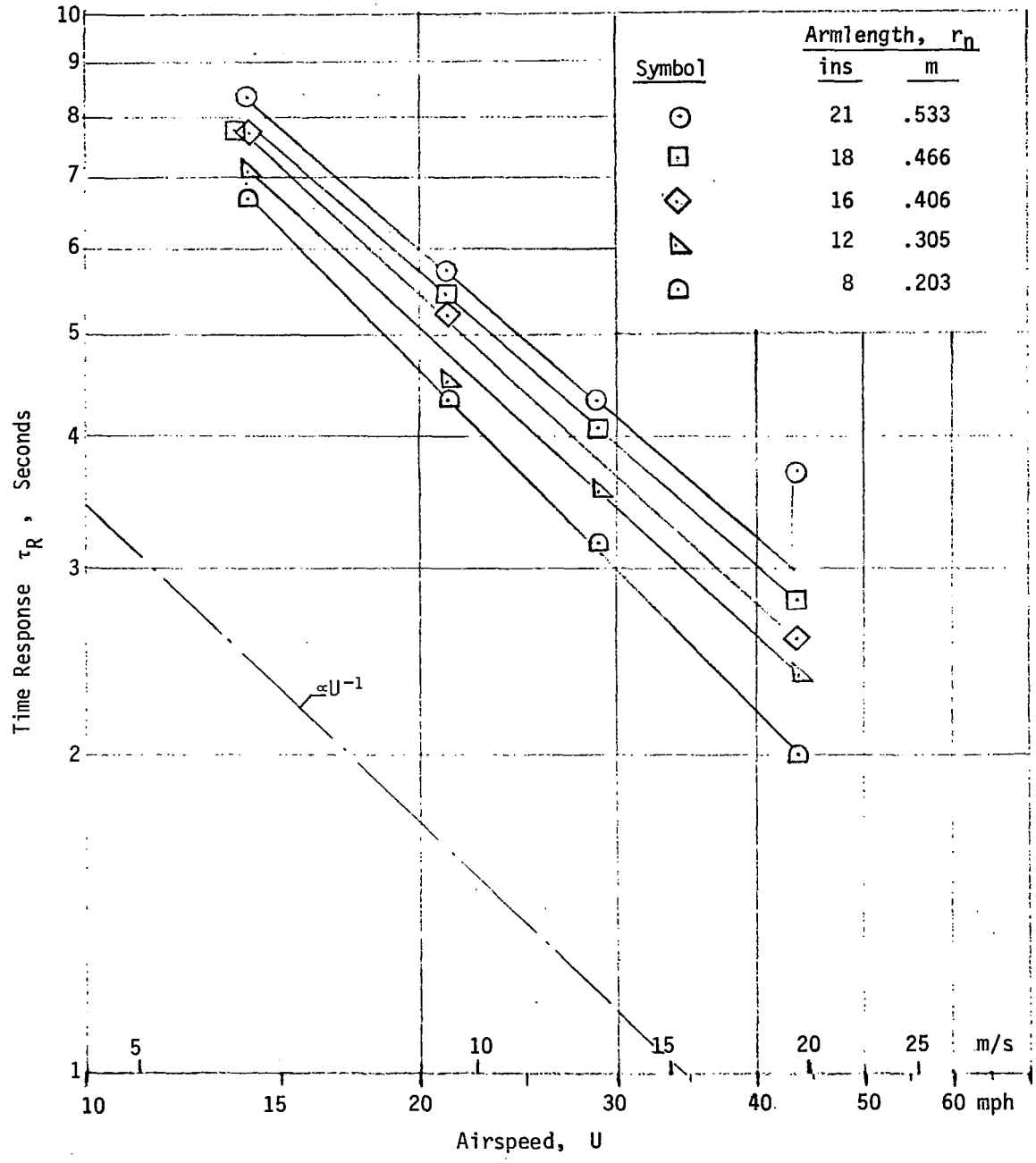

Figure 30. Variation of time response with airspeed for a single vane (AR = 5, No. 1 model) as affected by armlength r_n.

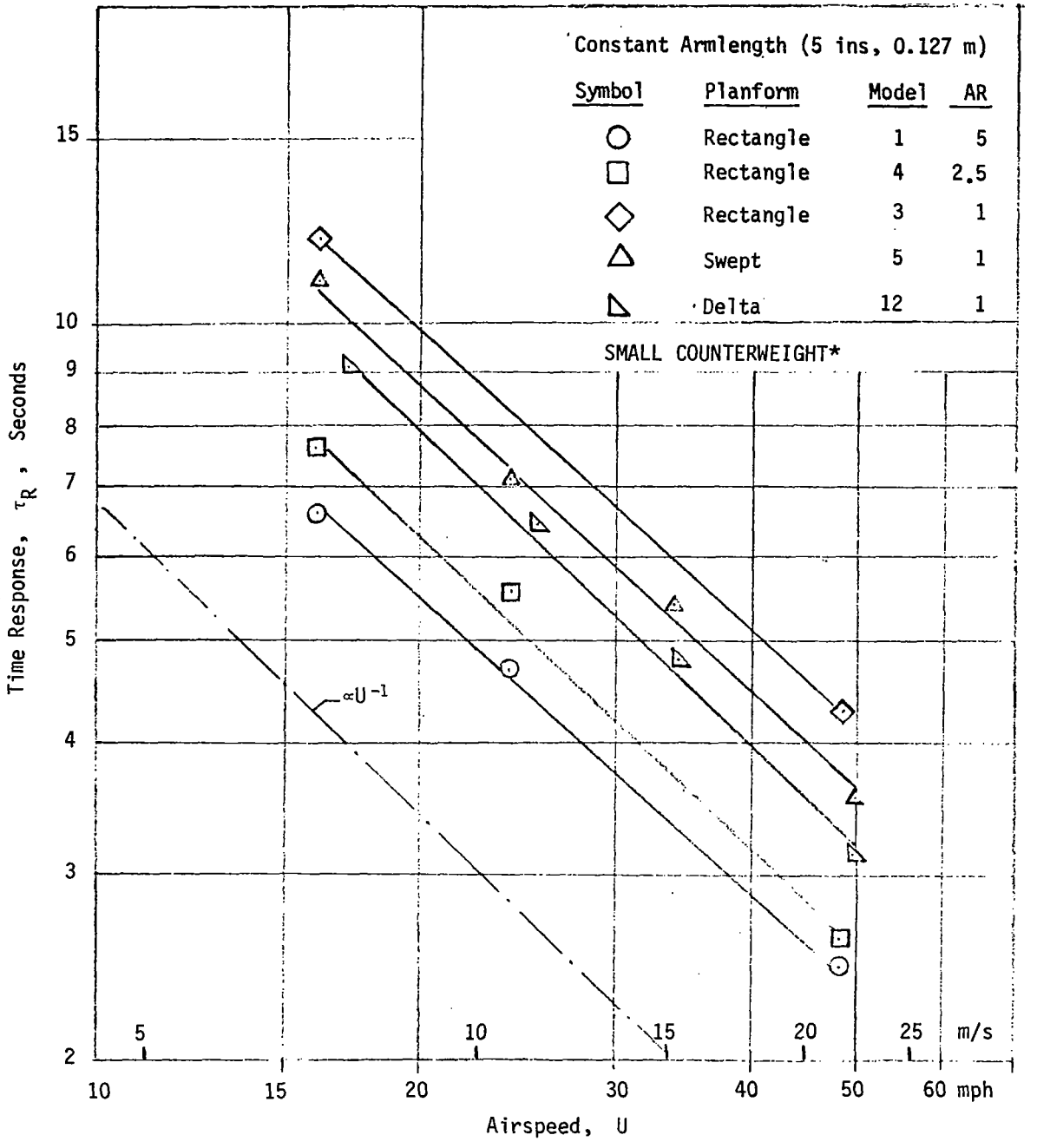

Figure 31. Variation of time response with airspeed of single vanes with constant armlength as affected by planform and aspect ratio.

* In all other figures the large counterweight was employed.

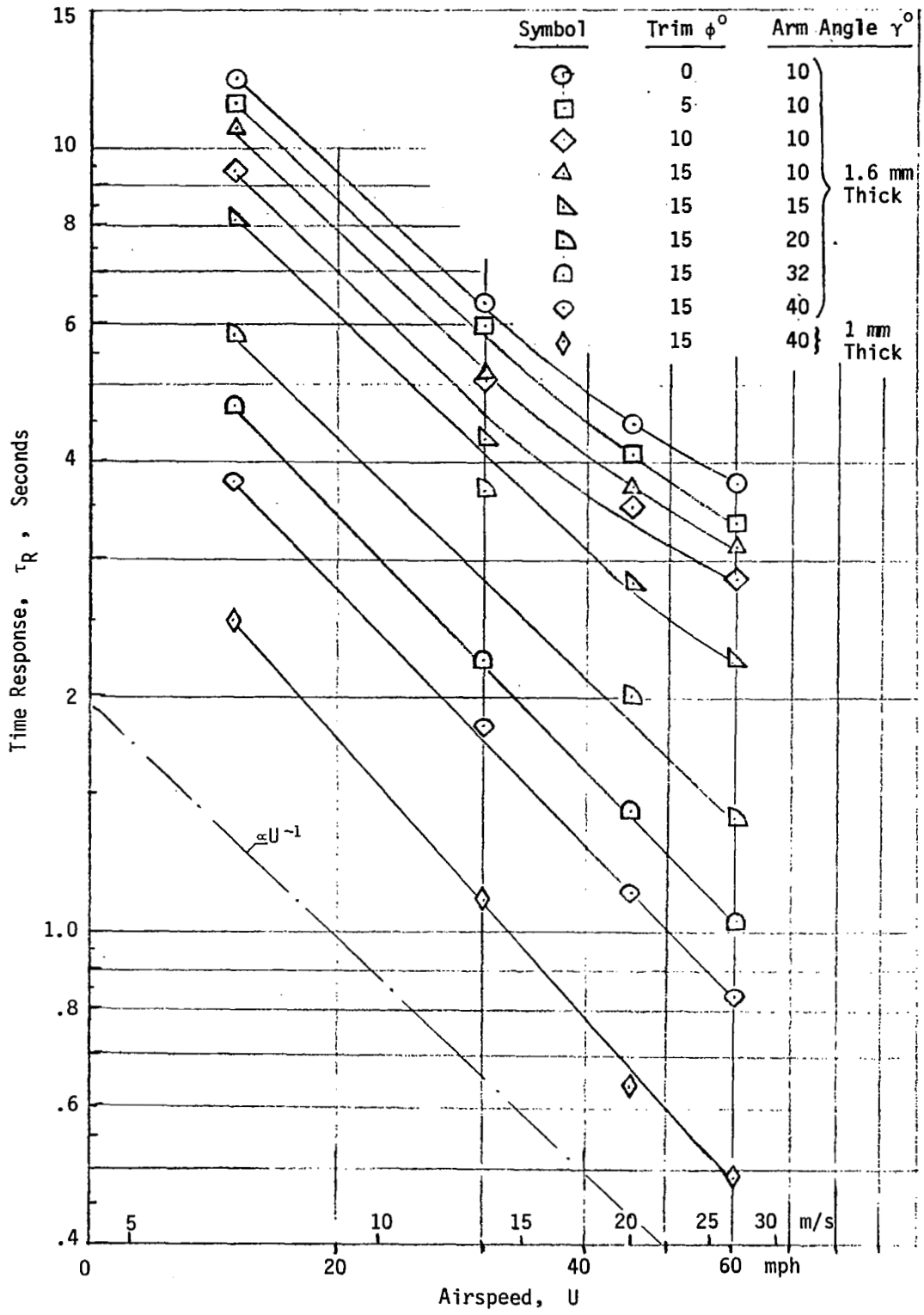

Figure 32. Variation of time response with airspeed for Bi-vanes as affected by arm and trim angle (γ and ϕ) and thickness.

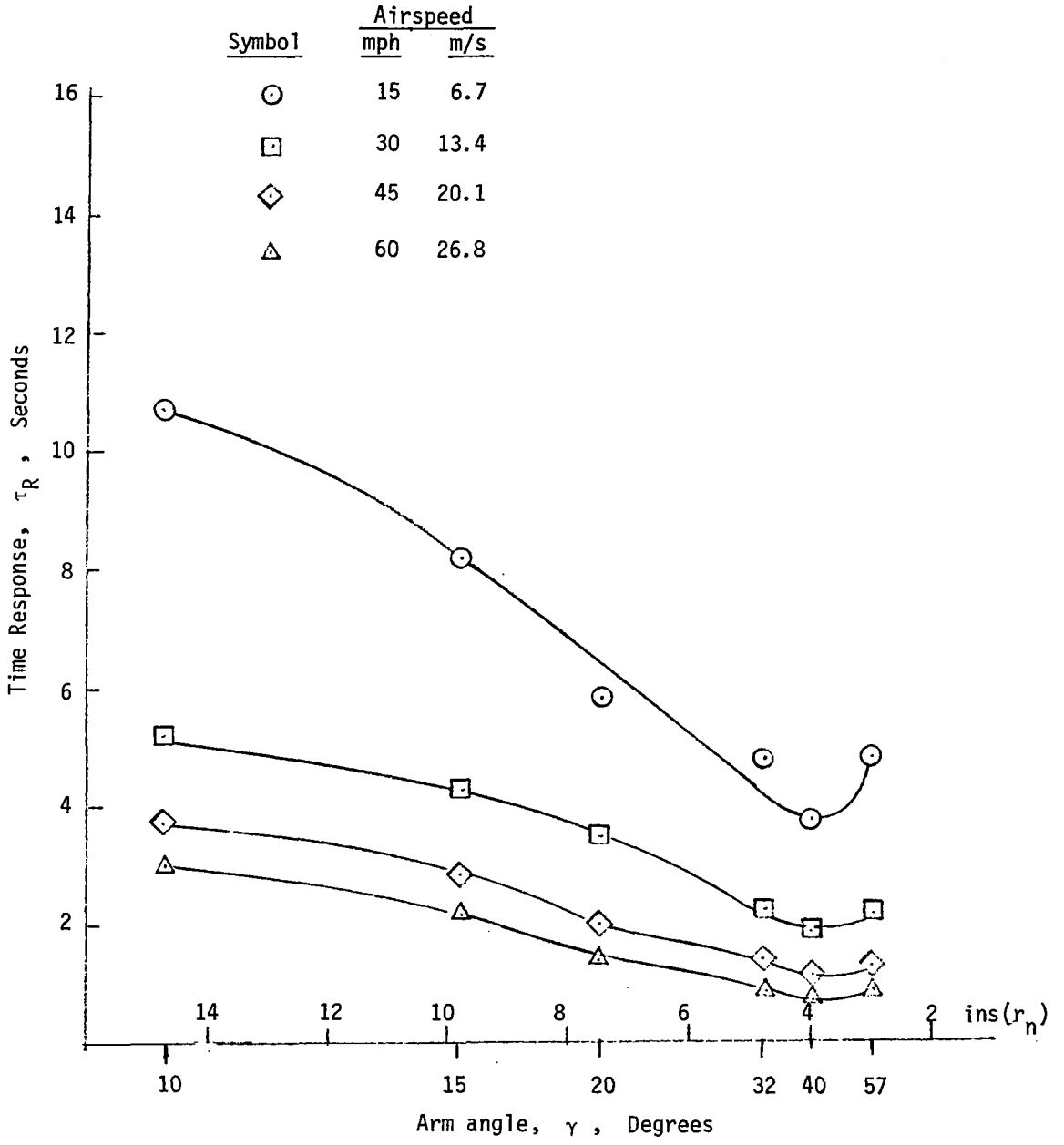

Figure 33. Variation of time response with arm angle γ (or length r_n) of bi-vanes as affected by airspeed.

Constant trim angle ϕ = +15°
Vane aspect ratio 2.5

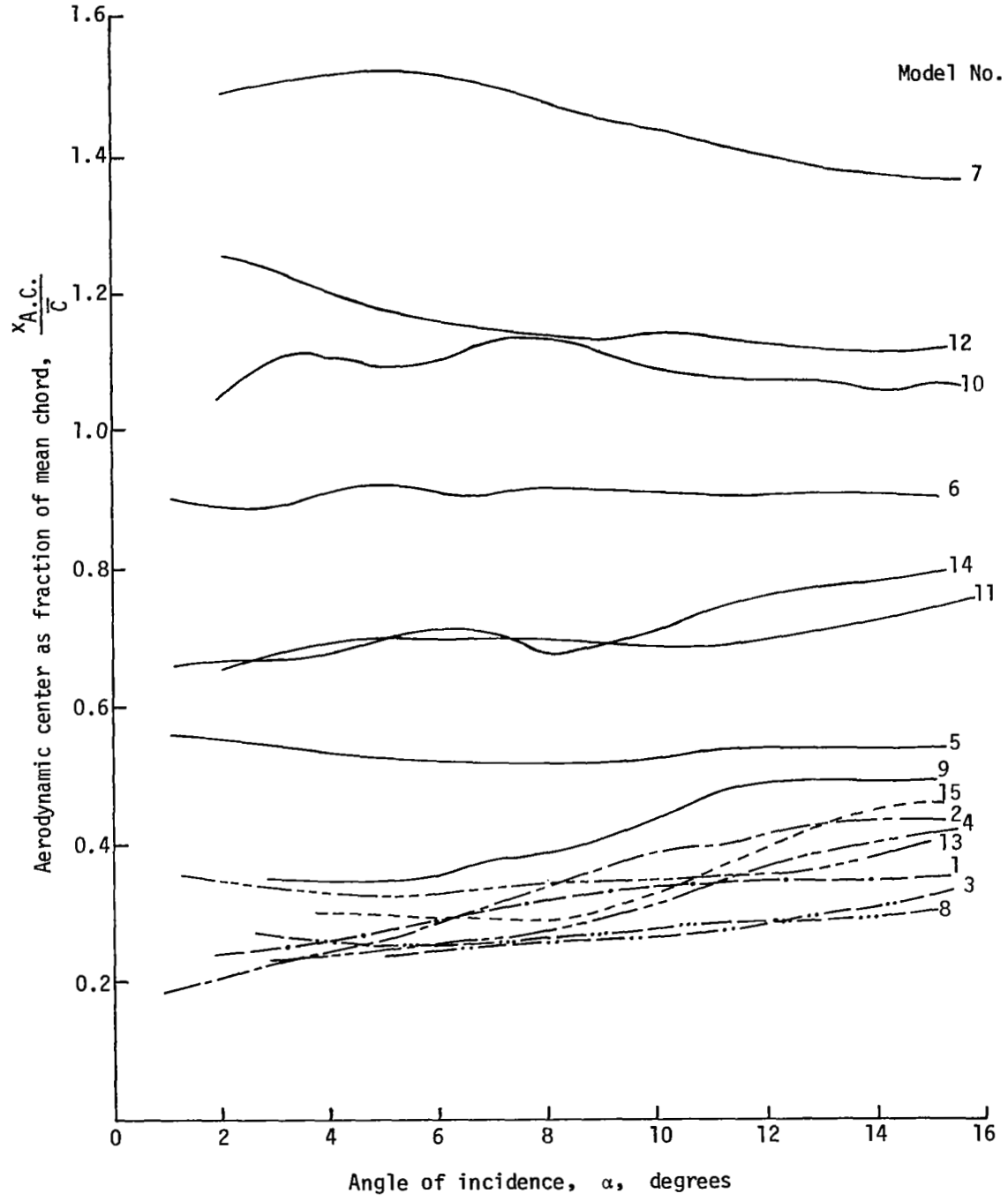

Figure 34. Variation of aerodynamic center with incidence.

APPENDIX A

BRIEF REVIEW OF LINEAR THEORY FOR ISOLATED WIND VANES

The oscillatory motion of a wind vane exposed to an airstream may be compared to the motion of a mass connected to the well-known mechanical spring and dashpot system, Fig. A1 (a). In the latter case, the mass displaced by distance x is returned by an active spring force F_s which is considered to be proportional to the displacement x:

$$F_s = -kx$$

where k is the spring constant. A passive force F_d, called damping, is generally assumed to be proportional to the velocity:

$$F_d = -d \frac{dx}{dt}$$

where d is the damping coefficient.

By Newton's Second Law, for dynamic equilibrium the forces must be balanced by the time rate of change of the momentum, hence,

$$F_s + F_d = \frac{d}{dt}(mv) = m \frac{d^2x}{dt^2}$$

Substitution for F_s and F_d results in a differential equation

$$m \frac{d^2x}{dt} + d \frac{dx}{dt} + kx = 0 \qquad A(1)$$

Assuming a solution of the form $x = e^{st}$, it follows that

$$(ms^2 + ds + k)\, e^{st} = 0$$

The roots of the bracketed term

$$S_{1\ 2} = \left[-\frac{d}{2m} \pm \sqrt{\left(\frac{d}{2m}\right)^2 - \frac{k}{m}} \right]$$

furnish the general solution

$$x = x_0 \exp\left(\left[s_1 + s_2 \right] t \right)$$

where $x = x_0$, when $t = 0$.

Critical damping is defined by the condition

$$\sqrt{\left(\frac{d}{2m}\right)^2 - \frac{k}{m}} = 0$$

which yields the relation between critical damping coefficient and spring constant

$$d = d_{crit} = 2\sqrt{km}$$

Similar reasoning can be applied to the motion of an oscillating wind vane. A vane is generally a flat plate of some plan configuration which is mounted to one end of a pivoted lightweight arm, while at the other end of the arm some counterweight is mounted for static balancing, Fig. A1 (b). When exposed to an airstream moving with velocity U , the vane is free to swing about the pivotal axis. If the vane is initially set at an angle to the airstream and released, the resulting motion is generally a damped oscillation.

The vane experiences an aerodynamic force which may be resolved into two components: a force F_n *normal* to the vane surface acting at its center of pressure, and F_a , a force acting parallel with the surface. If the vane surface lies in the centerline of the arm, the force F_n is also normal to the arm and is at r_n arm-length distance from the pivotal point.

When the vane is rotating about the pivotal point, the incidence angle β changes with time and the vane assumes a velocity normal to the arm $V_n = r_n \, d\beta/dt$. From the vectorial addition of U and V_n there results a relative velocity U_r , hence the relative angle of incidence β_r enclosed between the relative velocity and moment arm, Fig. A1 (c), is given by the relation

$$\beta_r = \tan^{-1}\left[\frac{U \sin \beta + r_n \frac{d\beta}{dt}}{U \cos \beta}\right]$$

For small angles of incidence $\tan \beta \approx \beta$ and $\cos \beta \approx 1$, hence

$$\beta_r \approx \beta + \frac{r_n \frac{d\beta}{dt}}{U}$$

When the vane is displaced from its center of equilibrium, the normal force F_n produces a returning torque $F_n r_n$ and under dynamic equilibrium condition

$$-F_n r_n = I \frac{d^2\beta}{dt^2}$$

where I is the moment of inertia of the oscillating mass system.

A unit angle torque is introduced

$$N = \frac{r_n F_n}{\beta_r}$$

which, upon substitution, yields

$$-N\beta_r = -N\left(\beta + \frac{r_n \frac{d\beta}{dt}}{U}\right) = I \frac{d^2\beta}{dt}$$

Upon rearranging terms, the oscillatory motion of the vane is described by the differential equation

$$I \frac{d^2\beta}{dt^2} + \frac{Nr_n}{U} \frac{d\beta}{dt} + N\beta = 0 \,. \qquad A(2)$$

Properties of vane motion, such as damping, frequency and time response will now be discussed in turn.

I. Damping

In comparing equation (2) with equation (1), it appears that the mass is replaced by moment of inertia I, the damping coefficient d by the term Nr_n/U, and the spring constant k by the unit angle-torque N. By introducing damping of the vane

$$D = \frac{Nr_n}{U}$$

the general solution of equation (2) may be written in a form similar to the solution of equation (1)

$$\beta = \beta_o \exp\left(\left[s_1 + s_2\right] t\right)$$

where

$$s_{1\ 2} = \left[- \frac{D}{2I} \pm \sqrt{\left(\frac{D}{2I}\right)^2 - \frac{N}{I}} \right] \qquad A(3)$$

and the initial displacement angle $\beta = \beta_0$ when $t = 0$.

Critical damping is defined by the condition

$$\left(\frac{D}{2I}\right)^2 - \frac{N}{I} = 0$$

hence

$$D = D_C = 2\sqrt{IN}$$

For subcritical damping

$$\left(\frac{D}{2I}\right)^2 < \frac{N}{I}$$

hence

$$S_{1,2} = \left[- \frac{D}{2I} \pm j \sqrt{\frac{N}{I} - \left(\frac{D}{2I}\right)^2} \right] \qquad A(4)$$

where $j = \sqrt{-1}$. By the identity $e^{\pm j\Theta} = \cos\Theta + j \sin\Theta$,

$$\beta = \beta_o e^{-\frac{D}{2I} t} \left\{(\cos \omega t + j \sin \omega t) + (\cos \omega t - j \sin \omega t)\right\}$$

$$= \beta_o e^{-\frac{D}{2I} t}\ 2 \cos \omega t \qquad A(5)$$

where

$$\omega = \sqrt{\frac{N}{I} - \left(\frac{D}{2I}\right)^2} \qquad A(5a)$$

is considered angular frequency of the damped oscillations.

One criteria of vane effectiveness is the rate of diminishing amplitude of oscillations. This is expressed by the damping ratio

$$\xi = \frac{D}{D_c}$$

Upon substitution for D and D_c one obtains

$$\xi = \frac{r_n N}{U} \Big/ 2\sqrt{NI} = \frac{r_n}{2U}\sqrt{\frac{N}{I}}$$

For evaluation of the damping ratio two procedures are open: *either* (a) to obtain N from aerodynamic force measurements on the vane; *or* (b) to measure the actual damping of the oscillatory motion.

Procedure (a). The aerodynamic force F_n normal to the moment arm is generally expressed as

$$F_n = C_n\ (1/2\ \rho U^2)\ S$$

With this value the unit angle torque becomes

$$N = \frac{F_n r_n}{\beta_r} = \frac{C_n}{\beta_r}\ 1/2\ \rho U^2 S\ r_n\ .$$

Introducing $a = \dfrac{C_n}{\beta_r}$

$$\xi = \frac{r_n}{2U}\sqrt{\frac{1/2a\ \ \rho U^2 S r_n}{I}} = k_1\left(\frac{a\ r_n^3\ S}{I}\right)^{\frac{1}{2}} \qquad A(6)$$

where $k_1 = 1/2\ \sqrt{(1/2)\rho}$. Equation (6) is employed to obtain the calculated damping ratio. For this calculated value of ξ it appears that the damping is practically independent of air speed because the variation of a with airspeed is relatively small.

In evaluating a the usual procedure is to substitute for C_n the lift coefficient C_L and for β_r the angle of incidence α .

Hence

$$a = \frac{C_n}{\beta_r} \simeq \frac{C_L}{\alpha}$$

Since for small angles of attack the lift curve slope of each surface employed for the wind vane is practically constant, we may write

$$a \simeq \frac{C_L}{\alpha} = \frac{dC_L}{d\alpha} = \text{const.}$$

The value of a may be obtained from aerodynamic tests on vanes.

Procedure (b). For damping to be established from experiments, the vane oscillations must be first recorded. The experimental damping ratio ξ then may be obtained from the decrease in amplitude of the oscillations.

Concerning damped oscillations, the envelope to the amplitude of peaks of oscillations is obtained from the critical condition. In this case the amplitude of the oscillations decreases logarithmically,

$$\beta = \beta_o e^{-\frac{D}{2I}t} \qquad A(7)$$

Counting the time lapse Δt between two consecutive oscillation peaks of the same sign, n and $n + 2$

$$\Delta t = t_{n+2} - t_n = \frac{2\pi}{\sqrt{\frac{N}{I} - \left(\frac{D}{2I}\right)^2}}$$

With this value

$$\beta_{n+2} = \beta_n \left\{ \exp \left[- \frac{D}{2I} \frac{2\pi}{\sqrt{\frac{N}{I} - \left(\frac{D}{2I}\right)^2}} \right] \right\}$$

Since for critical damping $D = \xi D_c$ and $D_c = 2\sqrt{IN}$, upon substitution the amplitude "ratio" of oscillation between two consecutive peaks of the same sign becomes

$$h = \frac{\beta_{n+2}}{\beta_n} = \exp \left[- \frac{2\pi\xi}{\sqrt{1 - \xi^2}} \right]$$

The symbol h is frequently referred to as "overshoot."

Between any m consecutive peaks the formula becomes

$$\frac{\beta_{n+m}}{\beta_n} = \exp\left\{-\frac{m\pi\xi}{\sqrt{1-\xi^2}}\right\} \qquad A(8)$$

where $m = 1, 2, 3, \ldots$

The damping ratio may be obtained by solving equation (8) for ξ. Denoting the reciprocal of the overshoot $\frac{1}{h}$, then

$$\ln\frac{1}{h} = \Lambda_m = \ln\frac{\beta_n}{\beta_{n+m}}$$

one obtains

$$\Lambda_m = \frac{m\pi\xi}{\sqrt{1-\xi^2}}.$$

Solving for ξ yields the experimental damping ratio

$$\xi = \frac{\Lambda_m}{\sqrt{m^2\pi^2 + \Lambda_m^2}}. \qquad A(9)$$

II. Frequency

The frequency of oscillations is of considerable interest. By Eq. A(5a), for damped oscillations the angular frequency

$$\omega_d = \sqrt{\frac{N}{I} - \left(\frac{D}{2I}\right)^2} \qquad A(10)$$

Setting $D = 0$ one obtains the natural angular frequency of undamped oscillations

$$\omega_n = \sqrt{\left(\frac{N}{I}\right)} \qquad A(11)$$

With the relations

$$\omega_d = \frac{2\pi}{t_d} = 2\pi f_d$$

and

$$\omega_n = \frac{2\pi}{t_\eta} = 2\pi f_n$$

one obtains from Eqs. (10) and (11)

$$\frac{t_n}{t_d} = \frac{f_d}{f_n} = \sqrt{1 - \frac{D^2}{4IN}}$$

Substituting $D = \xi D_c$ and $D_c = 2\sqrt{IN}$, and by combining Eqs. A(10) and A(11) the relation between natural and damped frequency becomes

$$f_n = \frac{f_d}{\sqrt{1 - \xi^2}} \qquad A(12)$$

Natural frequency may be expressed in terms of vane design. Substituting $N = a\left(\frac{1}{2}\rho U^2\right) Sr_n$ into Eq. A(11), one obtains

$$f_n = k_2 U\left(\frac{a\, r_n\, S}{I}\right)^{\frac{1}{2}} \qquad A(13)$$

where

$$k_2 = \frac{\rho}{2\sqrt{2}\,\pi} .$$

Equation A(13) is employed to obtain the calculated natural frequency. From this calculated value of f_n it appears that the natural frequency is directly proportional to airspeed.

In practice, the natural frequency may be directly obtained from the expression*

$$f_n = \frac{1}{\Delta t\,(6 - 2.27\xi)} \qquad A(14)$$

where both Δt and ξ are obtained from the recorded graph of oscillations.

III. Time Response

The time lapse counted for the oscillations to decrease from β_0 at $t = 0$ to some specified β_R at t_R is the time response of the vane. This parameter

---

* MacCready and Jex [2] recommend the use of $(6.0 - 2.4\xi)$ derived graphically, analytical derivation yields $(6 - 2.27\xi)$.

is extremely useful when comparing the performance of vanes.

Vane response time in terms of damping and natural frequency may be obtained from the envelope of the amplitude peaks given by the expression

$$\beta = \beta_o \exp\left(-\frac{D}{2I}\, t\right)$$

With $\beta = \beta_R$ when $t = t_R$ one obtains

$$\ln \frac{\beta_o}{\beta_R} = \frac{D}{2I}\, t_R$$

With $D = \xi 2 \sqrt{NI}$

$$\ln \frac{\beta_o}{\beta_R} = \xi \sqrt{\frac{N}{I}}\, t_R$$

Since natural frequency $f_n = \frac{1}{2\pi}\sqrt{\frac{N}{I}}$, the time response becomes

$$t_R = \frac{\ln \frac{\beta_o}{\beta_R}}{2\pi f_n \xi} \qquad A(15)$$

Considering that $\frac{1}{2\pi} \ln \frac{\beta_o}{\beta_R}$ is a constant, say K_3, time response becomes inversely proportional to the product of natural frequency and damping

$$t_R = \frac{K_3}{f_n \xi} \qquad A(16)$$

For comparative purposes, assume that $K_3 = 1$, thus one obtains the "specific" time response

$$\tau_R = \frac{1}{f_n \xi} \qquad A(17)$$

Combination of Eqs. A(6) and (13) with (16) yields

$$t_R = K \frac{1}{U}\left(\frac{I}{a\, r_n^2\, S}\right) \qquad A(18)$$

where

$$K = \frac{K_3}{K_1 K_2}\,.$$

Thus for a specified vane design response time appears to be inversely proportional to airspeed, $t_R \propto U^{-1}$.

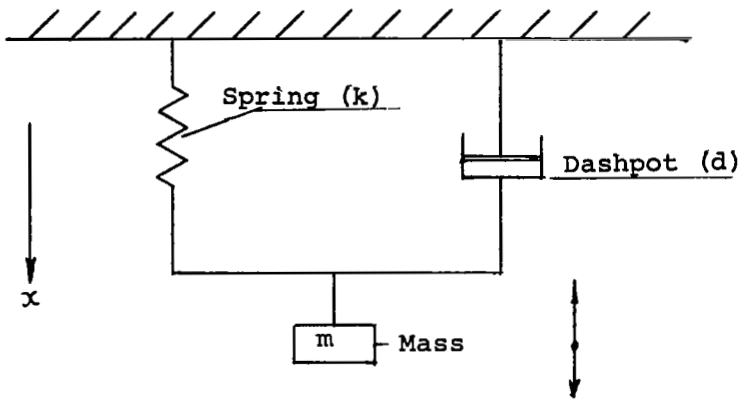

(a) Simple spring and dashpot mass system

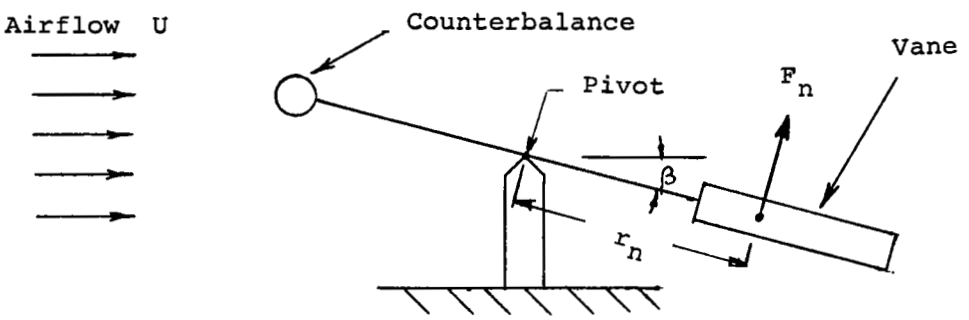

(b) Pivoted vane system provided with counterbalance

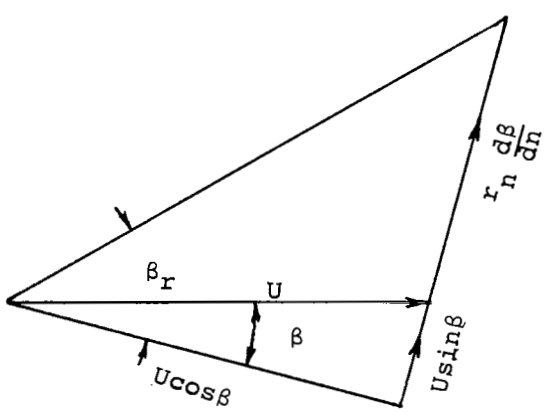

(c) Velocity Vector diagram

Fig. A1 - Schematic Diagrams pertaining to theory of wind vanes exposed to an airstream

APPENDIX B

DYNAMICS OF BI-VANES

Consider a pair of vanes, referred to as a bi-vane, consisting of flat surfaces, suitably mounted to an arm which is free to swing about a pivotal axis P as shown (a) on top of Figure B1. Here the vanes and the arms are shown to be aligned parallel with the airstream U, and the distance d between the vanes is split into equal halves so that each vane is located at $d/2$ distance from the system centerline. Since the vanes are hinged, they can be turned inward or outward, usually with equal vane setting "trim" angle ϕ. When turned outward $+\phi$ and when turned inward $-\phi$ angle will be indicated. For each vane, the aerodynamic center AC is considered at quarter-chord from the leading edge. The aerodynamic moment arm R_V, that is the distance located between the aerodynamic center AC and the pivot point P, encloses the angle γ with the flow direction as shown (b) in the center of Figure B1, where for this illustration both vanes are turned outward by an angle $-\phi$ from the flow direction.

In neutral or equilibrium position the system centerline $\mathbb{C}$ aligns parallel with the airflow and the aerodynamic forces, acting on the vanes, balance out. When, however, the system centerline $\mathbb{C}$ is displaced by an angle β from the flow direction, as shown (c) on bottom of Figure B1, the contribution of torque of each vane becomes unequal resulting in a net torque that will produce some damped oscillations when the vanes are "set free" from an offset position.

In the case of bi-vanes, in addition to lift, the drag forces also develop torque, hence for the vanes A and B, and with the notation shown (c) in Figure B1, the net torque about P (positive if anticlockwise) is given by

$$T = F_{LA}\, L_A - F_{LB}\, L_B - F_{DA} \cdot \ell_A + F_{DB} \cdot \ell_B$$

where

$$F_{LA}\, L_A = C_{LA}\, q\, S\, R_V \cos(\gamma + \beta)$$

$$F_{LB}\, L_B = C_{LB}\, q\, S\, R_V \cos(\gamma - \beta)$$

$$F_{DA}\,\ell_A = C_{DA}\,q\,S\,R_v\,\sin(\gamma + \beta)$$

$$F_{DB}\,\ell_B = C_{DB}\,q\,S\,R_v\,\sin(\gamma - \beta)$$

are the torque components and

S = projected surface area of <u>one</u> vane.

Upon defining a torque coefficient, averaged for the torque components

$$\overline{C}_v = \frac{T}{q\,S\,R_v}$$

one obtains

$$\overline{C}_v = C_{LA}\cos(\gamma + \beta) - C_{LB}\cos(\gamma - \beta) - C_{DA}\sin(\gamma + \beta) + C_{DB}\sin(\gamma - \beta) \qquad B(1)$$

Assuming that the vanes were <u>not</u> affected by multiplane interference, then the values of both C_L and C_D could be obtained from the experimental values of lift and drag coefficient of isolated flat vanes. However, this assumption did not bear out as the vanes were indeed affected by each other and the coefficients must be calculated accordingly.

In the "neutral" arm position when $\beta = 0$, each vane inclines to the flow direction by equal ϕ ; when, however with $\beta \neq 0$, A vane becomes inclined to the flow direction with the angle $\alpha_A = \phi - \beta$ while the B vane becomes inclined to the flow direction with the angle $\alpha_B = \phi + \beta$.

Let ϕ be specified and β be variable. As β increases one vane experiences increasing lift, while simultaneously the other experiences decreasing lift. Similar considerations apply to drag also.

Thus, for a β displacement, the simultaneous incidences at which the lift and drag coefficients of the vanes must be found from the C_L and C_D versus α curves, are

$$\alpha_A = \phi - \beta\ ,$$

and

$$\alpha_B = \phi + \beta$$

resulting in lift and drag coefficients of the A and B vanes respectively

$$C_{LA} = C_{L\alpha_A}, \quad C_{DA} = C_{D\alpha_A},$$

$$C_{LB} = C_{L\alpha_B}, \quad C_{DB} = C_{D\alpha_B}$$

In the case the vanes are set parallel with the stream $\phi = 0$, $\alpha = \alpha_A = \alpha_B = \beta$, thus

$$C_{LA} = C_{LB} = C_{L\alpha}$$

and

$$C_{DA} = C_{DB} = C_{D\alpha}$$

In this special case Equation (B1) reduces to

$$\overline{C}_v(\beta) = 2\cos\gamma(C_{L\alpha}\cos\beta + C_{D\alpha}\sin\beta) \tag{B2}$$

Curves of $\overline{C}_v$ plotted against β angle are shown in Figure B2, where the vane setting angle ϕ and the angle γ are parameters. Values of C_L and C_D for vanes A and B were read off at angles $\phi + \beta$ and $\phi - \beta$.

As in Appendix A, let unit angle torque* be defined as

$$N = \frac{F_v R_v}{\beta} = \left(\frac{\overline{C}_v}{\beta}\right) q\, SR_v$$

Thus damping ratio becomes

$$\xi = \frac{R_v}{2U}\sqrt{\left(\frac{\overline{C}_v}{\beta}\right)(1/2\,\rho U^2)\frac{SR_v}{I}}$$

$$= \sqrt{\frac{\rho}{8}}\sqrt{\left(\frac{\overline{C}_v}{\beta}\right)}\sqrt{\frac{R_v^3}{I/S}} \tag{B3}$$

---

* Note change of notation of C_n and r_n to C_v and R_v.

Various plots of calculated values of $(\overline{C}_v/\beta)$ against β are also shown in Figure B2 with the vane trim angle ϕ and the arm angle γ again used as parameters. Since the curves show considerable variation of $(\overline{C}_v/\beta)$ with β, *the assumption of N being constant does not hold generally for bi-vanes.* It holds only for $\phi = 0$, if β is not exceeding 4 degrees. Therefore, the necessary condition for linear theory to hold is not satisfied and the experimental results bear this out.

For vanishingly small angles of $(\overline{C}_v/\beta)$ write Equation (B3)

$$\xi = \sqrt{\frac{\rho}{8}} \sqrt{\left(\frac{d\overline{C}_v}{d\beta}\right)} \sqrt{\frac{R_v^3}{I/S}} \qquad \text{(B4)}$$

In order to obtain the slope of the curves $\frac{d\overline{C}_v}{d\beta}$ at $\beta = 0$, differentiate $\overline{C}_v$ with respect to β

$$\left(\frac{d\overline{C}_v}{d\beta}\right) = -C_{LA} \sin(\gamma + \beta) + \frac{dC_{LA}}{d\beta} \cos(\gamma + \beta) - -C_{LB} \sin(\gamma - \beta) - \frac{dC_{LB}}{d\beta} \cos(\gamma - \beta)$$

$$+ -C_{DA} \cos(\gamma + \beta) - \frac{dC_{DA}}{d\beta} \sin(\gamma + \beta) + -C_{DB} \cos(\gamma - \beta) + \frac{dC_{DB}}{d\beta} \sin(\gamma - \beta) .$$

With $\beta \to 0$, the lift and drag coefficients at ϕ incidence become

$$C_{LA} = C_{LB} = C_{L\phi}$$

and

$$C_{DA} = C_{DB} = C_{D\phi} .$$

Further, since $\alpha_A = \phi - \beta$ and $\alpha_B = \phi + \beta$, one obtains: $d\alpha_A = -d\beta$, $d\alpha_B = +d\beta$, hence

$$\left(\frac{d\overline{C}_v}{d\beta}\right) = -C_{L\phi} \sin\gamma - \frac{dC_{L\phi}}{d\alpha_A} \cos\gamma - C_{L\phi} \sin\gamma - \frac{dC_{L\phi}}{d\alpha_B} \cos\gamma$$

$$- C_{D\phi} \cos\gamma + \frac{dC_{D\phi}}{d\alpha_A} \sin\gamma - C_{D\phi} \cos\gamma + \frac{dC_{D\phi}}{d\alpha_B} \sin\gamma$$

Upon collecting terms, changing signs, and dropping the subscripts A and B, one obtains the slope of the $\bar{C}_v$ curves at $\beta = 0$ for *inwardly turned vanes* (ϕ-)

$$-\left(\frac{d\bar{C}_v}{d\beta}\right)_{\beta=0} = 2\cos\gamma\left[\frac{dC_{L\phi}}{d\alpha} + C_{D\phi}\right] - 2\sin\gamma\left[\frac{dC_{D\phi}}{d\alpha} - C_{L\phi}\right]$$

It may be shown that for *outwardly turned vanes* (ϕ+)

$$-\left(\frac{d\bar{C}_v}{d\beta}\right)_{\beta=0} = 2\cos\gamma\left[\frac{dC_{L\phi}}{d\alpha} + C_{D\phi}\right] + 2\sin\gamma\left[\frac{dC_{D\phi}}{d\alpha} - C_{L\phi}\right] \qquad \text{(B5)}$$

For parallel vanes ($\phi = 0$) since both $dC_{D\phi}/d\alpha = 0$ and $C_{L\phi} = 0$, Equation (B5) reduces to

$$-\left(\frac{d\bar{C}_v}{d\beta}\right)_{\substack{\beta=0\\ \phi=0}} = 2\cos\gamma\left[\frac{dC_{L0}}{d\alpha} + C_{D0}\right] \qquad \text{(B6)}$$

where $dC_{L0}/d\alpha$ is the lift curve slope and C_{D0} is the drag coefficient at $\alpha = 0$. The negative sign signifies the decrease in $\bar{C}_v$ with increasing β.

Curves of calculated $(d\bar{C}_v/d\beta)_{\beta=0}$ against vane setting angle ϕ are plotted in Figure B2 where γ is used as a parameter.

It appears from Figure B2 that the curves peak at about $\phi = 6$ degrees and are a strong function of the arm angle γ. While these curves show a similar pattern for $\phi = 0$, 5, and 10 degrees, a markedly different curve appears when ϕ attains 15 degrees. It is noted that as far as lift is concerned all values shown in Figures B2, (a), (b), (c), and (d) were calculated with the experimentally obtained lift coefficients (shown in Figure 15) of a rectangular bi-vane of aspect ratio 2.5, for reasons that these results include effects of bi-vane interference. However, as far as drag is concerned, the coefficients of a single vane shown in Figure 10 - of the same aspect ratio - were employed. For each $\phi = 0$, 5, 10, and 15 degrees (and one set of 20) fixed, angle β was varied stepwise using 1, 2, 4, 8, 12, 16, and 20 degrees. For example in

Figure B2b, $\phi = 5$ and assuming $\beta = 1$, $\alpha_A = 5 + 1 = 6$ and $\alpha_B = 5 - 1 = 4$. Hence $C_{LA} = 0.340$, $C_{LB} = 0.220$, $C_{DA} = 0.0583$, $C_{DB} = 0.036$ and so on. Again, the same lift and drag results were employed to calculate $(d\overline{C}_V/d\beta)_{\beta=0}$ by establishing $dC_{L\phi}/d\alpha$ and $dC_{D\phi}/d\alpha$ at the appropriate ϕ angle on the graph when $\alpha = 0$.

The predicted damping for bi-vanes (as already stated earlier) falls considerably below the experimental values. In Figure B3, the predicted damping is plotted against inertia ratio showing the decrease with increasing inertia for various arm angles and trim angles ϕ. It is particularly interesting to observe the increase in the discrepancy between the calculated prediction and the experimental results as trim increases. For zero trim $\phi = 0$, the discrepancy is fairly small and even with $\phi = 5$ degrees the prediction is reasonably acceptable. With $\phi = 10$ and 15 degrees, however, the experimental values far exceed the predicted figures and there is a strong suspicion that the forces are greater on the vanes because of bi-vane interference. Further studies in this field appear to be desirable.

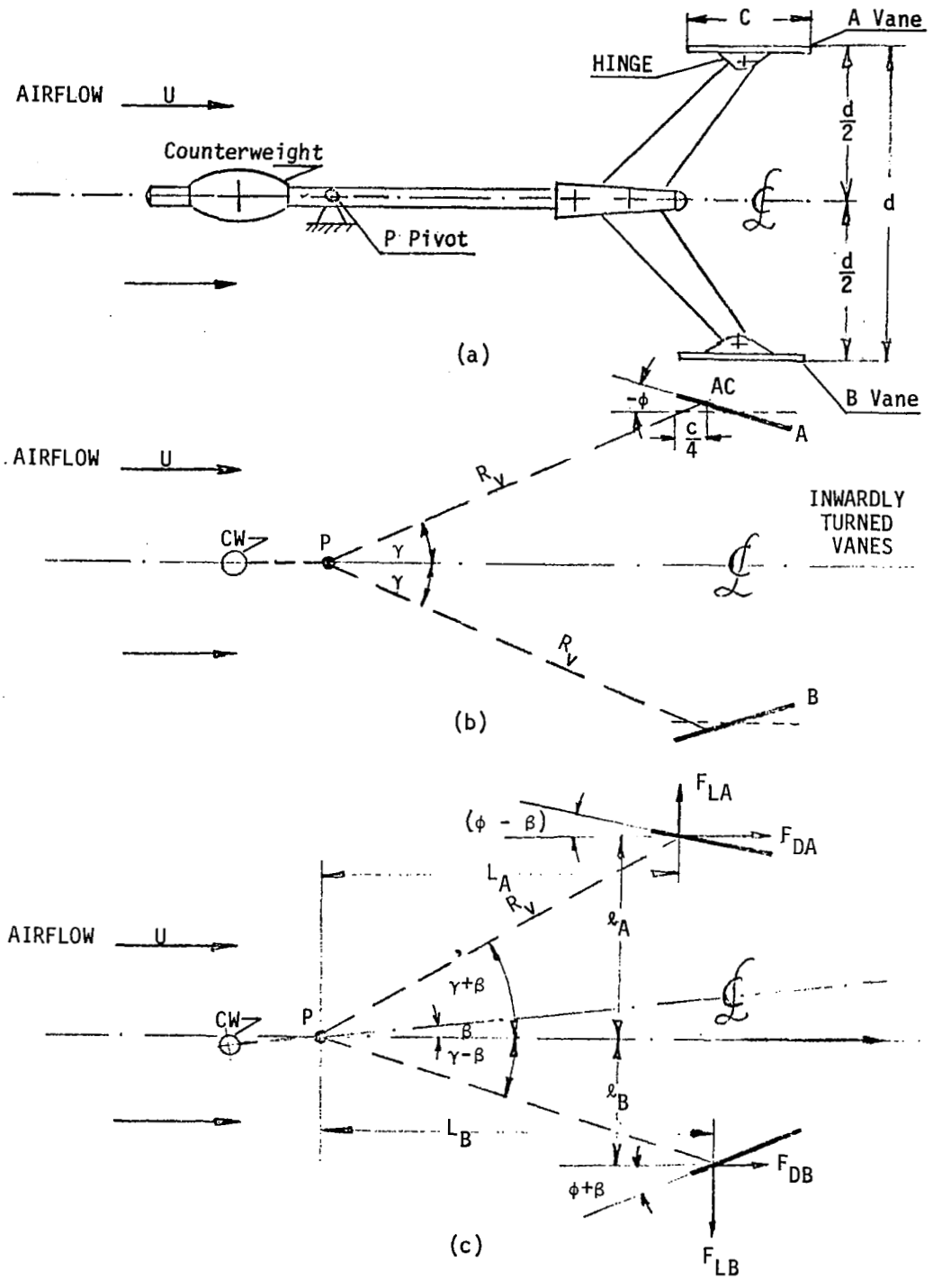

Figure B1. Schematic arrangement of bi-vanes.

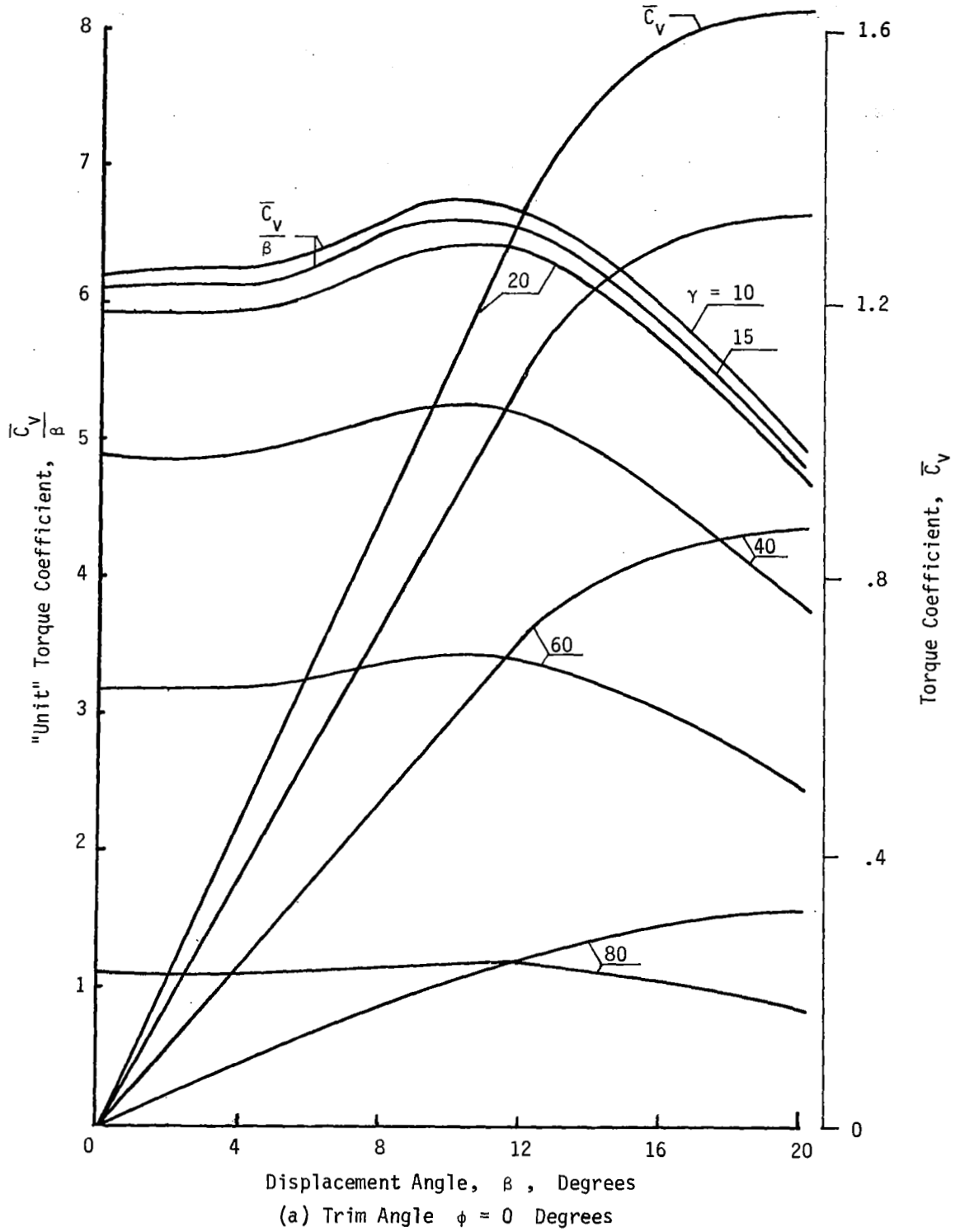

Figure B2. Variation of torque coefficient with displacement angle of bivanes.

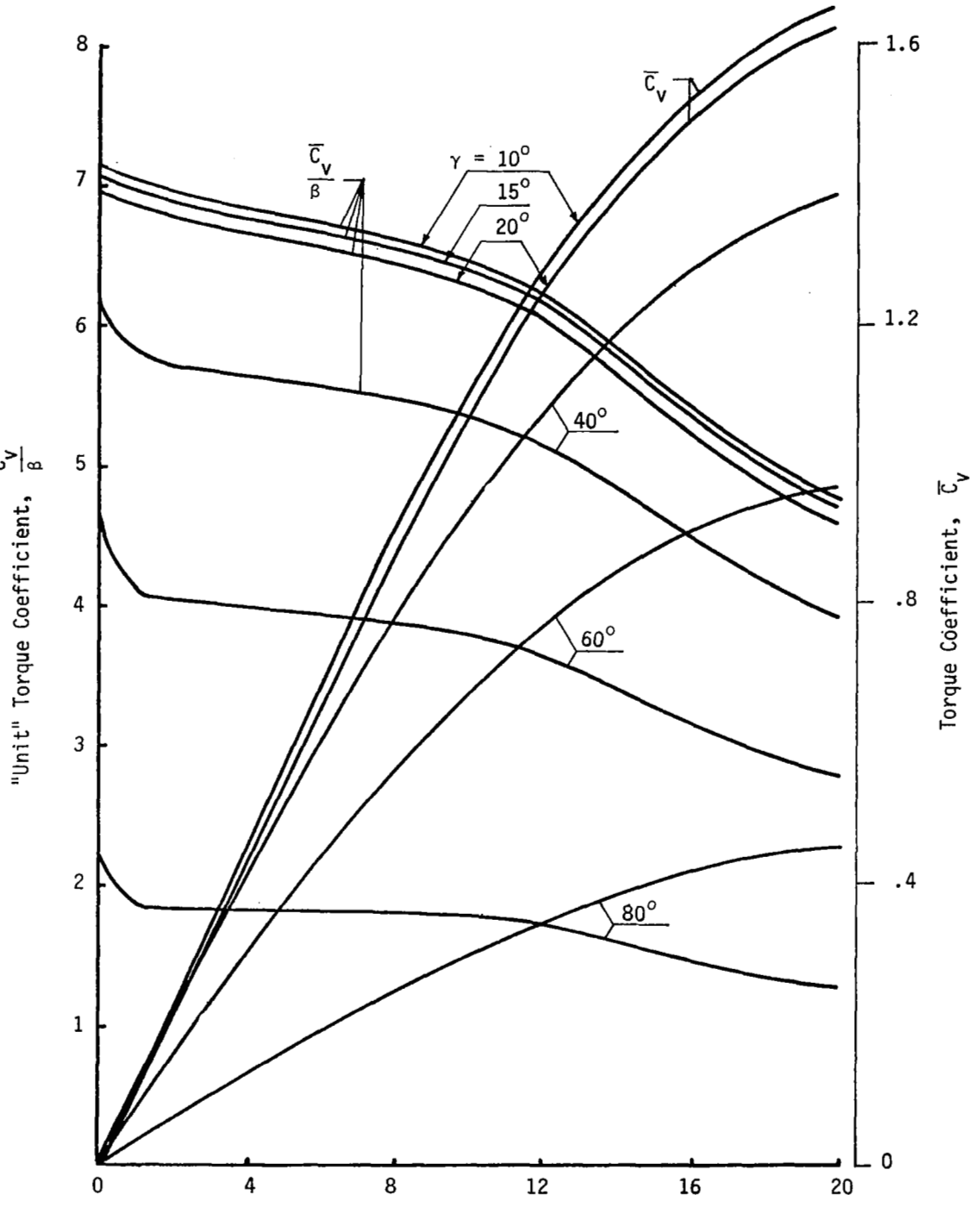

(b) Trim Angle $\phi = 5^\circ$

Figure B2. - Continued

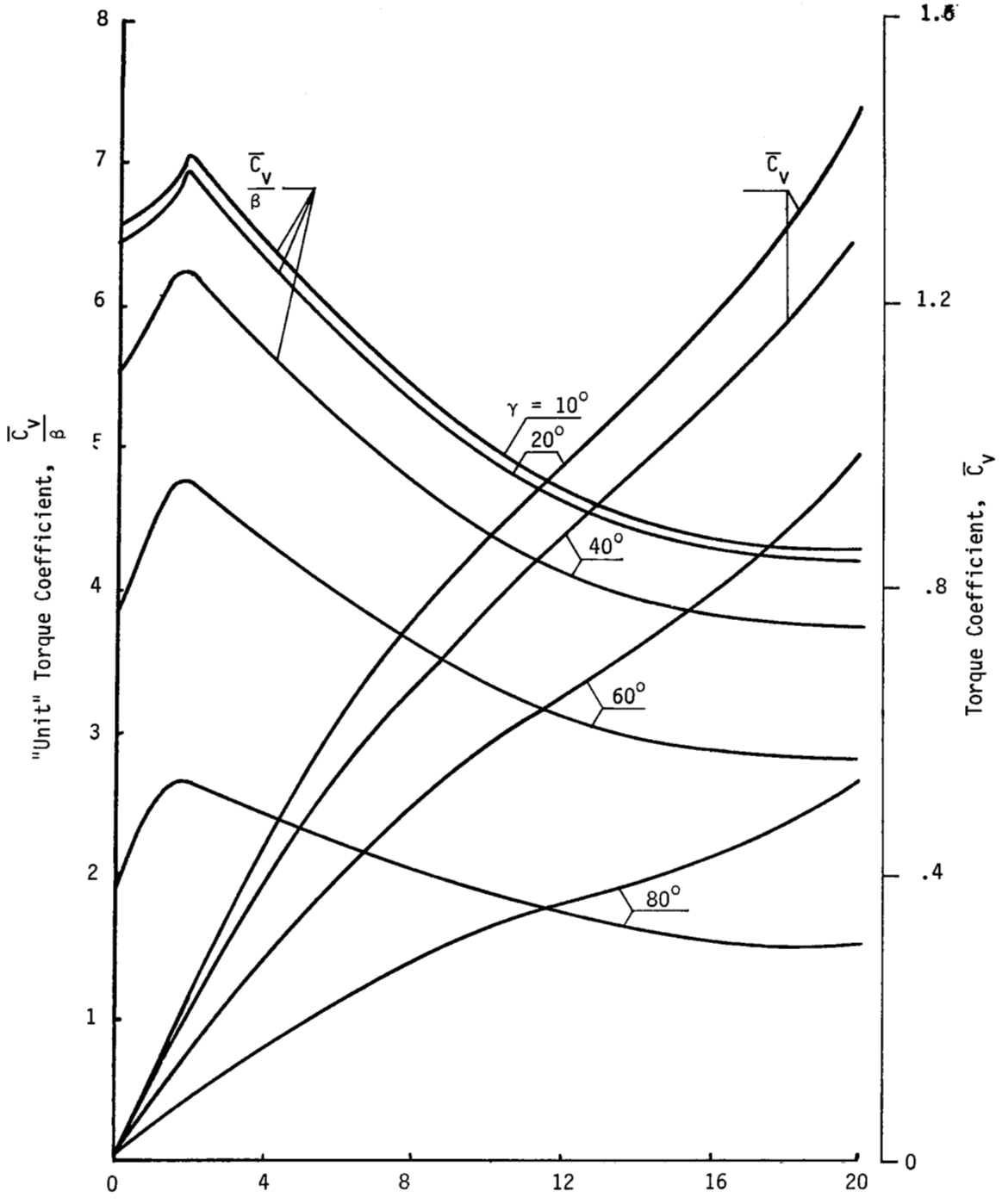

(c) Trim Angle ϕ = 10 Degrees

Figure B2. - Continued

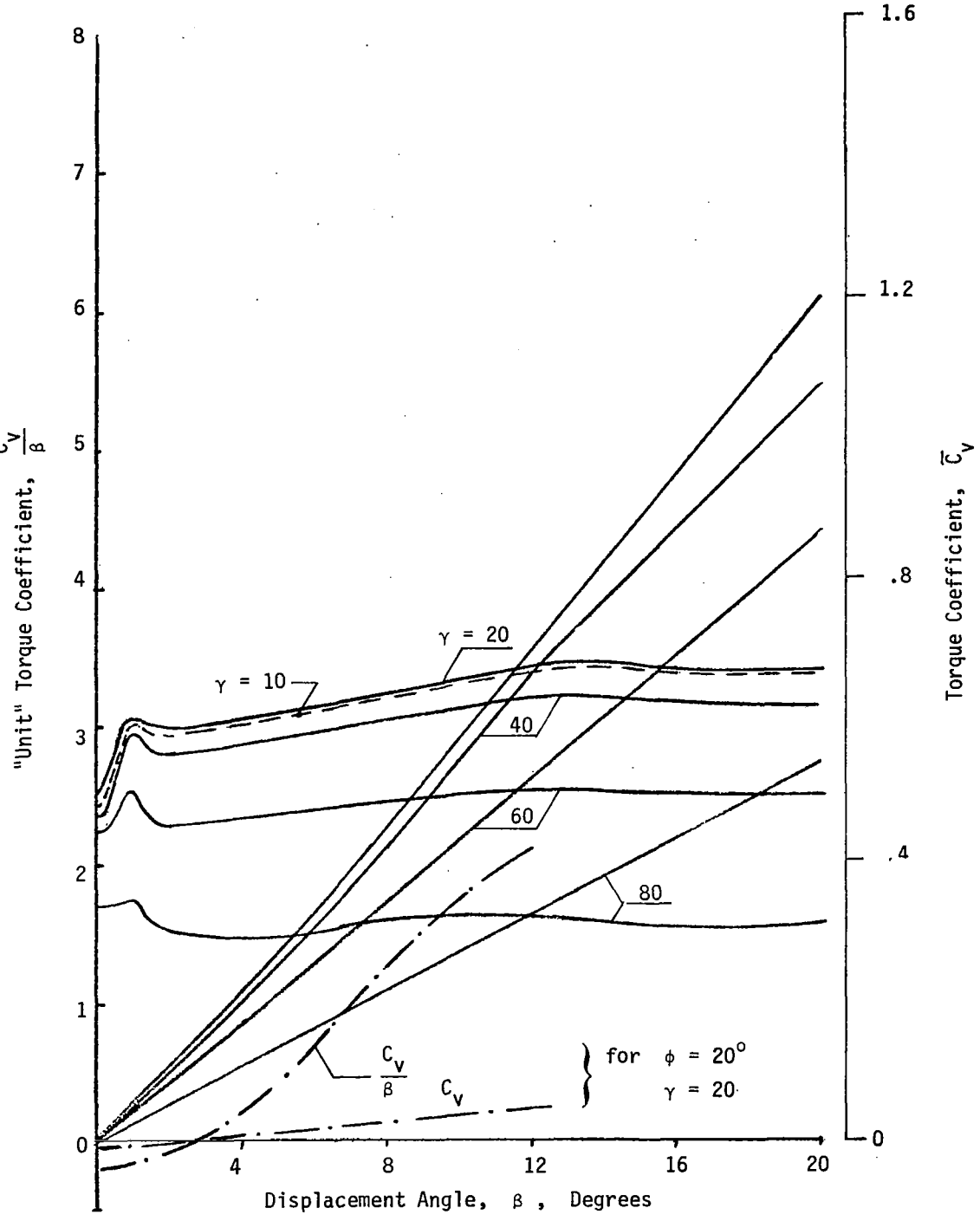

(d) Trim Angles ϕ = 15 and 20 Degrees

Figure B2. - Concluded

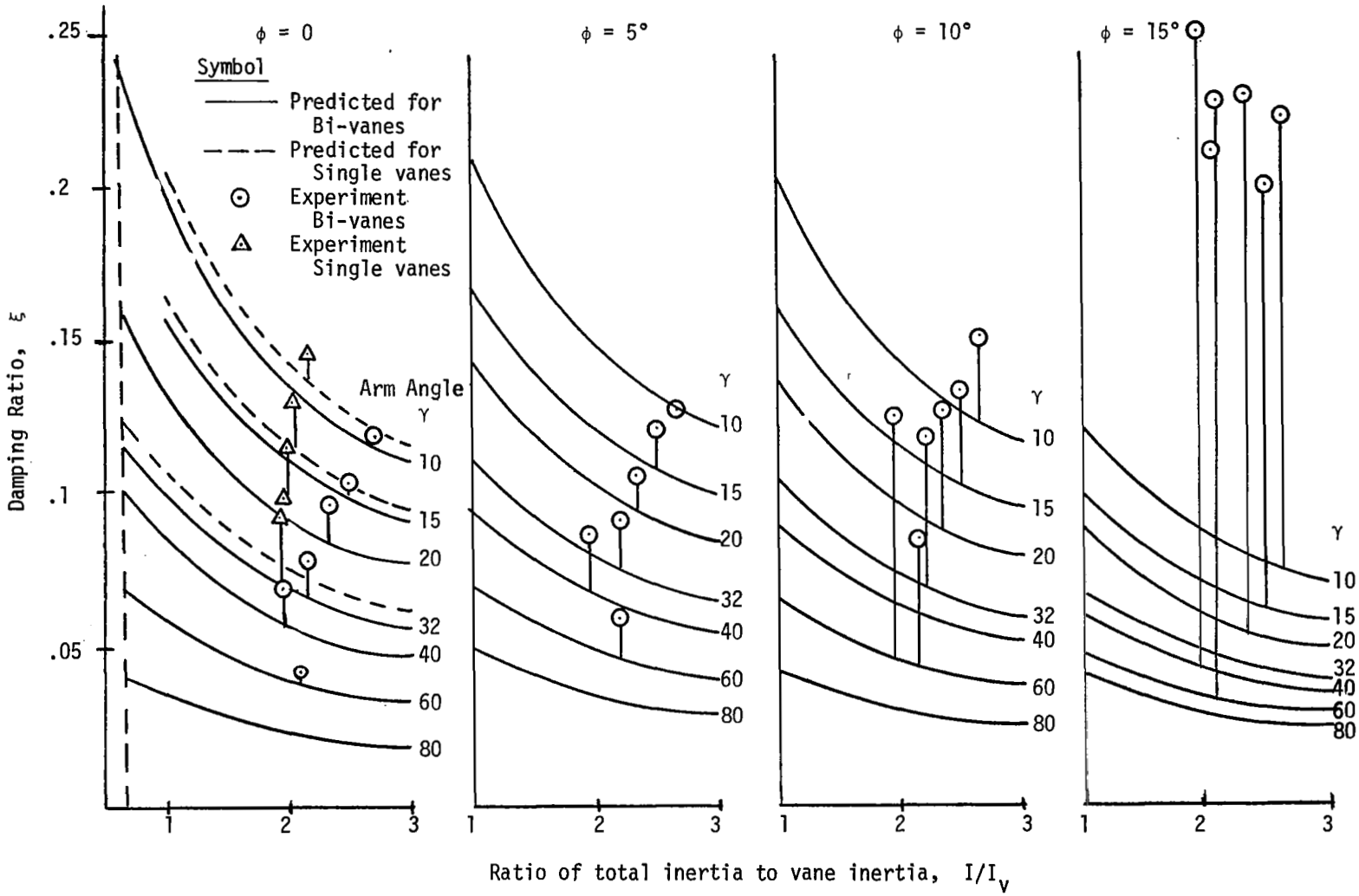

Figure B3. Variation of damping ratio of bi-vanes with vane inertia (I/I_V) for different arm (γ) and trim angles (ϕ).

APPENDIX C

INERTIA

The inertia I of a vane about the axis of oscillations

$$I = I_{C.G.} + I_x$$

where $I_{C.G.}$ is the inertia of the vane about its own center of gravity and I_x is the inertia of the vane about the axis of oscillations.

Accordingly, for a rectangular vane

$$I_{C.G.} = \frac{1}{12} bc^3 t\rho_v$$

and

$$I_x = bct\rho_v r^2_{C.G.}$$

where $r_{C.G.}$ is distance between the axis and C.G. of the planform. If the aerodynamic center is located at quarter chord from the leading edge $r_{C.G.} = r_n + \frac{c}{4}$ and upon substitution one obtains

$$I = bct\rho_v \left[\frac{c^2}{12} + \left(r_n + \frac{c}{4}\right)^2\right] .$$

To this quantity must be added the inertia of the shaft and of the counterweight balance to obtain the inertia of the system.

Upon expanding the bracketed term one obtains for a rectangular vane with the A.C. at quarter chord

$$I = kr_n^2 \left[1 + \frac{1}{2}\left(\frac{c}{r_n}\right) + .146 \left(\frac{c}{r_n}\right)^2\right]$$

where $k = bct\rho_v$.